

**INVESTIGATION OF THE GEOLOGY AND
MINERALISATION IN THE VICINITY OF THE GIBRALTAR I
DRILL HOLE, NORTH-WEST OF TARCOOLA, SOUTH
AUSTRALIA.**

Robert C Webb B Sc.



**Thesis submitted as a partial fulfillment for the
Honours Degree of Bachelor of Science**

**Department of Geology and Geophysics
The University of Adelaide
October 1992**

**NATIONAL GRID REFERENCE: SH 5737-III
(CARNDING 1:100 000 Map Sheet)**

Supervisor: R A Both

Perm. Loan

Miner. Proc.

ABSTRACT

The Gibraltar I drill site is located 38 km north-west of Tarcoola, South Australia, within the Middle Proterozoic Gawler Range igneous province. The drill core has sampled the Ealbara Rhyolite, a member of the Lower Gawler Range Volcanics. This unit in the vicinity of the drill hole may be subdivided into a number of variably welded rhyolitic ash flow tuffs and lavas, all showing similar degrees of deuteric alteration.

Tectonic implications of the host volcanic geochemistry are consistent with a tectonic model of emplacement proposed by Giles (1980, 1988).

Hydrothermal alteration and mineralisation is noted in outcrop in the vicinity of the drill hole, and in the drill core itself. A hematite bearing quartz breccia and chloritic microbreccia are present, along with areas of often intense silicification and sericitisation. The drill core mineralisation consists mainly of vein and disseminated pyrite, with minor chalcopyrite, sphalerite, galena, pyrrhotite and marcasite. Sericite and quartz comprise the major gangue minerals, with minor chlorite, fluorite and calcite present as accessory phases.

Sulfur isotope analyses performed on pyrite from the drill core reveal isotopic ratios consistent with a felsic igneous source for the sulfur. Such a source is most likely to be the rhyolite pile hosting the mineralisation.

Temperature estimates of the hydrothermal fluids responsible for the hematite-bearing quartz breccia and Gibraltar I mineralisation, on the basis of fluid inclusions and chlorite analyses, indicate a range of 190°C to 300°C, characteristic of an epithermal type hydrothermal system. Salinities obtained from the fluid inclusion analyses indicate low salt contents (< 2% wt NaCl equivalent).

Geochemical modelling of the hydrothermal system at 300°C suggests that much of the sulphide deposition occurred between pH's of 2.8 and 4.8, with log oxygen fugacities ranging from -36.5 to -33.0. These conditions are unsuitable for significant gold transport, due to the low solubilities of gold complexes present in such a fluid.

A convective, groundwater derived hydrothermal system is considered responsible for the mineralisation sampled by the drill core. In the presence of a heat source, superposition of a convective flow regime upon meteoric waters would occur. Continued cyclic flow at elevated temperatures would allow the fluids to become enriched in metals and sulphur, with deposition resulting from mixing with less evolved groundwaters. The heat source for this system was most likely a subvolcanic magma chamber associated with the extrusive rocks hosting the mineralisation.

CONTENTS

1. INTRODUCTION.....	1
1.1 Location and Description of Mapping Area	1
1.2 Previous Work and Mining Operations in the Area	1
1.3 Reasons for the Location of the Gibraltar I Drill Site	2
1.4 Aims of the Study	2
1.5 Methods of Study	3
2. GEOLOGICAL SETTING	4
2.1 Regional Geology	4
2.2 Local Lithological Descriptions.....	6
2.2.1 Unaltered Volcanics	6
2.2.2 Altered Volcanics	9
3. GEOCHEMISTRY OF THE VOLCANICS.....	11
3.1 Introduction	11
3.2 Classification of the Volcanics.....	11
3.3 Tectonic Setting.....	12
3.3.1 Previous Work.....	12
3.3.2 Major and Trace Element Variation Implications for Fractionation History.....	12
3.3.3 Tectonic Implications of the Geochemistry.....	13
4. LOCAL STRUCTURAL GEOLOGY.....	15
4.1 Jointing	15
4.2 Chloritic Microbreccia	16
4.3 Joint Zone	16
4.4 Quartz-Hematite Breccia.....	16
4.5 Barren Quartz Veins.....	17
5. HYDROTHERMAL ALTERATION AND MINERALISATION	18
5.1 The Vent Area.....	18
5.1.1 Mineralisation	18
5.1.2 Alteration Geochemistry	19
5.2 Altered Volcanics - Zone 1	20
5.3 Altered Volcanics - Zone 2.....	21
5.4 The Gibraltar I Drill Core.....	21
5.4.1 Introduction	21
5.4.2 Mineralogy and Paragenesis	22
5.4.3 Drill Core Geochemistry.....	23
5.5 Quartz - Hematite Breccia	25

6. PHYSICOCHEMISTRY OF THE GIBRALTAR I	
HYDROTHERMAL FLUIDS	26
6.1 Fluid Inclusion Microthermometry.....	26
6.1.1 Inclusion Types	26
6.1.2 First and Final Melt Temperatures.....	27
6.1.3 Homogenisation Temperatures.....	27
6.1.4 Summary	28
6.2 Chlorite Analyses.....	29
6.3 Sphalerite Analyses	30
6.4 sulphur Isotope Analyses.....	30
6.5 Geochemical Modelling of the Hydrothermal System Responsible for the Gibraltar I Mineralisation	32
6.5.1 Modelling in fO_2 vs pH Space	32
6.5.2 Modelling in fO_2 vs T Space	33
6.5.3 Gold Solubility (Fig. 6.5).....	33
7. GENETIC MODEL FOR MINERALISATION	34
7.1 Heat Source Driving the Hydrothermal System	34
7.2 Fluid / Metal / Sulphur Source and Transport.....	34
7.3 Relation of the Gibraltar I Mineralisation to nearby Hydrothermally Mineralised Zones	35
8. CONCLUSIONS	36

ACKNOWLEDGEMENTS

REFERENCES

LIST OF APPENDICES

1. Petrological Descriptions of thin and polished sections
2. Whole rock analyses
3. CIPW Normalisation Program
4. Gibraltar I drill Core Log
5. Fluid Inclusion Microthermometry
6. Chlorite Electron Microprobe Analyses
7. Sphalerite Electron Microprobe Analyses
8. Sulphur Isotope Analyses
9. Thermodynamic Equations

LIST OF FIGURES

- 1.1 Locality Plan of Gibraltar I drill site.
- 2A 1:3000 scale outcrop map.
- 2B 1:3000 scale interpretative map.
- 2C 1:3000 schematic cross-section
- 2.1 Modal classification of the volcanics.
- 3.1 Normative classification of igneous rocks.
- 3.2, 3.3 Volcanic discrimination plots using immobile elements.
- 3.4 Spidergram of selected major and trace element data.
- 3.5 Rb-Ba-Sr ternary plot indicating the degree of fractionation of rhyolites.
- 3.6 Discrimination diagrams for discrimination of A-type granites from I-, S- and M- type granites.
- 3.7 Tectonic regime plots for fresh and altered rhyolite samples.
- 4.1 Schematic representation of observed jointing in the porphyritic welded tuff.
- 4.2 Rose diagram of joint data from mapped area.
- 5.1 Alteration haloes of the Vent Area.
- 5.2 Variations of major and trace element abundances within the vent area.
- 5.3 Paragenesis of the Gibraltar I drill core.
- 5.4 Variation in whole rock geochemistry with depth down the Gibraltar I drill core.
- 6.1 Summary of fluid inclusion analyses.
- 6.1a Histogram of pyritic sulphur isotope ratios representing samples from the Gibraltar I drill core.
- 6.2 Histogram of temperatures generated from chlorite analyses.
- 6.3 Log fO_2 - pH diagram calculated for 300°C, $a_{K^+} = 0.1$, and $\Sigma S = 10^{-2.5}$ M.
- 6.4 Log fO_2 - temperature diagram calculated for $\Sigma S = 10^{-2.5}$ M and pH = 4.

6.4a Log fS_2 - fO_2 diagram calculated for 300°C. Chlorite data are plotted for the range $300 \pm 10^\circ C$.

6.5 Log fO_2 - pH diagram calculated for 300° C, $a_{K^+} = 0.1$, $\Sigma S = 10^{-2.5}$ M. Gold solubility contours are included.

LIST OF PLATES

1. Heavily embayed quartz within the porphyritic welded ash flow tuff.
2. Compactional layering within the porphyritic welded ash flow tuff.
3. Lithic fragment within the porphyritic welded ash flow tuff.
4. Axiolitic devitrification within the strongly welded ash flow tuff.
5. Compactional layering within the black glassy rhyolite.
6. Convolute flow banding within the rhyolite lava.
7. Quartz veins associated with the quartz-hematite breccia
8. Typical brecciation in barren quartz veins.
9. Jointing within the porphyritic welded ash flow tuff.
10. Typical sericitic brecciation within the Gibraltar I drill core.
11. Pyrite - bearing sericite associated with fluorite within the Gibraltar I drill core.
12. Brecciated aggregates of pyrite within a sericitic breccia vein.
13. Pyrite contained within a vein of sericite.
14. Disseminated aggregate of marcasite, chalcopyrite and pyrite.
15. Chalcopyrite hosted within a quartz vein.

1. INTRODUCTION

1.1 Location and Description of Mapping Area

The South Australian Department of Mines and Energy (SADME) Gibraltar I drill hole is located within the Gawler Craton, 38 km north-west of Tarcoola, South Australia, at latitude 30° 25' S and longitude 134° 20' E on the Carnding 1:100 000 geological map (Fig. 1.1). It is hosted within the Ealbara Rhyolite, a member of the Upper Middle Proterozoic Gawler Range Volcanics. The land is contained within Mulgathing sheep station, and may be accessed by a vehicle track running roughly west from the 535 km marker on the Tarcoola-Alice Springs rail line service road.

The outcrop in the vicinity of the drill site consists of a number of low relief ridges, trending south-south-east, covering an area of roughly 3x2 km. Surrounding sediment is Recent red-brown sandy clay, occasionally cemented by iron oxide or calcrete. The entire area is sporadically covered by salt bush, and acacia trees averaging about 3 m in height, indicative of the arid climate of the district.

1.2 Previous Work and Mining Operations in the Area

The area has been mapped by S. Daly at both 1: 250 000 and 1:100 000 for the Geological Survey of South Australia (Daly, 1985). A study of the area was carried out by E. Dubowski before and during the Gibraltar I drilling program in 1991 (Dubowski, 1992), with subsequent thin section petrology by Pontifex and Associates Pty. Ltd. (Purvis, 1991).

No mining operations local to the Gibraltar I drill site are known. The Tarcoola Goldfield produced a total of 2387 kg of gold at 3.7 g/t bullion between 1893 and 1988, with no production since that time (Daly et al., 1990). Gold was discovered at Glenloth, 40 km SE of Tarcoola, in 1901 and production now totals 280 kg. The Birthday quarry, approximately 23 km north east of Gibraltar I, is currently in operation producing aggregate for rail ballast from Gawler

Range Volcanics; of note are traces of disseminated pyrite and chalcopyrite within the extracted rock.

1.3 Reasons for the Location of the Gibraltar I Drill Site

The area local to the drill site was initially considered to be of interest by the SADME because of a magnetic anomaly delineated by regional aeromagnetic surveying within the Gawler Range Volcanics. Further interest was generated by subsequent remote sensing and ground magnetic surveying. The remote sensing data was of particular interest, as this outlined a patch of possibly silicified volcanics within an outcrop of hematite rich rock.

This was followed up by SADME with surface sampling for geochemical and thin section purposes. The resulting geochemical assaying revealed anomalous, but subeconomic, concentrations of gold, silver, copper, lead and zinc. The diamond drill hole was intended to test for evidence of higher concentrations of these elements.

Upon completion of geochemical assaying of the drill core, further subeconomic concentrations of the metals were found, however no ore grade abundances could be identified. The final drill core length totalled some 111 m through the Ealbara Rhyolite, with no other lithologies encountered.

1.4 Aims of the Study

The aims of the study presented here were:

(i) To observe and interpret the geology of the area in the vicinity of the Gibraltar I drill hole.

(ii) To investigate the mineralisation in the drill core and on the surface, using petrology, whole rock geochemistry, chlorite and sphalerite microprobe analyses, sulphur isotope analyses and fluid inclusion studies.

(iii) To define a feasible genetic model for this mineralisation, based on the above data.

1.5 Methods of Study

(i) Initial mapping of the defined area was performed in conjunction with a laser targetted theodolite and reflecting prism. This was used to avoid the inaccuracies of aerial photograph mapping, due to distortions. This method was abandoned in later mapping because of its time consuming nature, with all subsequent mapping on an air photo provided by SADME.

(ii) Petrological / petrographic inspection of 29 thin sections and 47 polished thin sections, from both outcrop and the Gibraltar I drill core. The sections examined include those previously prepared for SADME by Pontifex and Associates.

(iii) Whole rock XRF analysis of 45 personally collected outcrop samples, along with the inspection of 20 outcrop and 26 drill core geochemical analyses provided by SADME.

(iv) Sulphur isotope analysis of 9 samples of pyrite from the drill core.

(v) Fluid inclusion microthermometry performed on 6 outcrop and 1 drill core sample.

(vi) 10 electron microprobe analyses of sphalerite to investigate fO_2 conditions associated with deposition of the mineralisation.

(vii) Electron microprobe analysis of 5 drill core thin sections to determine chlorite compositions.

(viii) Applications of thermodynamic data on the sulphide and gangue mineralogy to generate further understanding of the associated hydrothermal fluid.

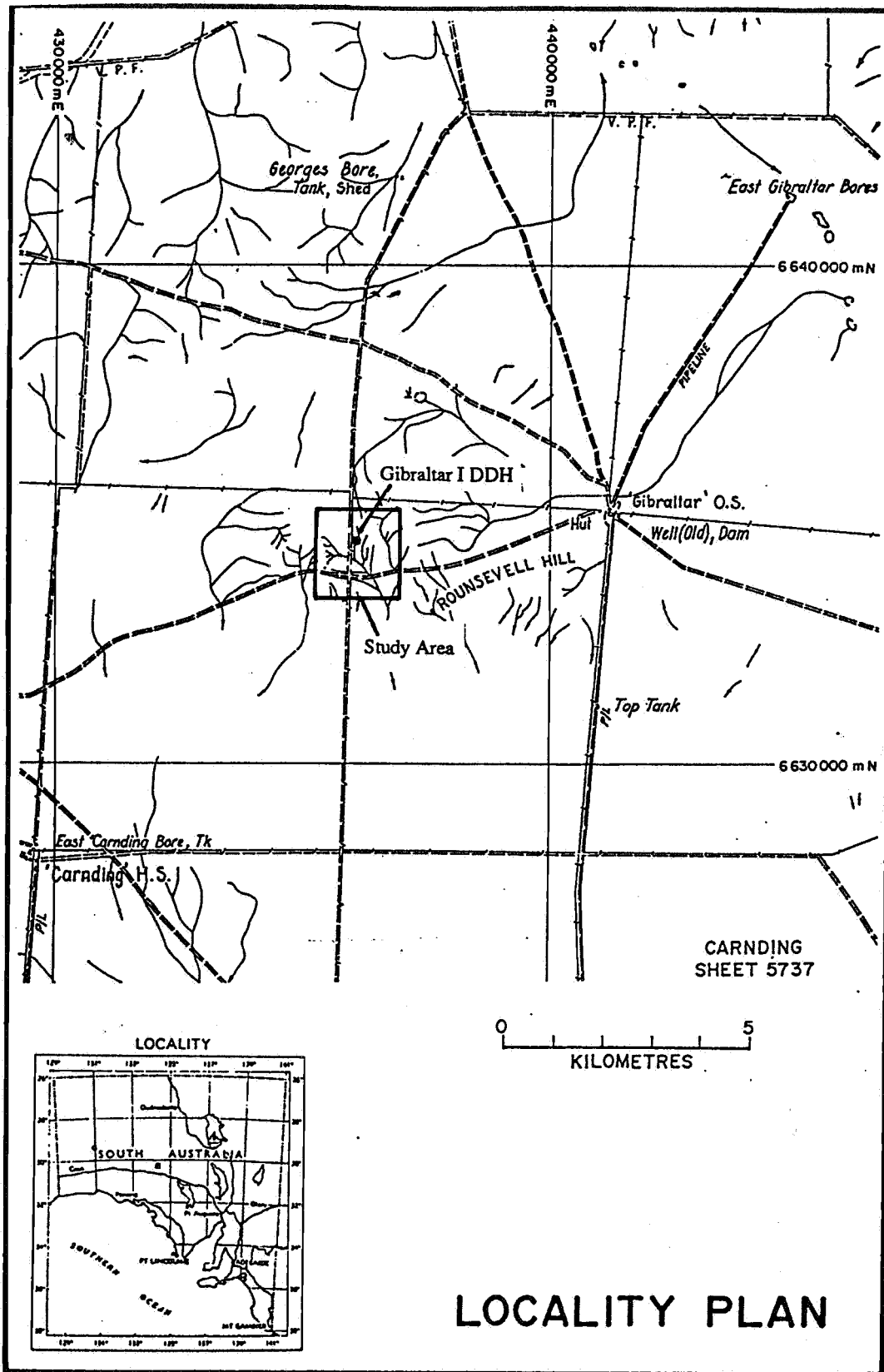


Figure 1.1 Location of the Gibraltar I drill site.

2. GEOLOGICAL SETTING

2.1 Regional Geology

The basement unit throughout the district is considered to be the Archaean Mulgathing Complex. The complex comprises gneisses and granitoids interlayered with quartzites, calc-silicates and marbles; rare metabasic extrusions and dykes are also present. This unit outcrops both 15 km north and south of the Gibraltar I drill site, possessing folds with north-westerly and north-easterly axial orientations.

Two phases of magmatism are recognised in this complex; the Early Proterozoic intrusions of the Kimban Orogeny, and the Middle Proterozoic Gawler Range Volcanics / Hiltaba Suite igneous complex. The Kimban Suite of intrusions were associated with orogenic development between 1820-1580 Ma, according to Rb-Sr age data (Webb et al., 1986). These intrusions now comprise I-type granites, granulites and gneisses. Locally, the suite is represented by a microcline-quartz-plagioclase granite outcropping 8 km north-west and 9 km north-east of the drill site.

Post-Kimban anorogenic activity is represented by the Middle Proterozoic Gawler Range Volcanics (GRV) and the comagmatic Hiltaba Suite. The GRV are locally divided into two general units; the Lower GRV and the Upper GRV. The lower GRV are characterised as scattered outcrops of basalt (Konkaby Basalt), dacite and rhyolite (Ealbara Rhyolite), which possess moderately steep dips. Steeply dipping exposures at Birthday Quarry suggest thicknesses in the order of 1500 m. Outcrop occurrences of the Konkaby Basalt are rare; one example is found at Konkaby Dam, 30 km east of the drill site. In the vicinity of the drill site, the Lower GRV outcrop is predominantly representative of the acidic end members. The Upper GRV are described as being thick, areally extensive, flat lying sheets of porphyritic dacite and rhyodacite. This unit dominates outcrop of the GRV as a whole within the Tarcoola district. Extrusion of the GRV has been dated (using U-Pb concordia) as having occurred over a short time interval around 1572 ± 2 Ma (Fanning et al., 1988).

10 km south of the drill site, a geophysically interpreted lineament strikes north-west, extending for up to 300 km in each direction. This feature is proposed to be a basement fault, and appears to mark the south-west boundary of the extruded GRV (Daly, 1985). A similar lineament is interpreted 10 km north-east of the drill site, although there the GRV extend beyond the interpreted feature.

Intruding the Gawler Range Volcanic pile is the comagmatic Hiltaba Suite Granite. This is commonly observed to be a pink, leucocratic, medium to coarse grained biotite-poor granite or adamellite, commonly porphyritic in places (Daly, 1986). Evidence for the intrusive nature of the relationship is found at a number of localities within the district, eg. at Jenner's Knob and near Birthday Quarry, 11 km south-east and 25 km north-east. of Gibraltar I respectively. An outcrop of Hiltaba Granite 2 km west-north-west of the drill site is visibly brecciated, with quartz-epidote veining associated with sphalerite. Intrusion of these granites has been U-Pb dated at 1514 ± 16 Ma (Cooper et al, 1985).

Numerous volcanic dykes intrude the GRV, and are correlated to the Wittabee volcanics (Daly, 1986). These are commonly of rhyolitic to dacitic composition, rarely andesitic and basaltic.

The sedimentary record in the district begins in the Late Jurassic, with the Algebuckina Sandstone. This is a kaolinitic, fluvial quartz arenite, possessing cobbles derived from the basement and volcanics. Near the Gibraltar I drill hole, this unit apparently occurs as large clasts cemented in calcrete and iron oxide. Post Jurassic lithologies are absent in the area, aside from supposedly Tertiary silcrete caps on some ridges. One such cap is present on a hill 2 km west of Gibraltar I. Pleistocene sediments, characteristically red-sandy clays, are the predominant soil cover in the area.

2.2 Local Lithological Descriptions

Mapping of the Ealbara Rhyolite within the vicinity of the Gibraltar I drill core has revealed the presence of a number of discrete volcanic units and zones of alteration. Outcrop and interpretative maps of the area are presented in the back cover of this thesis (Figs. 2A, 2B) along with an interpretative schematic section (Fig. 2C). Classification of the individual fresh volcanic units described below have been conducted using the observed mineral abundances of each, based on a scheme proposed by Streikeisen, 1975 (Fig. 2.1). All plot within either the alkali rhyolite or rhyolite fields. A summary of the characteristics of each unit is presented below, based on hand specimen and thin section descriptions found in Appendix 1.

2.2.1 Unaltered Volcanics

Porphyritic Welded Ash Flow Tuff

This unit is a porphyritic, jointed and welded rhyolitic ash flow tuff. It makes up at least 60% of the outcrop in the mapped area. Phenocrysts of quartz, orthoclase and plagioclase constitute 40% of the total rock. Quartz is commonly embayed (Plate 1) and feldspars demonstrate some degree of sericitisation, generally coupled with hematisation. Such alteration has been noted at other localities within the GRV (Giles (1980, 1988), Jagodzinski (1985), Robertson (1989), and was deuteric in nature, as distinct from hydrothermal. In situ fragmentation is also a common feature in quartz phenocrysts, caused by thermal cracking on eruption.

The groundmass is commonly black, purple or dark green in hand specimen, the colour being a function of iron content. Devitrified glass shards and lithic fragments are common, indicative of pyroclastic eruption. Weak compaction layering is commonly observed, the unit only displaying a minor degree of welding (Plate 2).

Lithic fragments are abundant, commonly possessing alkali feldspar and quartz phenocrysts within a groundmass of similar mineralogy (Plate 3). Occasionally, this groundmass displays a granophyric texture.

This unit appears to underlie the brown flow banded tuff unit (see below).

Strongly Welded Ash Flow Tuff

This unit appears distinct from the porphyritic welded tuff described above, due to a much higher iron oxide content in the groundmass. As a result, this rock has a distinct orange-red outcrop colour. Further, discontinuous flow bands are visible in hand specimen, the result of syn-welding flowage. Thus, the degree of welding within this unit is greater than that of the porphyritic welded tuff. Axiolitic devitrification is observed along the edges of these flow bands (plate 4).

Phenocrysts of quartz and feldspar are in equal abundance, together making up 25% of the total rock volume. Alteration of the phenocrysts is similar to that displayed in the porphyritic welded tuff, although hematisation of the feldspars is quite intense, making them indistinguishable with regard to individual feldspar types.

This unit appears to have formed contemporaneously with the porphyritic welded tuff, and thus appears to be overlain by the brown flow banded tuff discussed below.

Black Glassy Rhyolite

Three localised outcrops of this unit has been identified in the north-west corner of the map. A petrological description by Purvis (1991) suggests this unit to possibly be a welded breccia of collapsed pumice, superficially similar to the Yardea Dacite, a member of the Upper GRV. It is, however, richer in quartz phenocrysts which are strongly resorbed, with weak sericitisation noted in the feldspars. The groundmass of this unit is flattened and finely devitrified, demonstrating a high degree of compaction, as indicated by the draping of glass shards around the phenocrysts (Plate 5).

Due to the lack of outcrop, the stratigraphic position of this unit with respect to the other units in the area is uncertain.

Brown Flow Banded Ash Flow Tuff

Characteristically, this unit is a red-brown, flow banded rhyolite, showing features attributed to pyroclastic eruption similar to those units discussed above. Marked variations in

groundmass colour, amount of flow banding and phenocryst population, occur along and across strike of the flow band orientations. It appears that such colour variations (eg brick red, purple) are a function of the iron oxide content of the groundmass. The total phenocryst volume of this rock is rarely more than 15%, much less than the other tuffaceous units mentioned above, although the degree of alteration of these crystals is similar. Coarse perthitic textures within the alkali feldspars are commonplace. Within the drill core, quartz abundance is variable; although usually more abundant than the feldspars, it occasionally drops as low as 5%, suggesting that some layers within this unit are in fact rhyodacitic in composition.

Referring to the Figures 2A and 2B, it appears the flow banding orientation of this unit is contorted around contacts with the porphyritic welded and the strongly welded tuffs, suggesting flowage over these units to have occurred during deposition of the flow banded rhyolite. Thus, this unit is considered to be younger than those units. The flow banding throughout the area dips steeply (generally greater than 50° both east and west). Further, the Gibraltar I drill core did not sample any other lithologies, suggesting that this unit extends vertically downwards for at least 110 m. Daly (1986), has suggested the lower GRV to have been subject to folding, with the fold closures now absent, presumably due to erosion. This may explain the banding orientations and drill core findings, however qualification of this proposal in the mapped area would require information on younging directions.

Rhyolite Lava

Of special note are the heavily contorted, strongly flow banded rhyolitic rocks adjacent to "East Boundary Creek", a creek named by the author which is present on the eastern side of the mapped area (Plate 6). These have been interpreted as lavas, and appear to have exploited palaeotopographic lows during viscous flow, similar to the topography existing at the present. These lavas appear syndepositional with the brown flow banded tuff, yet appear tectonically unfolded, suggesting that the folding event may have occurred while these volcanics were still capable of flow. All of these lavas have been quartz-sericite altered and possibly represent local extrusive portals, through which subsequent hydrothermal fluids permeated.

Similar, small bodies of strongly layered rhyolite are hosted within the brown flow banded rhyolite outcrop; these have also been designated as lavas, although they may in fact represent localised areas of viscous flow that occurred during accretion of the hot volcanic pile.

Rhyolite Dyke

A rhyolite dyke, present in the south-west corner of the mapped area, is distinguished by its massive, brick red outcrop morphology, and large (up to 5 mm) quartz phenocrysts. It appears discordant to the tuffaceous units, however no distinct thermal alteration is observed on the contact with the tuffs, suggesting intrusion occurred while the volcanic pile was still hot.

2.2.2 Altered Volcanics

A brief introduction to the areas of altered volcanics is presented below. A detailed discussion of the alteration mineralogy associated with each alteration body may be found in chapter 5.

Vent Area

This patch of alteration has previously been described as a vent, possibly volcanic (Daly, pers. comm.). The alteration is located within the porphyritic welded tuff and centred on a patch of brecciated volcanics. Intense, knotted flow banding is observed to surround this breccia body, delineated by red limonitic stringers. Away from the central area, where alteration is intensely sericitic, silicic and rarely kaolinitic, the alteration is predominantly sericitic (distinct from deuteritic processes).

The author's own interpretation of the genesis of the vent, in particular the brecciated core, is that it may be the result of autobrecciation due to explosive eruption. The knotted flow banding may be the product of viscous rhyolitic flow at the rim of the autobrecciated area. Thus, the surrounding alteration haloes are probably the result of later hydrothermal activity within the breccia body, a consequence of the associated high permeability.

Altered Volcanics Zone 1

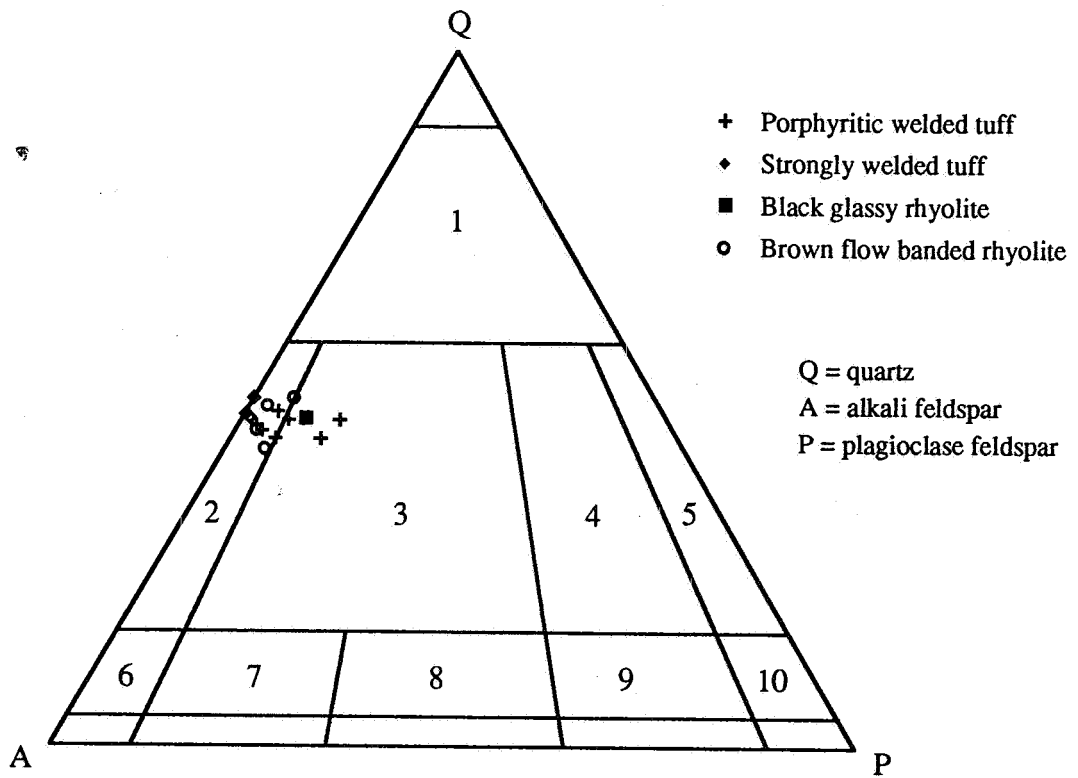
This peanut-shaped zone consists of white, silicified and sericitised rhyolite, with a minor clay component to the alteration. Lithic fragments are abundant, suggesting this to be an agglomeratic lens contained within the brown flow banded rhyolite.

Altered Volcanics Zone 2

This zone of alteration is located above the Gibraltar I drill hole within the brown flow banded rhyolite, and is a surface expression of the hydrothermal alteration and mineralisation found within the drill core.

Quartz-Sericite Rock

Spotted throughout the mapped area (Fig. 2A) but particularly in the south-west corner of outcrop, the brown flow banded rhyolite has been variably silicified and sericitised. Commonly, only feldspars have been mildly sericitised, however, rare obliteration of phenocrysts and most volcanic textures has been observed in hand specimen. The occurrence of this altered rock displays no observable pattern, and suggests that hydrothermal activity within the mapped area was pervasive, without any apparent structural control.



- | | | | |
|---|-----------------|----|-----------------|
| 1 | - | 6 | alkali trachyte |
| 2 | alkali rhyolite | 7 | trachyte |
| 3 | rhyolite | 8 | latite |
| 4 | dacite | 9 | andesite |
| 5 | - | 10 | basalt |

Figure 2.1 Modal volcanic rock discrimination diagram after Streikeisen (1975).

3. GEOCHEMISTRY OF THE VOLCANICS

3.1 Introduction

Geochemical analysis of 30 fresh and altered outcrop samples were performed to investigate the major and trace element geochemistry of the volcanics. A further five outcrop and 26 drill core samples, provided by SADME, have also been used for this purpose. There were two main aims of this geochemical study; to classify the volcanics, and to consider the implications of their geochemistry on possible tectonic settings associated with their generation and emplacement.

3.2 Classification of the Volcanics

Two schemes of chemical classification have been applied here to categorise the volcanics; the CIPW normative mineral method of Streckisen and LeMaitre (1979), and the immobile element method of Winchester and Floyd (1977).

Figure 3.1, following Streikeisen and LeMaitre (1979), differentiates volcanic rocks based on normative mineralogies. Geochemical data from the freshest outcrop samples were used for each lithology, with the CIPW normative calculations made using a BASIC computer program (Appendix 4). All resulting data points plot within the alkali feldspar rhyolite field. On comparison with Figure 2.1 (Chapter 2), these results are in general agreement with the modal classification.

Figures 3.2 and 3.3 (after Winchester and Floyd, 1977) use abundances of the immobile elements Zr, Ti, Nb and Y, along with SiO₂, for discrimination. Due to the deuteric and hydrothermal alteration prevalent within the observed lithologies, such plots are useful as they minimise discrepancies generated by mobilisation of other elements. Thus, geochemical data from relatively fresh outcrop volcanics, along with all variably altered drill core and vent area samples, were applied to this classification scheme.

Of the fresh outcrop volcanics, all but one plot within the rhyolite field in Figures 3.2 and 3.3; the one point in question representing a sample of brown flow banded tuff. However, Blissett (1975) observed that it is common in the Gawler Range Volcanics for mineralogically defined rhyolites to display uncharacteristically low total SiO₂. Almost all drill core samples plot

within the rhyolite, rhyodacite and trachyte fields, in agreement with the findings in Chapter 2. Vent area samples reside within the rhyolite field (with the exception of one point residing in the comendite / panttellerite field), but are displaced to higher silica contents due to silicification.

3.3 Tectonic Setting

3.3.1 Previous Work

Past geochemical studies on the Gawler Range Volcanics have been performed by a number of authors; Giles (1980, 1988), Jagodzinski (1985) and Robertson (1989). From these studies, a consistent conclusion has been reached: that of bimodal volcanism associated with basaltic magmatism. More specifically, Giles (1980, 1988) proposed that the felsic members of the Gawler Range Volcanics developed in response to high temperature, dry partial melting of granulitic, sialic material at depth in the crust. The heat required could have been supplied during an episode of crustal rifting and / or underplating by basic magmas associated with mantle diapirism. The resulting volcanic activity was bimodal in nature, with the basic and felsic volcanics being derived from physically separate, but temporally related, sources.

3.3.2 Major and Trace Element Variation: Implications for Fractionation History

A spidergram has been constructed to establish the normalised elemental variation of the rhyolite for each lithology (Figure 3.4). This has been compared to a minimally fractionated body, namely an 18 sample average of the Konkaby basalt (Flint, in press). This locally outcrops 12 km east of the Gibraltar I drill hole.

The resulting spidergram patterns for the rhyolites are indicative of significant fractionation in comparison to the basalt. Barium, strontium, phosphorus and titanium are all clearly depleted, with rubidium, thorium and potassium all enriched. Removal of plagioclase from the melt during earlier fractionation would account for the depletion of barium and strontium. Phosphorus and titanium were probably lost during crystallisation of apatite and ilmenite. Potassium is present in alkali feldspars and is therefore enriched in the rhyolites. Rubidium is

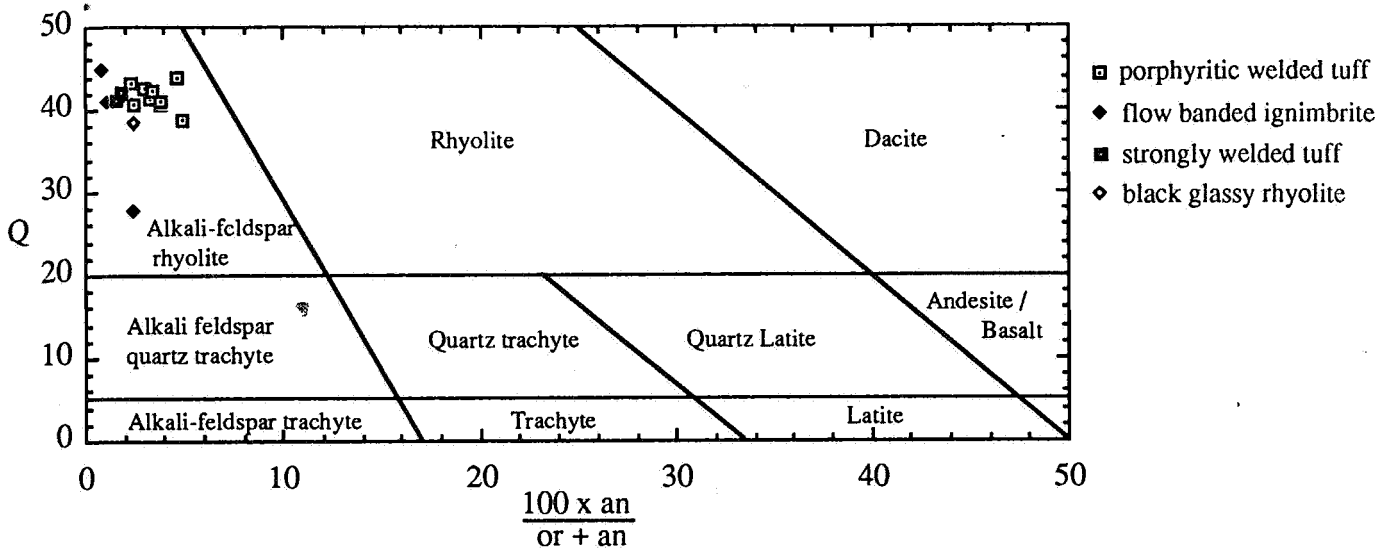


Figure 3.1 Normative classification of igneous rocks after Streckeis and LeMaitre (1979).

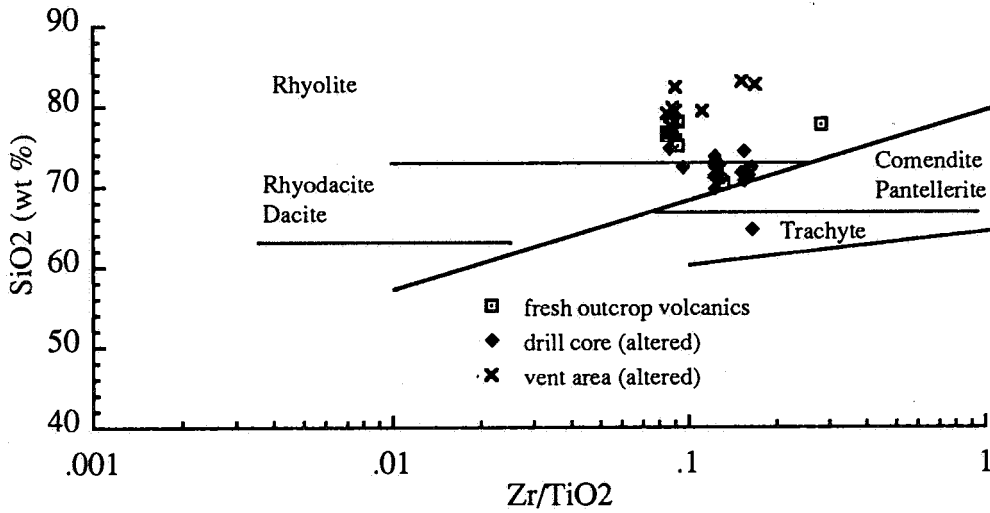


Figure 3.2 Volcanic discrimination plot of SiO₂ vs Zr/TiO₂ after Winchester and Floyd, 1977.

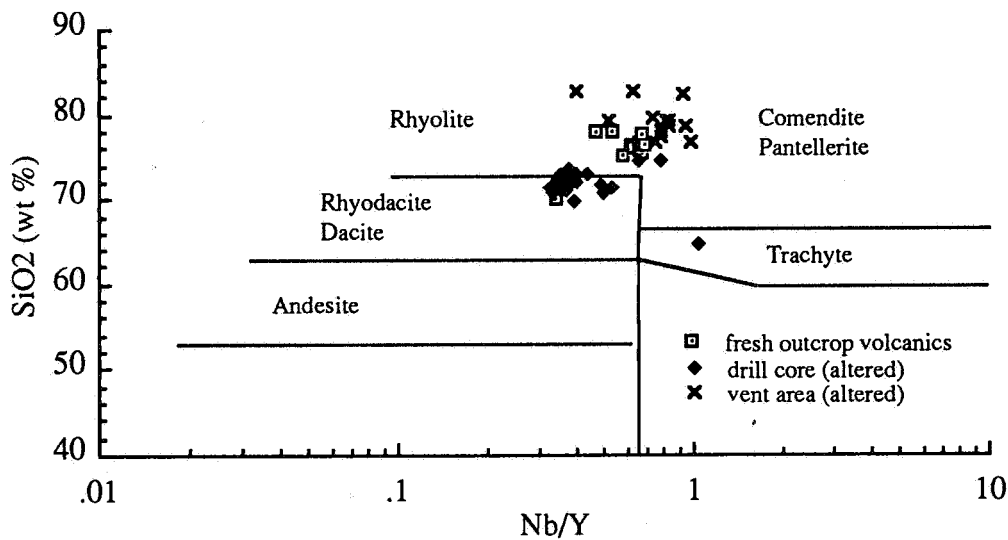


Figure 3.3 Volcanic discrimination plot of SiO₂ vs Nb/Y after Winchester and Floyd, 1977.

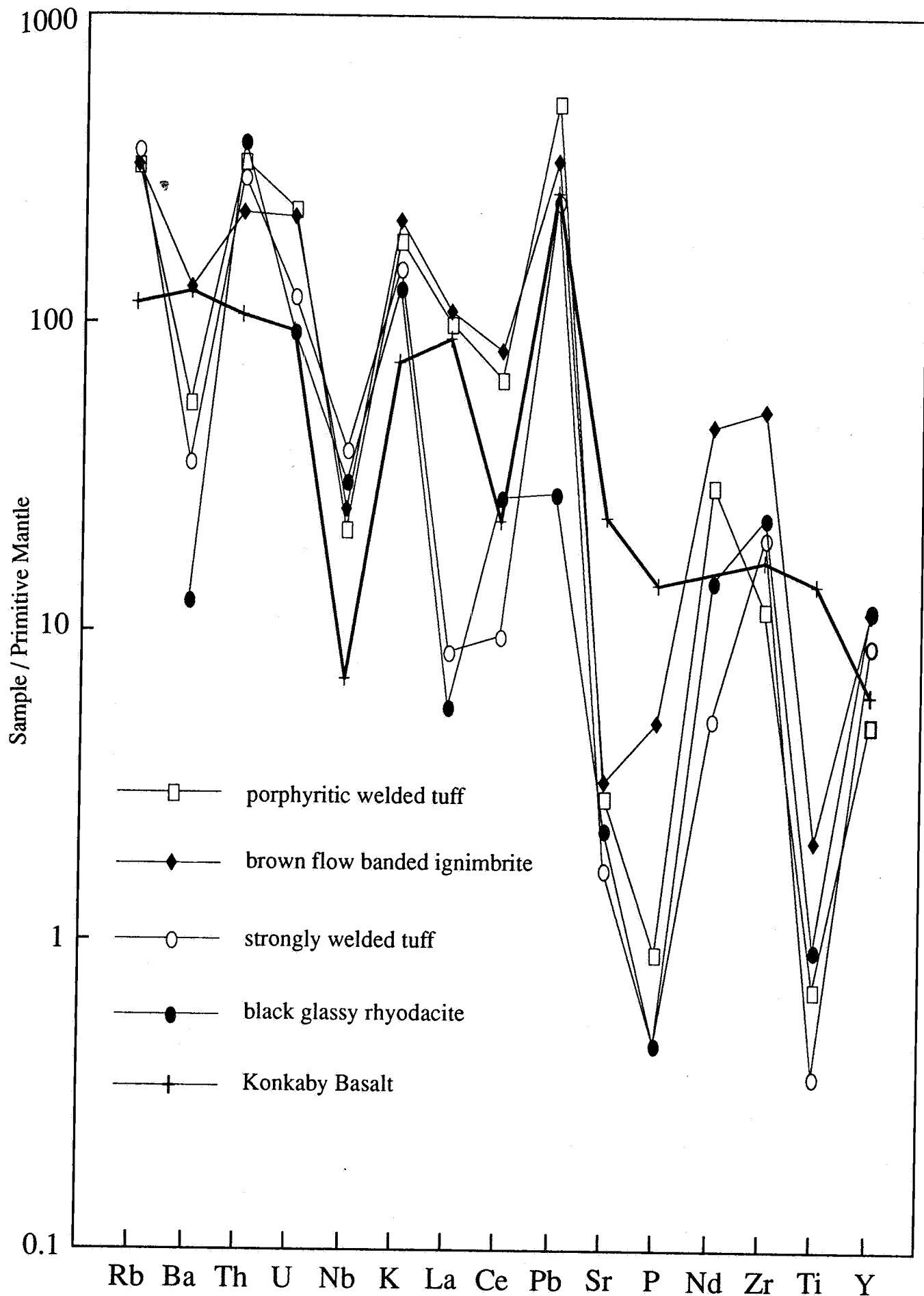


Figure 3.4 Spidergram of selected major and trace element data, normalised to primitive mantle (Sun and McDonough, 1989).

geochemically similar to potassium, occupying sites within alkali feldspar, hence its enrichment. Thorium is incompatible with the early formed mafic minerals, and is thus enriched in the rhyolites relative to the basalt.

The degree of fractionation of the rhyolites has been investigated using a rubidium-barium-strontium ternary plot proposed by Bouseily and Sokkary (1975). Figure 3.5 demonstrates that most of the rhyolites plot within the normal granite field, indicating that the degree of fractionation, although significant, is not anomalously high.

3.3.3 Tectonic Implications of the Geochemistry

Of interest is the high Ga/Al ratio within the samples. This has been interpreted by Collins et al. (1982) to be diagnostic of A-type (anorogenic) granites, on the basis of studies of granites from the Lachlan Fold Belt, Victoria. Plots of selected major and trace elements versus Ga/Al have been used by Whalen et al. (1987) to differentiate A-type granites from I-type and S-type and M-type granites, using geochemical data on granitic suites throughout the world. Applying the rhyolite data of the present study to such diagrams (Figure 3.6), the data either plot within the A-type granite field, or inside the I-S-M-type granite field. At higher Ga/Al ratios the data points reside in the A-type field. Note that it is possible for highly fractionated I- and S-type granites to bear an artificial A-type Ga/Al signature. However, the degree of fractionation obtained from the Rb-Ba-Sr ternary diagram indicates little anomalous fractionation occurred within the source associated with the rhyolites, suggesting the A-type classification to be credible.

Pearce et al. (1984) have subdivided granites according to their intrusive settings, based on trace element and silica abundances. These divisions include ocean ridge granites (ORG), volcanic arc granites (VAG), within plate granites (WPG) and collision granites (Syn-COLG). Each exhibits distinctive trace element characteristics. Data from fresh outcrop, altered drill core and vent area samples have been plotted, as several plots involve the use of immobile elements. In all, five diagrams have been used in this study (Fig. 3.7). The data points demonstrate consistent tendencies to plot either in the within plate granite field or the volcanic arc and collisional granite

fields. Pearce et al. (1984) noted that unusually high degrees of crustal contamination may displace within plate granite chemistries into volcanic arc granite or a collisional granite chemistries.

The above geochemical findings are consistent with the model proposed by Giles (1988), based on two key criteria. Firstly, magmatism associated with the local rhyolites reveals an A-type geochemical signature. A-type granites are commonly associated with rifting environments (Collins et al. 1982) and Giles proposed such an environment to have been active during the extrusion of the GRV. Secondly, the within plate granite signature is also supportive of intracontinental rifting, as Pearce et al. have described such granites to display affinities with attenuated crust. However, the interpretation of why many of the data points in Figure 3.7 plot within the volcanic arc and collisional granite fields is more complex. In light of Giles' model, it may be possible to explain this phenomenon by anomalous degrees of crustal contamination. If sialic material was present at depth in the crust, such material could have displaced the geochemical signature of any within plate granite into the volcanic arc / collisional granite field (as this material would most likely bear a VAG or syn-COLG signature). If this was indeed the case, then this facet of the geochemistry is fully consistent with Giles' proposition.

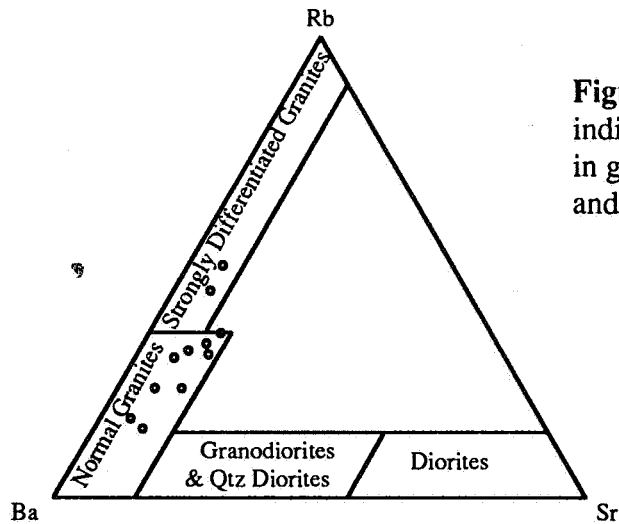
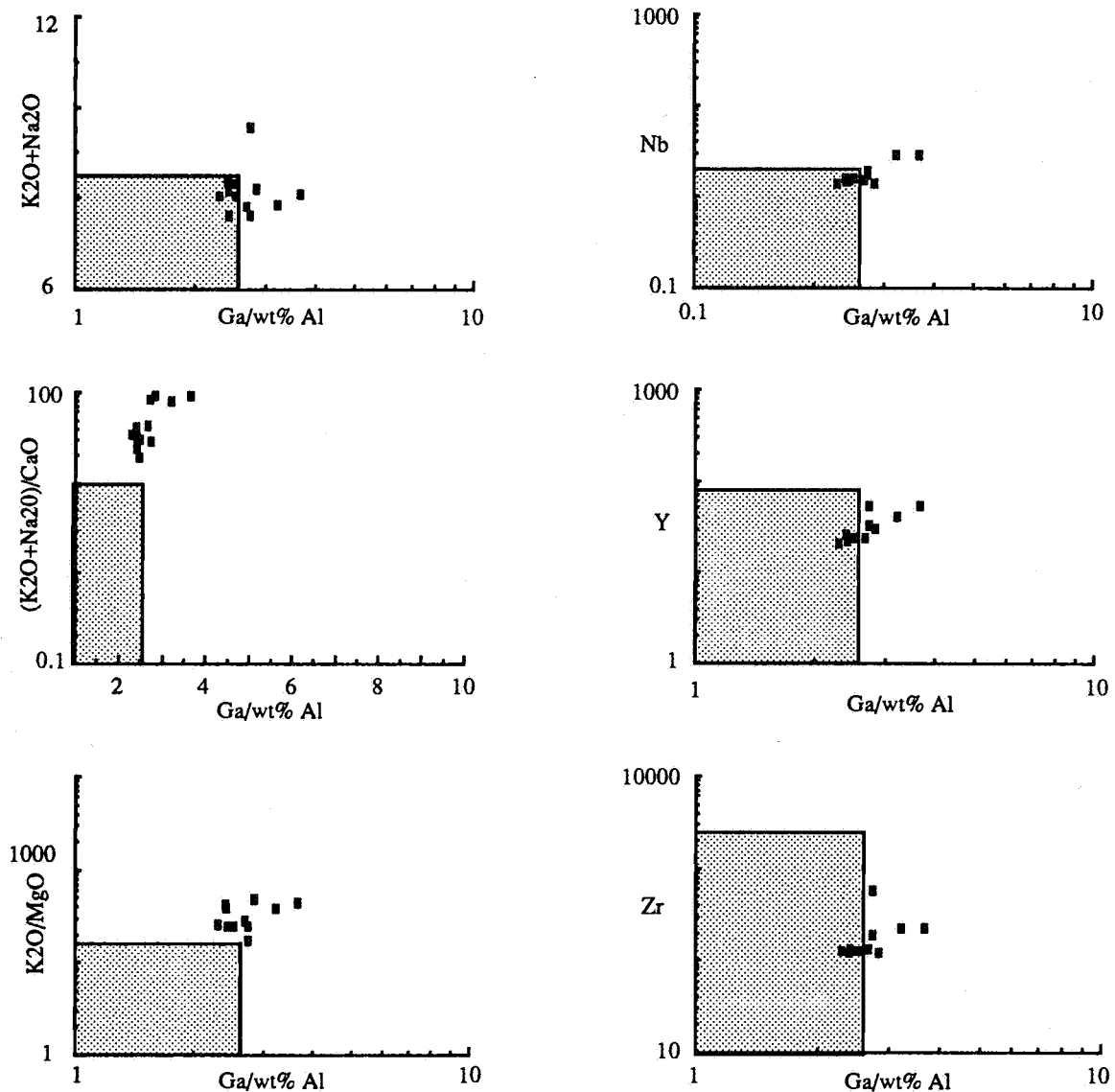


Figure 3.5 Rb-Ba-Sr ternary plot indicating the degree of fractionation in granitic rocks, after El Bouseily and El Sokyry (1975).



Figures 3.6 Diagrams for the discrimination of A-type from I-, S- and M-type granites, after Whalen et al. (1987). The stiped region indicates the proposed field for the latter three granite types, while the area outside this is considered to be the A-type granite field.

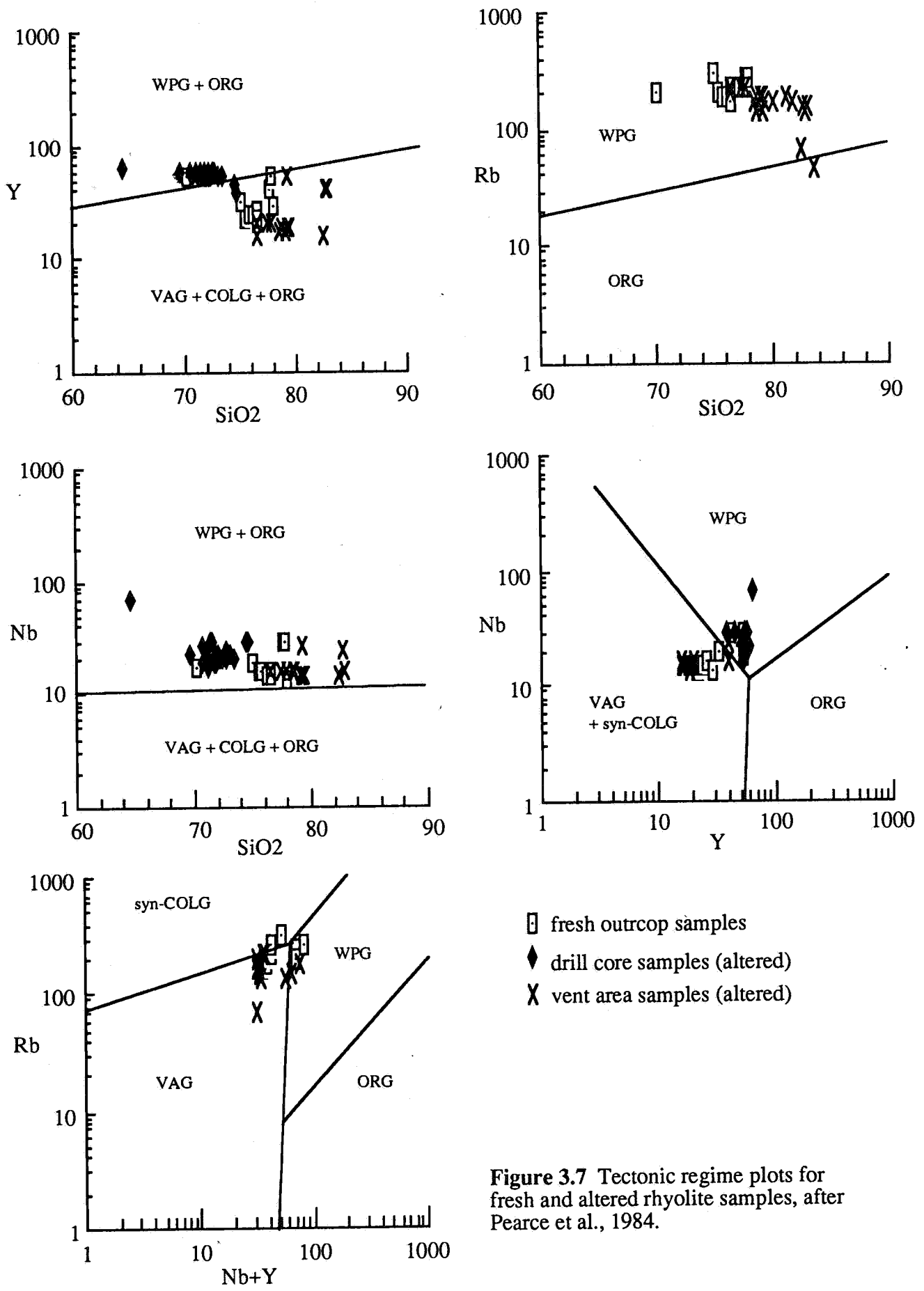


Figure 3.7 Tectonic regime plots for fresh and altered rhyolite samples, after Pearce et al., 1984.

4. LOCAL STRUCTURAL GEOLOGY

A number of important structural features are evident within the mapped area (Figs. 2A, 2B and 2C). Jointing within the volcanics, along with the presence of breccias, quartz veins and an intensely jointed zone will be discussed here in an attempt to resolve any stress fields previously active, and to place some control on the timing of the mineralising events.

4.1 Jointing

Subvertical to vertical jointing is apparent in all of the lithologies present, presumably associated with contraction due to cooling of the volcanic pile. However, jointing within the porphyritic welded tuff demonstrates a distinctive joint pattern (Plate 9 and Figure 4.1) of a dominant joint system striking around 315° , crosscut by two joint sets at 45° to the first. This joint pattern is consistent over most of this unit's outcrop. Unlike the other lithologies in the area, banding and layering within the porphyritic welded tuff is generally weak, thus joint systems are less likely to open along such a fabric. Instead, this joint pattern is interpreted as the result of brittle extensional deformation in a regional stress field. Within the other units, joint sets have been noted trending near 315° , however such sets are usually secondary to a number of other joint sets, developed in response to contractional cooling.

A rose diagram of joint data taken from a number of lithologies displays a clear peak near $135^\circ / 315^\circ$ (Figure 4.2). Referring back to Figure 4.1, extensional strain occurs orthogonal to the dominant joint system. Evidence for regional extension at this orientation is found by way of the subsurface Gairdner Dyke Swarm, found in drill holes several hundred kilometres north of Gibraltar I. Aeromagnetic data indicate a north-westerly trend for these basic dykes, which are presumed to be related to failed intracontinental rifting during the Late Proterozoic. Recent samarium-neodymium dating has revealed emplacement ages of 802 ± 35 Ma and 867 ± 40 Ma. (Jian-Xin Zhao, pers. comm., 1992). Thus, it is proposed that the majority of north-westerly trending joint systems in the Gibraltar I area are the result of extensional stresses imposed during this rifting event.

Such an interpretation places controls on the likely age of the mineralisation within the area. All mineralised zones are characterised by this jointing but show no sign of fluid flow through the joints. It is unlikely that any hydrothermal system would not have taken advantage of such joint systems, and hence, it is inferred that mineralisation occurred prior to the rift event.

4.2 Chloritic Microbreccia

The outcrop evidence for this breccia body is limited (Fig. 2A). A line of trees trends north-west across the map area, rooted in a thin corridor of alluvium. The outcrop within this area consists of green, microbrecciated rock, hosting abundant chlorite (thin section A972-C141) or hydrothermal biotite (thin section A972-C143). This breccia trends parallel to the extensional joint system mentioned above, suggesting it to be the result of the same regional event. However, this does not explain why only one such corridor of brecciation formed. Hence, the timing of development of the chloritic microbreccia is unconstrained.

4.3 Joint Zone

Located north of the vent area, this corridor possesses joints generally striking north-west, parallel to the extensional jointing mentioned above. Based on remote sensing imagery provided by SADME, this zone is interpreted to have a north-westerly trend either side of the vent area. However, the joint zone itself, where found in outcrop, strikes in a more westerly direction. Although most likely attributable to the same stress field that formed the joint sets discussed above, the cause of perturbation in the north-westerly orientation proximal to the vent area is unresolved in the present study.

4.4 Quartz-Hematite Breccia

This breccia is hosted within the brown flow banded ash flow tuff. It consists of 0.1 mm to 1 cm wide crosscutting quartz veins, commonly possessing abundant specular to earthy hematite. Its presence in outcrop is patchy, but does appear to follow a trend indicated in Figure 2B. The chloritic microbreccia appears truncated by this body, thus a fault has been inferred along the path of the quartz-hematite breccia (Fig. 2C).

Two quartz-vein sets are evident in hand specimen (Plate 7). Thin section petrology performed by Purvis (1991) on three samples provided by SADME revealed two important points with respect to this quartz veining in this breccia body:

(1) The earlier quartz vein set (vein quartz I) consists of coarse to prismatic quartz crystals up to 7 mm long, occasionally showing evidence of strain in the form of microfracture lamellae. The later quartz vein set (vein quartz II) is generally fine-grained and granular, demonstrating no deformational lamellae.

(2) Quartz phenocrysts within the host rock also show evidence of deformation.

Thus, there is evidence for both extensional and compressional deformation within the breccia. At least three deformational events are recognisable:

(1) Extensional deformation associated with brecciation and deposition of vein quartz I.

(2) Compressional deformation associated with the formation of strain lamellae within both vein quartz I and quartz phenocrysts of the host rock.

(3) Extensional deformation associated with the brecciation and deposition of vein quartz II.

4.5 Barren Quartz Veins

Discontinuous quartz veins are spotted throughout the mapped area and appear parallel to the quartz-hematite breccia (Fig. 2A). These veins commonly expand into breccias (Plate 8), suggesting them to represent a barren equivalent of the quartz-hematite breccia, or at least to have developed during the same (as yet unresolved) deformational event associated with quartz-hematite breccia formation.

Plate 1 Heavily embayed quartz phenocryst within the porphyritic welded ash flow tuff. The material infilling the groundmass is a cryptocrystalline aggregate of quartz and sericite (thin section A972-28M, transmitted cross-polarised light).

Plate 2 Compaction layering within the the porphyritic welded ash flow tuff. The mild draping around the quartz phenocryst is indicative of syn-depositional compaction and welding (thin section A972-28M, transmitted plane light).

Plate 3 Quartz phytic lithic fragment within the porphyritic wlded tuff. The microcrystalline intergrowths of quartz and feldsapr associated with the quartz phenocryst define the edges of this fragment (thin section A972-28M, transmitted, cross-polarised light).

Plate 4 Axiolitic devitrification at the edges of a flow layer within the strongly welded ash flow tuff (arrowed). This is a common devitrification texture within all the units studied (thin section A972-C119, transmitted cross-polarised light).

Plate 5 Compaction layering within the black glassy rhyolite. The distinct draping of elongated quartz and feldspar masses over the quartz phenocryst is indicative of a heavier degree of compaction and welding than is seen in plate 2 (thin section RS 1089, transmitted plane light).

Plate 6 Contorted flow banding observed at an outcop of the rhyolite lava. Severe contortion is evident directly adjacent to and above the hammer.

Plate 7 Quartz veining in the quartz-hematite breccia. The schematic diagram in the left-hand corner of the photo differentiates the two separate veining events 1 and 2. The former vein set is comprised of two orthogonal vein populations.

Plate 8 Typical brecciation of the host rock associated within barren quartz veins. Alteration of the host rock is sericitic in nature, as is indicated by a whitening of feldspar phenocrysts.

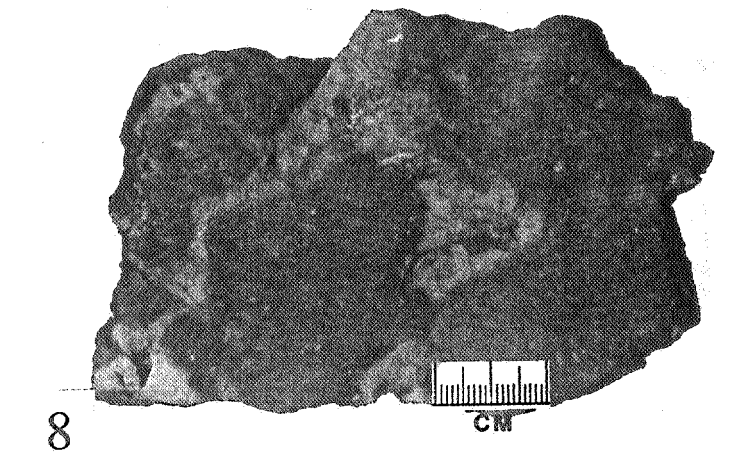
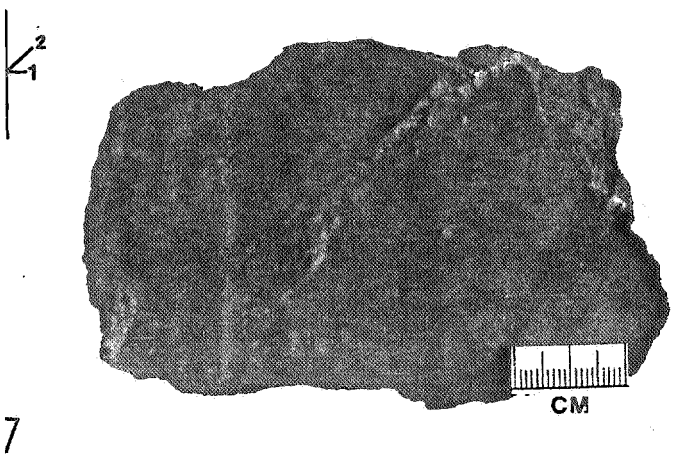
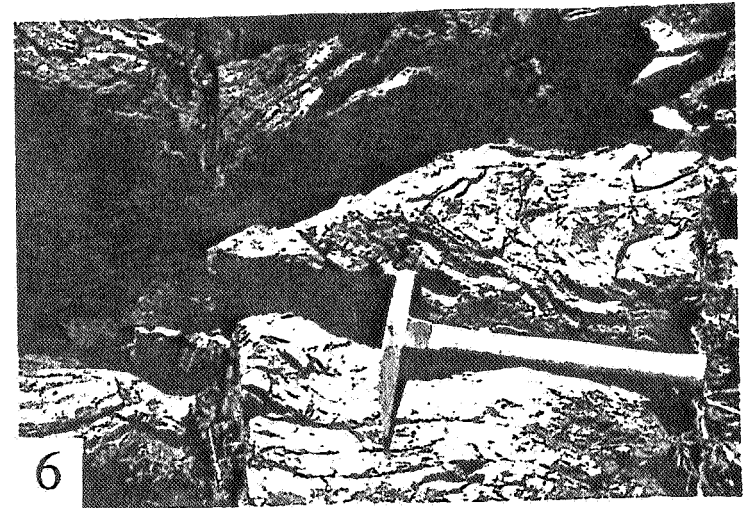
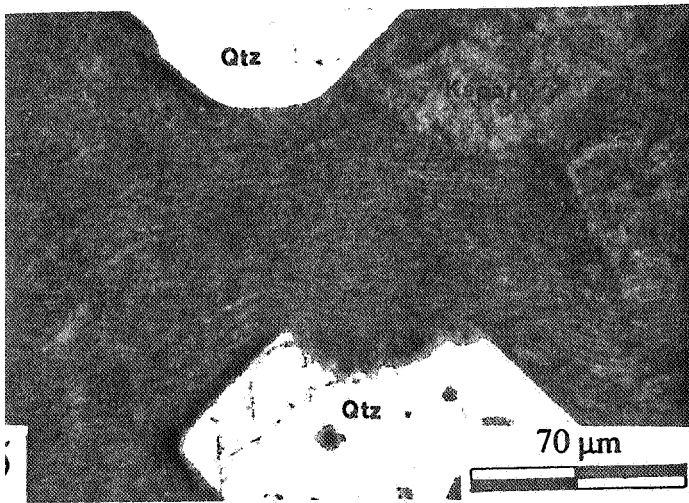
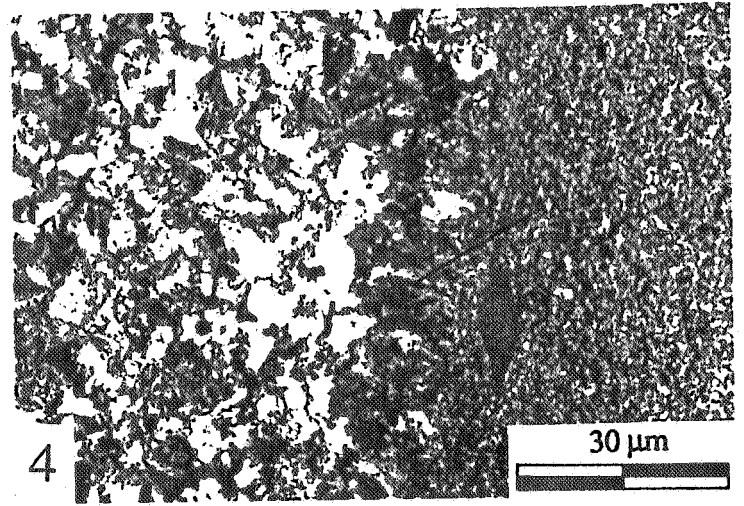
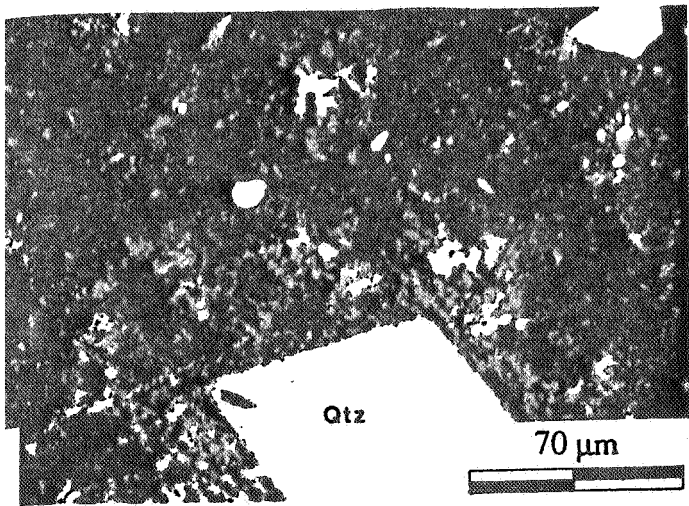
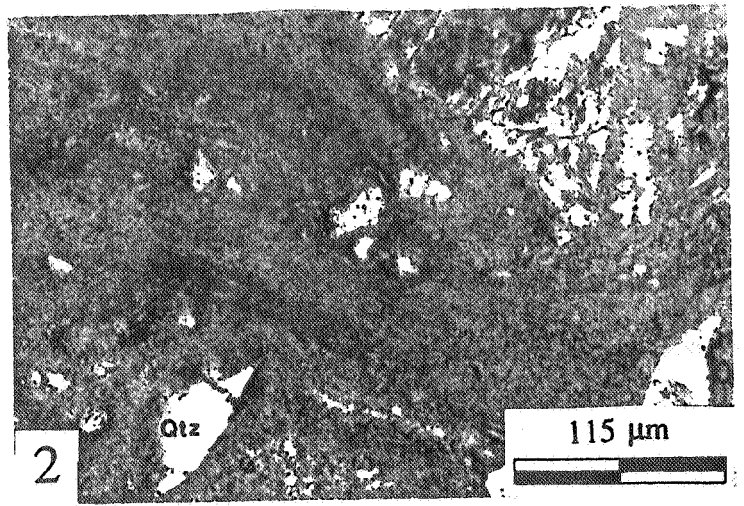
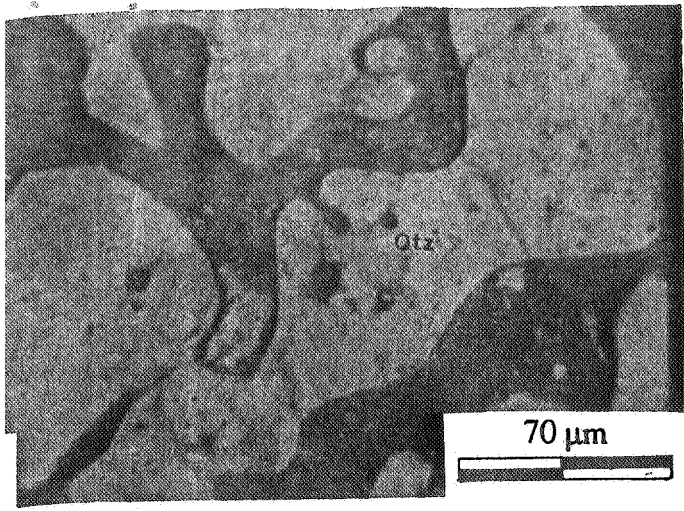


Plate 9 Jointing within the porphyritic welded ash flow tuff. The hammer is orientated at 320°, parallel to a dominant joint set; two sets may be distinguished crosscutting this at approx. 45°.

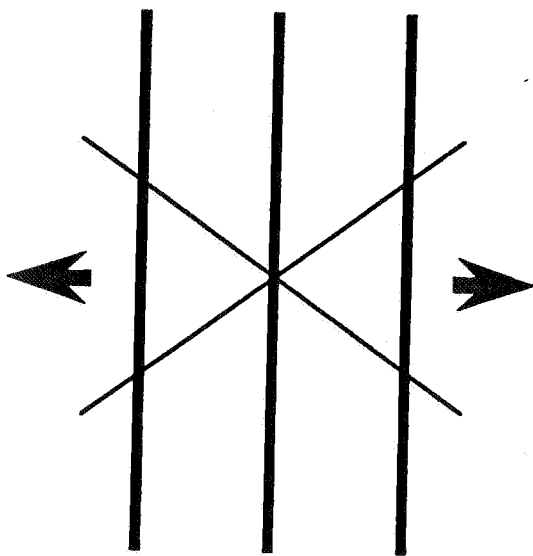


Figure 4.1 Schematic representation of observed jointing within the porphyritic welded tuff (Plate 9). Extension is parallel to the arrows.

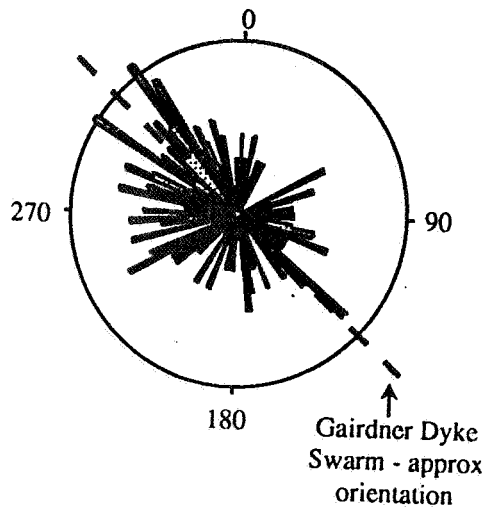


Figure 4.2 Rose diagram of joint data from mapped area.

5. HYDROTHERMAL ALTERATION AND MINERALISATION

Within this chapter, the characteristics of mineralisation associated with quartz-hematite breccia, “vent” area and the Gibraltar I drill core will be discussed separately. Possible relations between these will be discussed in Chapter 7. Note that the different *zones* of alteration within the volcanics are depicted in Figures 2A and 2B, whereas alteration *haloes* surrounding the vent area are presented in Figure 5.1, below.

5.1 The Vent Area

5.1.1 Mineralisation

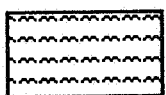
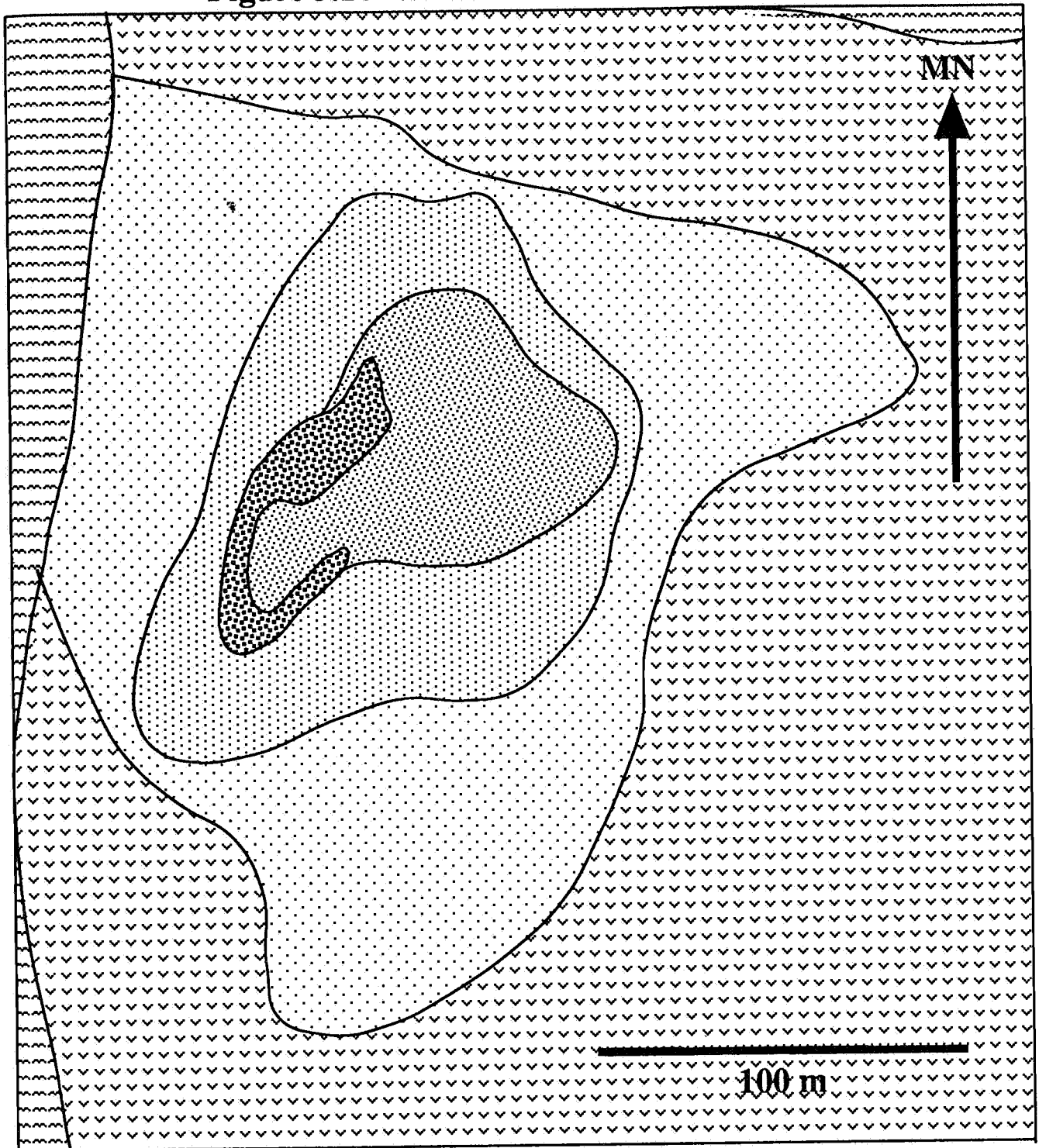
The alteration mineralisation in the vent area consists almost completely of sericitisation and silicification, with kaolinite rarely observed. Three, roughly concentric alteration haloes have been delineated, based on the presence and intensity of the observed alteration mineral species. These are centred on the autobreccia body shown in Figure 5.1

Halo 1 (the outermost halo) is characterised by light sericitisation of the feldspar phenocrysts, with groundmass feldspar also demonstrating sericitisation. Alteration intensity increases from halo 1 to halo 2, where no feldspar remains in the groundmass, and all feldspar microlites and phenocrysts are completely sericitised. Phenocrystic sericite commonly coarsens to muscovite. Some silicification of the groundmass is noted, with the increased quartz content a result of sericite consumption. Halo 3 exhibits the most intense level of alteration, with silicification the dominant alteration process. Little sericite remains in the groundmass, and quartz replacement of feldspar phenocrysts and sericite is noted.

Kaolinite as a dominant alteration mineral species occurs in rare patches of up to 1m diameter within alteration halo 3. Microprobe analysis reveals it is also commonly present in trace amounts, associated with sericite within these haloes.

Sulphide mineralisation is scarce throughout the vent area. The only sulphide mineral observed is pyrite, present as very fine grained euhedra within quartz phenocryst embayments. Presumably, the host quartz has protected any such pyrite from oxidation during

Figure 5.1 Alteration Halos of the Vent Area



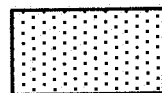
Alluvium



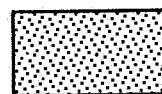
Fresh Volcanics



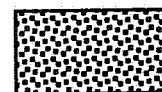
Alteration Halo 1



Alteration Halo 2



Alteration Halo 3



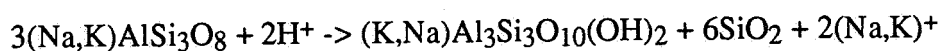
Autobreccia

weathering. The origin of this pyrite is uncertain; it may have been deposited within the quartz embayments during hydrothermal activity, or it may have been initially incorporated into the phenocrysts during their formation in the subvolcanic magma chamber.

Within halo 3, goethite is present as veins (up to 0.5 mm wide) and disseminations (up to 1 mm diameter), clearly pseudomorphing pyrite. These veins characteristically follow relic flow bands, suggesting the hydrothermal fluid utilised this textural weakness for fluid flow. Goethite is also commonly associated with patches of sericite at sites of feldspar phenocryst replacement, however no textural evidence exists to suggest this goethite has replaced pyrite.

5.1.2 Alteration Geochemistry

Geochemical analyses of 20 outcrop samples obtained from the vent area have been used to compare the bulk chemistry between the proposed alteration haloes and the surrounding host rock. The two dominant types of alteration, sericitisation and silicification, are the most likely controls of bulk chemical variation from halo to halo and may be described by the following reaction:



(1)

alkali feldspar

sericite

quartz

(modified after Henley, 1984)

Various elements investigated have been plotted against Al_2O_3 wt%, assumed to be an immobile element, to observe any changes in bulk chemistry (Fig. 5.2). Silica displays a clear trend of enrichment from halo 1 to halo 3, no doubt an increase in the degree of silicification. Sodium demonstrates a simple depletion trend, with most sodium removed from samples within the alteration haloes. This removal may be explained by the fact that sericitisation of alkali feldspars will release more sodium from the system per mole of altered feldspar than potassium, as sericite possesses a lower sodium content than that of the alkali feldspar.

Potassium abundance within halo 1 is similar to that of the unaltered samples; only in haloes 2 and 3 do depletions occur. Such depletions are due to the dilution effect of high SiO₂ abundance, along with the loss of this element during sericitisation and silicification.

Calcium exhibits a general trend of decreasing abundance from unaltered host to halo 3 areas. Calcium is most likely to reside in the plagioclase feldspars, which is present only as an accessory mineral in the volcanics. Thus, the loss may be attributed to the release of calcium ions from plagioclase into the fluid system during sericitisation.

Magnesium demonstrates only a minor decrease in concentration from the unaltered host tuffs to Halo 3. No significant magnesium bearing mineral phase has been identified in petrological studies, suggesting that this decrease is most probably due to dilution as distinct from mineral alteration.

5.2 Altered Volcanics - Zone 1

Mineralogy

The fragment rich lithology associated with this zone of alteration displays silicification and sericitisation in both the groundmass and the fragments themselves. Minor amounts of clay are also present. Disseminated limonite boxworks after pyrite are pervasive throughout much of the central part of this altered outcrop (Figs. 2A and 2B). Localisation of alteration within this body is most likely due to high permeability induced by the fragment rich lithology, with fluids accessing weaknesses along the edges of the fragments.

Geochemistry

One geochemical analysis of this zone, for a sample taken from an area of low alteration intensity, demonstrates a 2% increase in silica content (78.3 wt%) when compared to the surrounding rhyolite, along with a heavily depleted sodium concentration (now <0.1 wt%). Such a depletion is similar to that observed in the vent area, and indicates that, even with minimal alteration, sodium is an extremely mobile element. No anomalous metal contents were found.

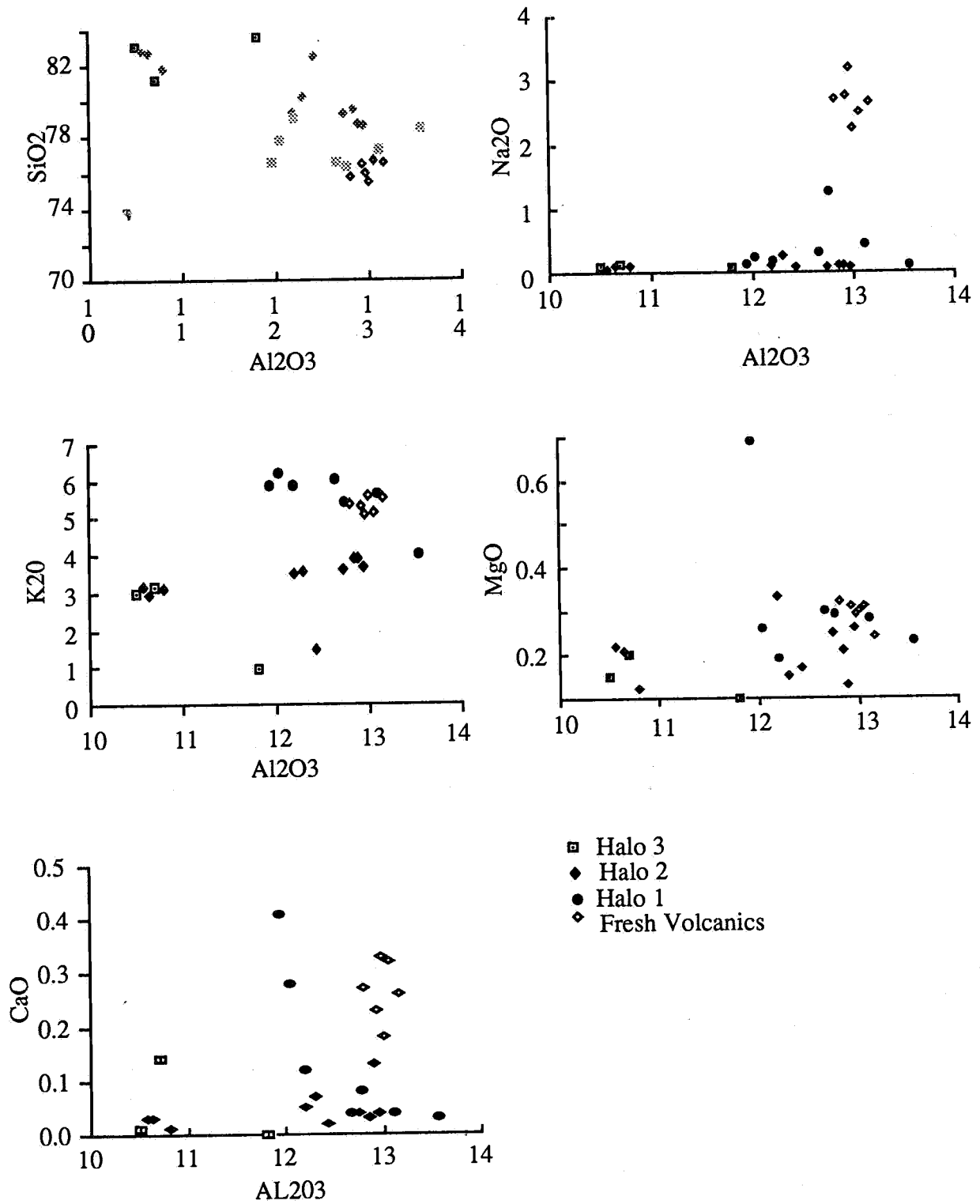


Figure 5.2 Variations of major element abundances within the vent area.

5.3 Altered Volcanics - Zone 2

Mineralogy

Alteration mineral species are more varied in this alteration zone than in those discussed above. Sericitisation and silicification are still dominant, however chlorite and some clays are also present. No distinct patterns or haloes of this alteration can be distinguished, although intensities of sericitisation and silicification are generally congruent. Most of the more intense alteration appears to be centred around lenses of the tuffs rich in fragments. As with altered volcanics - Zone 1, this association may be explained due to the higher permeability in these fragment rich bodies compared to the surrounding volcanics, and thus hydrothermal fluids would preferentially enter (and alter) these areas. Alteration in this zone is much less intense than in the vent area.

Mineralisation bears a marked similarity to the vent area in that pyrite, the only sulphide observed, resides within quartz phenocryst embayments. The boxwork rich areas within Zone 2 (Figs. 2A, 2B) are associated with the most intense patches of silicification and sericitisation.

Alteration Geochemistry

Five altered samples, taken from various locations within Zone 2 (see appendix 2) show fluctuations in major element abundances, with silica up to 74.9 wt% and sodium depleted to .13% (from an ambient average of 1.64 %) for one sample. This is indicative of the intensity of alteration in this zone; the alteration is probably less intense than that observed in the vent area.

5.4 The Gibraltar I Drill Core

5.4.1 Introduction

The Gibraltar I drill hole, collared at the eastern edge of the Zone 2 altered volcanics, dips beneath this altered outcrop at 65°, sampling a hydrothermally altered and mineralised sequence for all of its 110 m length. Alteration at depth in the core differs from that observed at the

surface, as little host rock modification has occurred. Feldspar phenocrysts are commonly still recognisable, as complete alteration of such crystals is rare.

Unlike the Zone 2 altered volcanics (presumably a surface reflection of hydrothermal mineralisation encountered in the drill core) where most of the sulphides have been weathered out of the host rock, the mineralisation at depth is present in pristine form. Thus, a more detailed discussion of this mineralisation may be made here, by way of the development of a paragenetic sequence. Further, 26 geochemical analyses of the core have been made available by SADME for investigations of bulk chemical variations down core.

5.4.2 Mineralogy and Paragenesis

Extensive petrological work by Purvis (1991) on the Gibraltar I drill core has been used here to develop an understanding of the paragenetic history of the mineralisation. The majority of the sulphide mineralisation is only present at depths between 30 m and 80 m. However, alteration and gangue mineralisation occurs throughout the length of the core. Most of the alteration and sulphide mineralisation is associated with, or is proximal to, zones of microbrecciation. Most of the breccia zones rarely exceed a few centimetres width, and are infilled with sericite, quartz, and pyrite (Plate 10).

The paragenesis of the ore and gangue mineralogy within the Gibraltar I drill core may be broken down into two generalised stages of mineral precipitation and alteration. (Fig. 5.3) This does not imply each stage was mutually exclusive; some overlap is quite possible.

Stage 1

This phase of mineralisation involved microbrecciation resulting in the deposition of sericite, quartz, chlorite and both disseminated and breccia-hosted pyrite. Sericite dominates the gangue mineralogy, making up most of the vein fill material (Plate 11). Breccia veins vary in thickness from less than 1 mm up to several centimetres. Disseminated pyrite grains up to 0.3 mm display a euhedral habit, while pyrite within the breccia vein system occurs as separate and grouped euhedral to subhedral crystals (rarely up to 2 mm), having also undergone brecciation (Plates 12 and 13).

Anhedral inclusions of sphalerite (up to 0.1 mm), chalcopyrite (up to 0.2 mm), galena (up to 0.01 mm) and pyrrhotite (up to 0.05 mm) within the pyrite are indicative of synchronous deposition (Plate 12). Rare marcasite is also observed as inclusions with the chalcopyrite (Plate 14).

Rarely, fluorite is associated with the sericite / quartz / chlorite veining, in particular where the breccia veins are greater than 1 mm wide (Plate 11). It is most probable that such locations were originally vugs, with the fluorite precipitating in these late in the stage 1 sequence.

Stage 2

Stage 2 mineralisation is characterised by veins of calcite, albite and epidote crosscutting the stage 1 vein systems. Minor chlorite, quartz and sericite are also noted in this vein generation. Associated euhedral pyrite crystals are contained within these veins, along with traces of very fine grained subhedral galena and euhedral chalcopyrite (Plate 15). Rare examples of chalcopyrite having replaced pyrite can be seen within the calcite veins.

Limonite atolls are infilled with chlorite pseudomorphing pyrite; such a replacement texture suggests chlorite was indeed being deposited throughout most of the paragenetic sequence.

"Post Stage 2"

Alteration and mineral deposition occurred after stage 2, and was probably supergene in nature. Goethite is prevalent throughout the drill core as very fine grained disseminations, presumably pseudomorphing pyrite. These commonly display colloform textures. Late stage fractures throughout the deeper parts of the core display limonite coatings. The lack of any crystalline iron mineral species within these fractures suggest such coatings are probably derived from supergene remobilisation of pyrite at shallower depths in the volcanic pile.

5.4.3 Drill Core Geochemistry

The lack of heavy alteration of the host rock at most depths down the core is reflected in the geochemistry (Fig. 5.4). Silica contents, averaging approximately 73 wt %, rarely exceed 74 wt%, indicative of the lack of silicification. Sodium, often almost completely removed

Plate 10 Typical sericitic brecciation within the Gibraltar I drill core. Fine stringers of sericite (hosting traces of pyrite) erratically cut through the host rock (brown flow banded ash flow tuff).

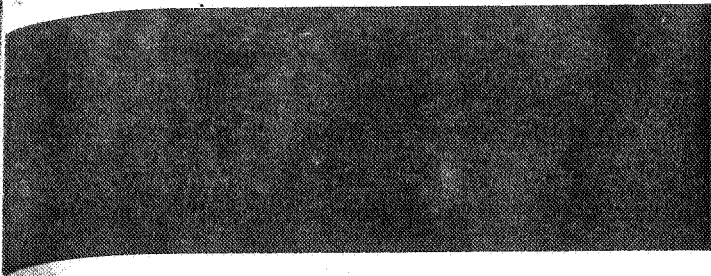
Plate 11 Euhedral pyrite (py) (opaque), hosted in a sericite (Ser) vein. Fluorite (Flr), demonstrating a characteristic purple colour, occupies the centre of the vein to the right of the field of view. (polished section RS 799, transmitted light).

Plate 12 Brecciated aggregates of pyrite (Py) within a sericitic breccia vein. Anhedral inclusions of sphalerite (Sph) indicate the syn-depositional nature of these two minerals (polished section A972-GI 104.1, reflected light).

Plate 13 Pyrite (Py) contained within a vein of sericite. The pyrite crystals commonly subhedral habits, suggesting that sericite precipitation occurred soon after the onset of nucleation of the pyrite, thus hindering the formation of euhedral pyrite crystals (polished section RS 823, reflected light).

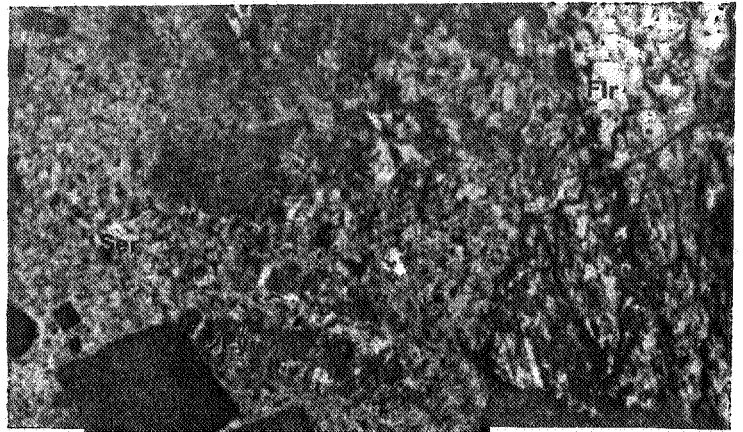
Plate 14 Disseminated aggregate of marcasite (Ma), chalcopyrite (Cpy) and pyrite (Py). Chalcopyrite is present as a replacement of euhedral pyrite, with the euhedral marcasite crystal apparently unaffected by this replacement (polished section RS 812, reflected light).

Plate 15 Chalcopyrite (Cpy) hosted within a quartz vein (polished section RS 816, reflected light).



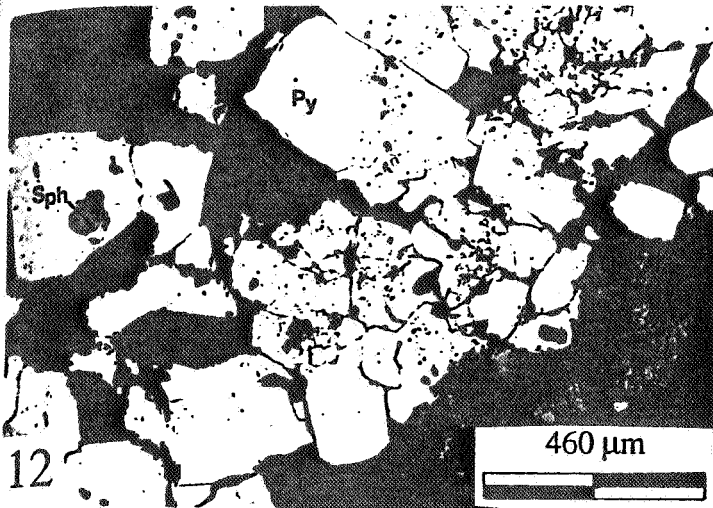
10

2 cm



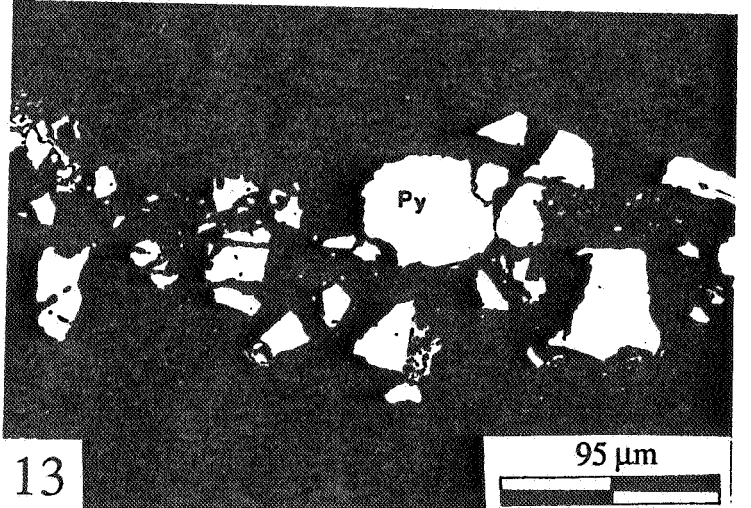
11

30 μ m



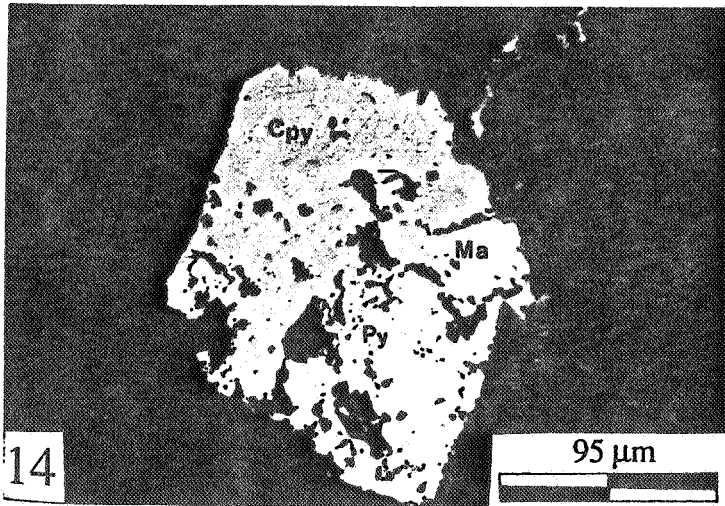
12

460 μ m



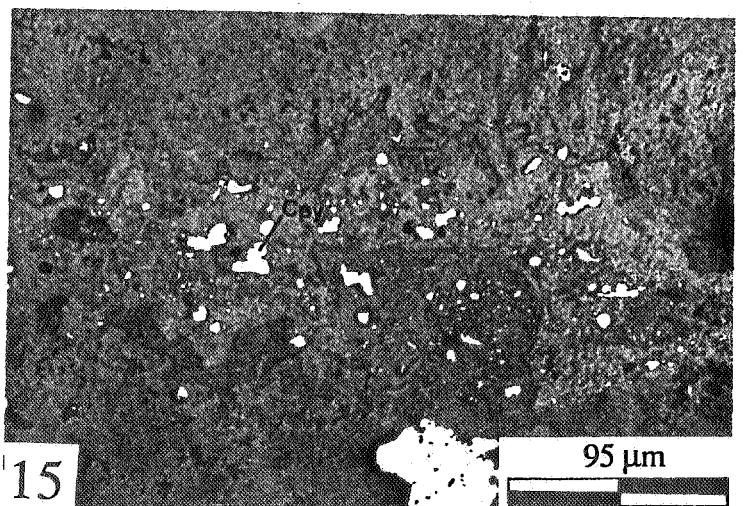
13

95 μ m



14

95 μ m



15

95 μ m



PARAGENETIC DIAGRAM OF THE GIBRALTAR I
MINERALISATION

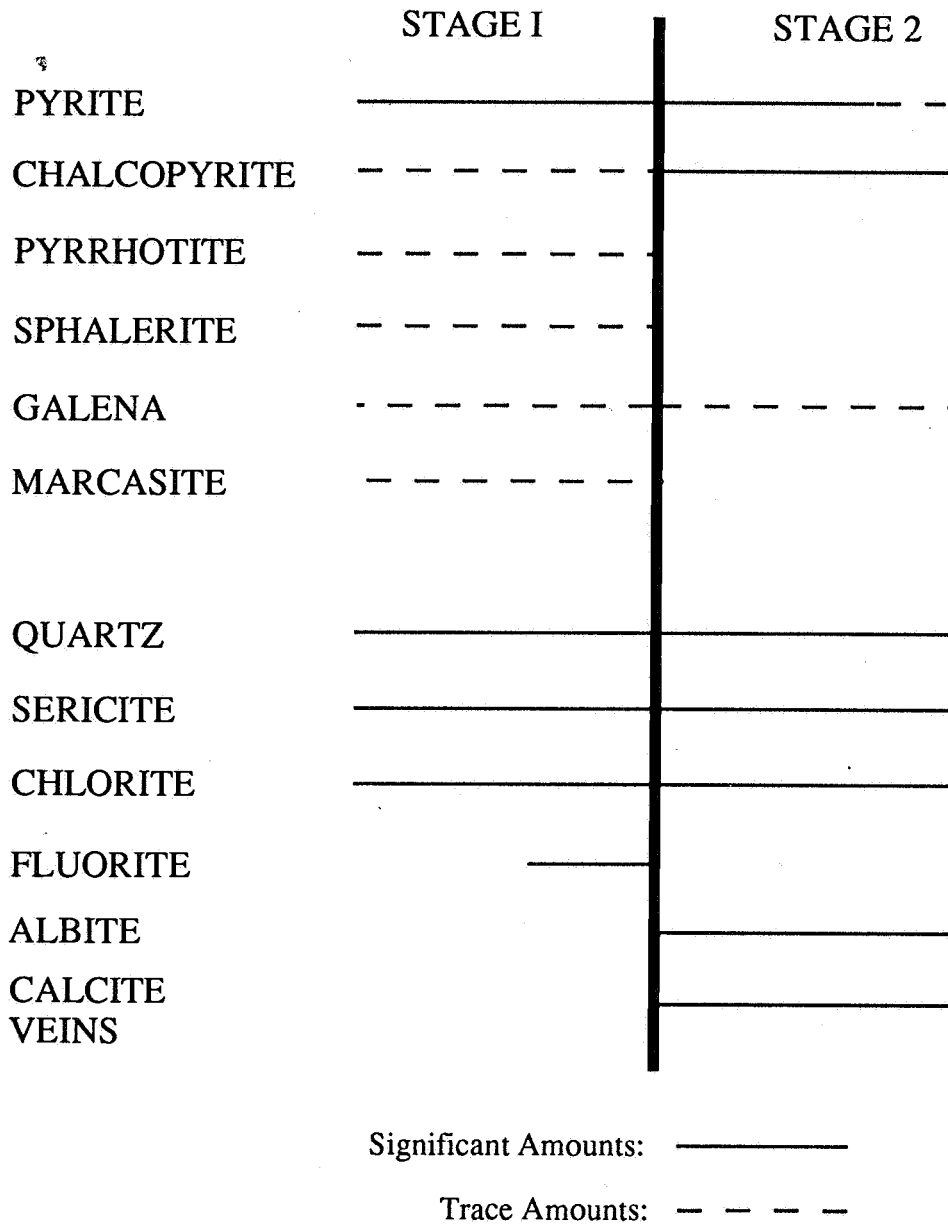


Figure 5.3 Paragenesis of the Gibraltar I drill core.

from surface samples, has abundances around 1 wt% Na₂O, with fresh samples possessing values of around 2%.

Potassium and sodium exhibit inverse trends down the core. Such a consistent trend indicates that similar pervasive chemical changes along the core have controlled the abundance of these two elements.

Alkali feldspars in the core often display perthitic textures, indicating high sodium contents within these crystals. Moderate sericitisation of the feldspars would result in the release of sodium, while maintaining the level of potassium concentration. Further, sericitisation may be associated with the uptake of K⁺ ions from solution, creating an increase in potassium abundance at the expense of sodium. The increase of sodium at the expense of potassium may be attributed to hydrothermal albitisation of the alkali feldspars, in which potassium is substituted by sodium within the feldspar lattice. Unfortunately, due to the fact that none of the geochemical samples corresponded exactly to the thin section samples made from the core, it is hard to establish the applicability of the above reactions to the geochemistry.

Magnesium and calcium both display trends distinct from sodium and potassium, indicating these elements were controlled by separate chemical processes. Calcium peaks are undoubtedly due to the presence of calcite veins, possibly along with greater abundances of plagioclase. The most likely control of magnesium abundance within any sample would be the corresponding amount of chlorite. One peak at 38 m corresponds to a zone of chlorite - sericite - quartz veining, while two peaks at deeper levels correlate with a chlorite - bearing fracture stockwork zone.

Base metal abundances display congruent down core trends in concentration, with copper, lead and zinc all exhibiting local maxima at 45 m and around 95 m. Gold maxima (up to of 0.004 ppm), generally correspond to the base metal trend, although no strong association is recognised between the gold and any particular base metal. Silver, where detected, peaks (up to 1 ppm) at depths corresponding to local lead maxima, suggesting galena to be a likely host.

Comparing major elements to the base and precious metals, no clear trend may be distinguished. However, high metal abundances roughly correspond to sodium, potassium and

calcium peaks. Certainly, many of the major element peaks are caused by the presence of albite, sericite and calcite veins, and so the above observation is probably due to the presence of sulphide minerals within these veins. Such an interpretation is consistent with petrological observations.

5.5 Quartz - Hematite Breccia

Mineralisation

Earthy and specular hematite is observed within the quartz veins present in this breccia. As mentioned in Chapter 4, two quartz veining episodes have been interpreted. Petrological work undertaken in this study suggests hematite mineralisation to be associated with the first vein set, based primarily on observations from hand specimen and thin section A972-C134 (Plate 15) sampled at the northern end of the breccia outcrop. However, petrological examination of thin sections provided by SADME, sampled at a location 200 m south of A972-C134 display hematite mineralisation within the second vein set (Purvis, 1991). Thus, it is most likely that hematite mineralisation was associated with both veining events, with the degree of mineralisation varying along the length of the breccia body.

Geochemistry

Geochemical assaying by SADME has revealed anomalous concentrations of silver (6 ppm) and gold (0.004 ppm). Sampling during the current study has also revealed anomalous zinc (130 ppm). No mineral phases responsible for these enrichments were observed under the microscope.

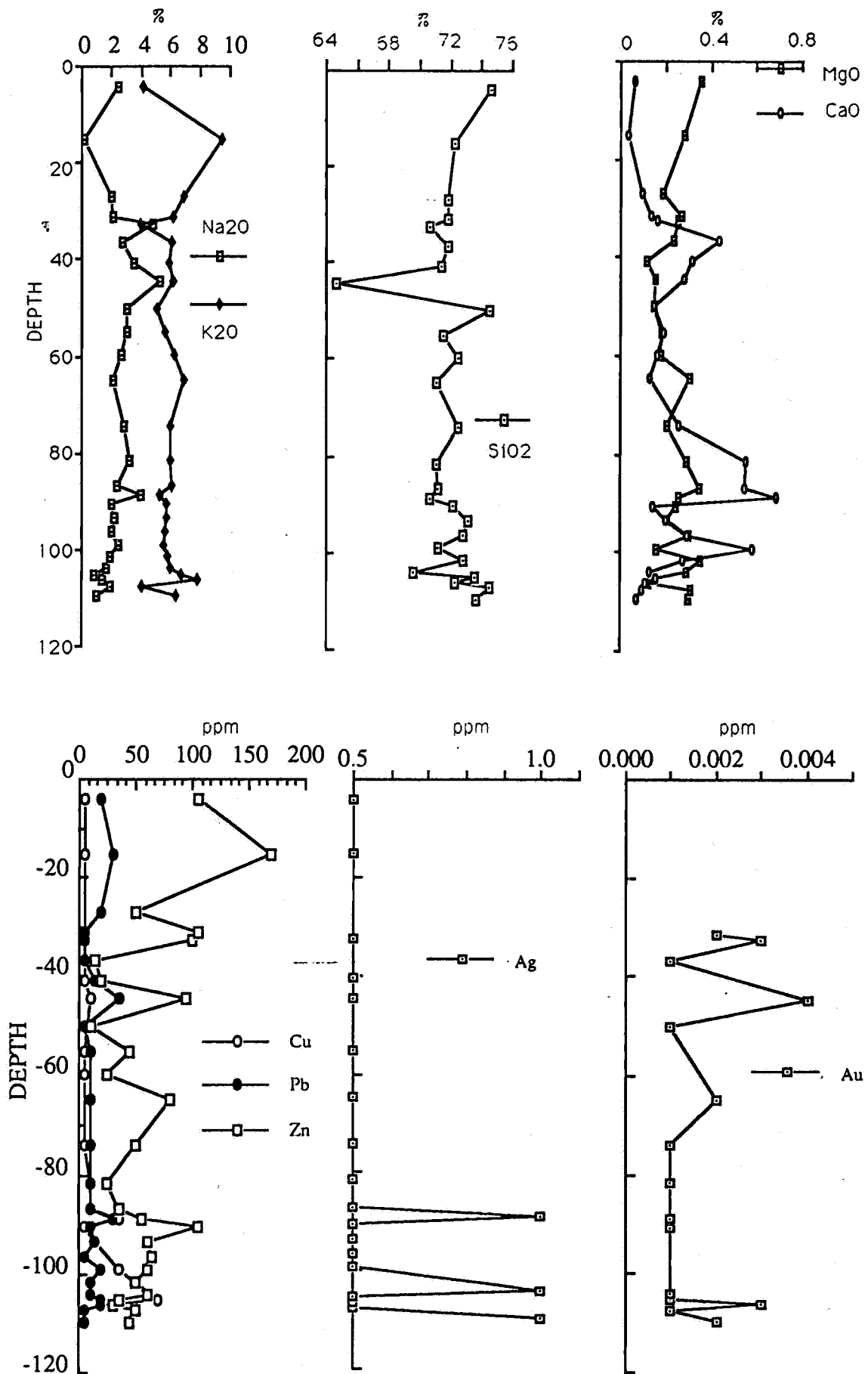


Figure 5.4 Variation in whole rock geochemistry with depth down the drill core.

6. PHYSICOCHEMISTRY OF THE GIBRALTAR I HYDROTHERMAL FLUIDS

6.1 Fluid Inclusion Microthermometry

Samples for fluid inclusion studies were gathered from four outcrop (quartz) and one drill core (fluorite) location. Of the outcrop samples, two were obtained from the quartz-hematite breccia, and two from barren quartz veins. Fluid inclusion microthermometry was performed in order to determine the nature and concentration of any free salts in the hydrothermal system, along with the temperature of the fluid. The eutectic temperature (T_e) is dependent on the solute species present, whereas the final melting temperature (T_f) is controlled by the overall salinity and the homogenisation temperature (T_h) is representative of the temperature of the fluid at time of entrapment as an inclusion. Results are summarised in Figure 6.1.

On completion of all fluid inclusion microthermometry, a total of 15 inclusions had been analysed; two from the drill core fluorite (A972-DDH) 12 from the quartz-hematite breccia, and 1 from the barren quartz vein.

6.1.1 Inclusion Types

All primary and secondary fluid inclusions analysed demonstrated irregular morphologies. Sizes varied from $24 \times 13 \mu\text{m}$ to $3 \times 4.5 \mu\text{m}$. All fluid inclusions appeared to possess 2 phases (L+V), however most specimens were hosted in cloudy quartz, making optical recognition of further phases difficult. It is this problem which has restricted the available T_e , T_m and T_h data. Heterogeneous trapping is noted in the quartz-hematite samples, with amount of vapour between 5% and 50 % by volume. The two fluorite fluid inclusions demonstrated 5% and 10% vapour, indicating a more homogeneous trapping (although more data would be required to substantiate this).

6.1.2 First and Final Melt Temperatures

(1) Fluorite (A972-DDH)

The drill core fluorite fluid inclusions, both primary, have eutectic temperatures of -53.2° and -59.0°C . This is in accordance with a $\text{H}_2\text{O}-\text{NaCl}-\text{CaCl}_2$ solution (Shepherd et al., 1985). Final melting occurred at -1.0° and -0.5°C , respectively, indicating salinities of approximately 1% to 0.5% NaCl equivalent (Shepherd et al., 1985).

(2) The Quartz-Hematite Breccia (A972-S184, A972-C134)

Primary Inclusions

Primary inclusions produced eutectic temperatures between -27.8° and -39.5°C , based on available data. This also suggests an $\text{H}_2\text{O}-\text{NaCl}-\text{CaCl}_2$ mixture, but with a higher Na:Ca ratio than in the fluorite fluid inclusions. Final melting temperatures of -0.8° to -1.8°C clearly indicate a low salinity (1-3% NaCl equivalent) for the trapped fluid.

Secondary Inclusions

These inclusions resulted in eutectic temperatures of -26.0° and -39.4°C , with final melting at -1.3° , -1.5° and -1.7°C , similar to the primary fluid inclusions.

(3) The Barren Quartz Vein (A972-C23)

One secondary fluid inclusion analysed within this sample yielded a eutectic temperature of -35.4°C , and a final melt temperature of -0.5°C . This suggests a similar salt type and content (low concentration) to the fluid inclusions in the quartz-hematite breccia.

6.1.3 Homogenisation Temperatures

(1) Fluorite

The two primary fluid inclusions in the fluorite yielded homogenisation temperatures of 168.4° and 200.2°C . This suggests deposition at a relatively low temperature of deposition with respect to common hydrothermal systems. This will be discussed further in chapter 7.

(2) Quartz-Hematite Breccia

Primary Inclusions

Primary fluid inclusions have homogenisation temperatures ranging from 198.5° to 296.5°C, with an average of 246.7°C. This is consistent with epithermal style deposits, which characteristically lie within the range of 200-300°C (Hayba et al., 1985).

Pseudosecondary and Secondary Inclusions

Data from secondary inclusions produced homogenisation temperatures between 130°C and 195°C, with an average of 167.6°C. These are thus significantly lower than the homogenisation temperatures obtained on the primary inclusions, and indicate a decrease in the temperature of the hydrothermal fluid with time.

6.1.4 Summary

From fluid inclusion data above, 3 main points can be made regarding the hydrothermal fluid physicochemistry:

- (i) Salinities of the fluids responsible for the mineralisation in the drill core, quartz-hematite breccia and the barren quartz vein are all low (below 3% NaCl equivalent).
- (ii) Temperatures for the deposition of the fluorite (~160°-200°C) are significantly lower than those associated with the quartz-hematite breccia (200°-300°C).
- (iii) Salt species present in the fluorite inclusions are similar with those associated with the quartz-hematite breccia and barren quartz vein, but are present in different abundances.
- (iv) Homogenisation temperatures associated with the quartz-hematite breccia are consistent with an epithermal type hydrothermal fluid.

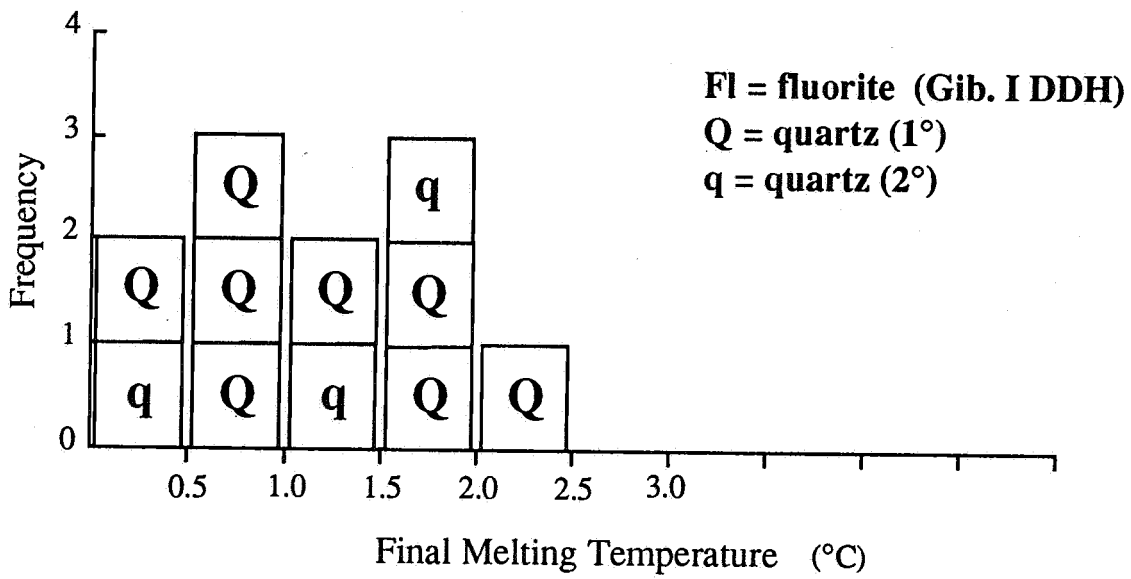
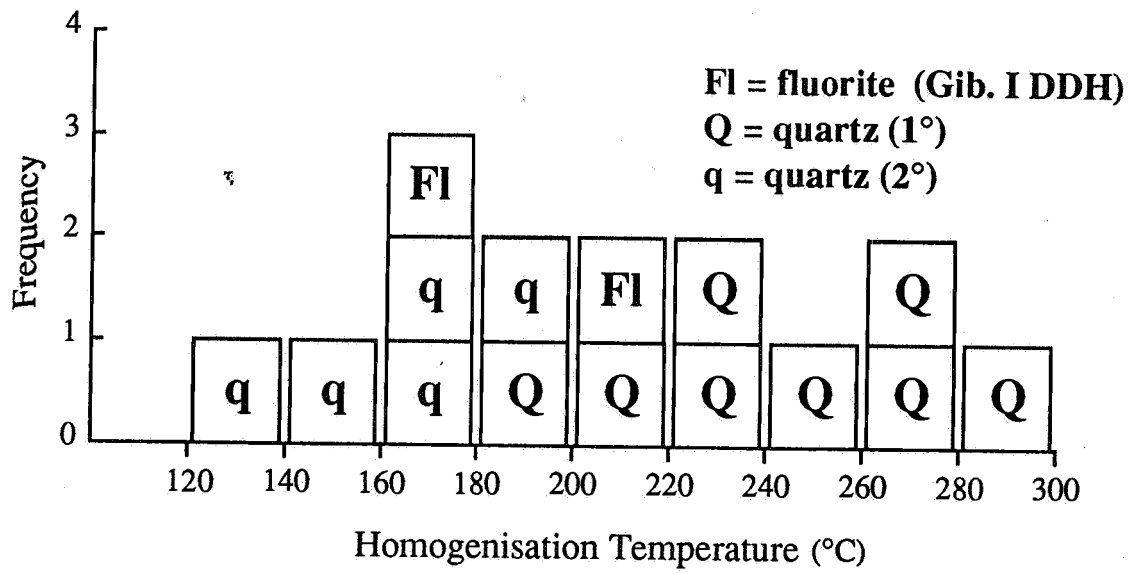


Figure 6.1 Summary of fluid inclusion analyses

6.2 Chlorite Analyses

Quantitative electron microprobe analyses were performed on 59 chlorite grains within the Gibraltar I drill core to determine theoretical temperatures, oxygen fugacities and sulphur fugacities of the hydrothermal fluid responsible for formation.

Using the abundances of the major metal ions within each chlorite, the above parameters were calculated using a six component chlorite solid solution model (Walshe, 1986). Chlorites in textural equilibrium with pyrite, along with those replacing alkali feldspar and associated with quartz phenocryst embayments are included in the 59 analyses, with the results presented in Appendix 5. A summary of the findings are presented below.

General Summary

The chlorite data set as a whole demonstrated temperatures between 89° and 327°C (average 240°C), log oxygen fugacities within the range -64.0 to -31.0 (av. -41.6), and log sulphur fugacities from -9.8 to -26.7 (av. -15.4). A histogram of the temperature data is presented in Figure 6.2.

Chlorites Associated with Pyrite Veining

Chlorites associated with pyrite-bearing veins demonstrate temperatures ranging from 105° to 305.°C (average 246°C), log oxygen fugacities between -62.6 and -34.3 (average -41.5), and log sulphur fugacities from -26.7 to -11.5 (av. -15.4). Considering the temperature data more closely, a mode exists at 290°-310°C, suggesting much of the pyrite was deposited within this temperature range. The chlorite data gathered in this study were largely from veins associated with Stage 1 mineralisation (Fig. 5.3), hence it appears the early part of pyrite deposition occurred around 300°C.

Chlorites Associated with Quartz Embayments

20 chlorites, located within embayments of quartz phenocrysts, were analysed to investigate temperatures associated with this alteration. Resulting temperatures range from 215° to 327°C, averaging 295°C. Of the 20 analyses, 18 lie within 282° to 327°C, suggesting that chlorites deposited within the quartz embayments precipitated from fluids with temperatures of around 300°C, similar in temperature to chlorites associated with Stage 1 mineralisation mentioned above. Thus, it is likely that both these populations chlorites were deposited during Stage 1 mineralisation.

Chlorite Replacing Pyrite

12 analyses were performed on chlorites pseudomorphing relict pyrite. Results yielded a temperature range from 89° to 258°C, with an average of 190°C. Any replacement of pyrite must be post stage 1 at least, thus a negative temperature gradient appeared to be prevalent after this phase of the paragenetic sequence, based on such a low average temperature.

6.3 Sphalerite Analyses

11 electron microprobe analyses of sphalerite present in the drill core were performed in order to further constrain oxygen fugacities during deposition. 11 points analysed in two sphalerite inclusions in pyrite gave a range of 11.28 to 13.31, with an average of 12.56 mole %. The content of sphalerite may be used to calculate fO_2 conditions in the fluid (Craig and Scott, 1974). At 300°C the FeS contents of the Gibraltar I sphalerites correspond to log oxygen fugacities between -33.0 and -33.1. (Fig. 6.2)

6.4 Sulphur Isotope Analyses

Sulphur isotope analyses were made of 9 samples of pyrite extracted from the drill core, and the resulting sulphur isotope ratios were expressed as $\delta^{34}S$ relative to the Canon Diablo Troilite. All samples were taken from depths between 44.64 and 104.4 m; sampling was restricted at other depths due to the lack of available pyrite.

Results

The results obtained are shown in Figure 6.1a. The $\delta^{34}\text{S}$ values are tabulated in Appendix 7. $\delta^{34}\text{S}$ values range between -2.8 and 4.8‰, averaging 2.0‰. The values show a narrow range; 8 out of 9 lie between 0.4 and 4.8‰, suggesting relative homogeneity of the $\delta^{34}\text{S}$ values throughout the body of the mineralisation.

Interpretation

According to Ohmoto and Rye (1979), $\delta^{34}\text{S}$ values of sulphide minerals in most igneous bodies are within the range of $0 \pm 5\%$, based on the sampling of igneous rocks from the Western United States of America. A more recent compilation of data by Ohmoto (1983) suggests a distinction between mantle derived and crustally enriched igneous bodies. Palaeozoic granitoids in Japan, contaminated by crustal assimilation, contain sulphides with $\delta^{34}\text{S}$ values between 2 and 9‰, while those free of this addition are characterised by $\delta^{34}\text{S}$ values in the range of -10 to -1‰ (Ohmoto, 1983 after Ishihara, 1981).

Using the above observations, the sulphur isotope data in this study are consistent with an igneous source for the sulphur. According to the findings of Ishihara (1981), 8 of the 9 values are consistent with a sulphur source of crustally enriched granitoids.

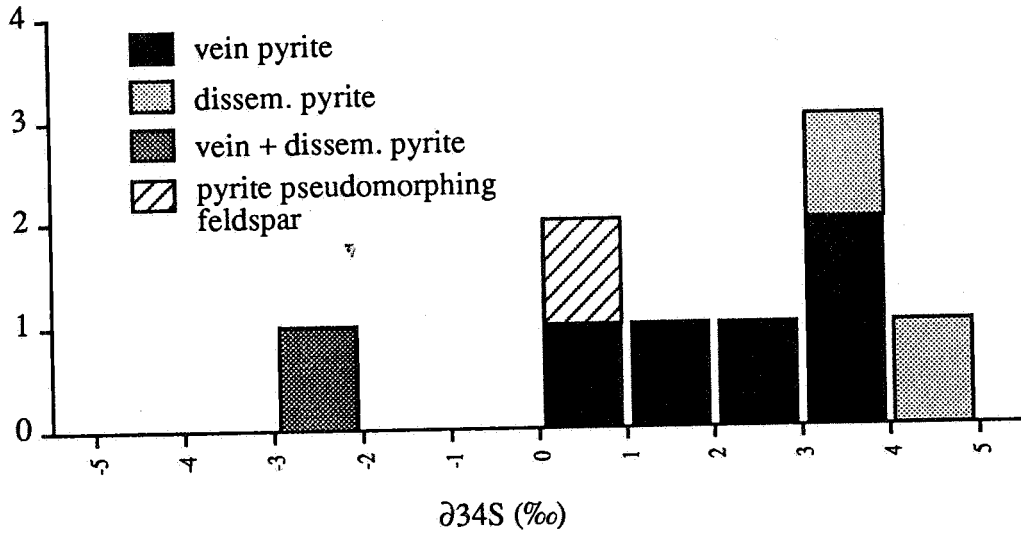


Figure 6.1a Histogram of pyritic sulphur isotope ratios ($\delta^{34}\text{S}$), representing samples from the Gibraltar I drill core.

6.5 Geochemical Modelling of the Hydrothermal System Responsible for the Gibraltar I Mineralisation

The paragenetic, fluid inclusion, chlorite and sulphur isotope studies described above are combined here, in order to generate a practical genetic model of the mineralisation within the Gibraltar I fluids. Chemical equations and the associated thermodynamic data used are presented in Appendix 9. The modelling has been performed for a fluid with a total sulphur content of 10^{-2.5} M.

Temperature data from the chlorites (Fig. 6.2) demonstrate a wide temperature distribution. However, a mode between 290° and 310°C is evident. Also, considering the fact that a mode at around 300°C exists for chlorites associated with pyrite, a temperature of 300°C was selected as an initial modelling parameter in fO_2 - pH space.

6.5.1 Modelling in fO_2 vs pH Space

Using thermodynamic data from Huston and Large (1989), an fO_2 vs pH diagram was constructed for 300°C, to constrain the possible pH and fO_2 conditions of pyrite deposition (Fig. 6.3). The stability fields of kaolinite, sericite and alkali feldspar were plotted on the basis of $a_{K^+}=0.1$. Pyrite is intimately associated with sericite in the drill core, thus a pH range of 2.8 to 4.8 is suggested for the fluid at the time of deposition. A pH of 4 was thus assumed for further calculations, it being an integral value relatively central to the sericite stability field.

Overlaying the pyrite stability field with contours of sphalerite iron content (Fig. 6.3), the sphalerite data previously calculated indicates oxygen fugacities of between -33.0 and -33.1 log fO_2 . In view of the limited data available for the sphalerites, this should only be seen as a guide, rather than limiting fO_2 values for sphalerite, and hence pyrite deposition.

Chlorite temperature data for those associated with pyrite yielded log oxygen fugacities between -33.5 and -36.6, indicating there is reasonable agreement with the oxygen fugacities calculated from the sphalerite data.

6.5.2 Modelling in fO_2 vs T Space

Using a pH of 4 (see above), a diagram of fO_2 vs T has been constructed (Fig. 6.4). Chlorite data mostly plot within the pyrite stability field (consistent with this being the dominant phase in the drill core mineralisation), and demonstrate a trend of decreasing $\log fO_2$ with decreasing temperature. A number of points lie within or near the magnetite or pyrrhotite fields, and all are distal from the hematite-pyrite buffer. These results are consistent with a plot of $\log fS_2$ against fO_2 (Fig 12), and the with microscopic findings; no hematite has been observed, and rare pyrrhotite inclusions in pyrite are present. All chlorite data plot within the chalcopyrite stability field, consistent with an observed absence of bornite within the drill core.

6.5.3 Gold Solubility (Fig. 6.5)

Gold in most hydrothermal systems is considered to be transported as either a bisulphide complex ($Au(HS)_2^-$) or a chloride complex ($AuCl_2^-$). Given the low salinities of all fluid inclusions sampled within the Gibraltar I area, it is reasonable to assume that any gold complexing via chloride would be minimal. Using the data for sulphide complexing of gold by Shenberger and Barnes (1989), solubility contours were constructed for $Au(HS)_2^-$ in fO_2 vs T space at pH 4. This plot demonstrates that no solubilities > 0.01 ppb intersect the proposed fluid conditions during deposition of the minerals in stage 1 of the paragenesis. Thus, significant gold deposition would be minimal. Note that lowering the temperature expands contours in the pyrite field to lower pH, hence significant gold deposition could be possible only if the hydrothermal system was operating at lower temperatures. Secondary fluid inclusion homogenisation temperatures, and temperature data obtained from analyses of chlorites replacing pyrite, indicate a decrease in the temperature of the hydrothermal fluid with time. Thus, it is possible that significant gold transportation and deposition could have occurred during this time, however, none is evidenced in the Gibraltar I drill core.

Figure 6.2 Histogram of temperatures generated from chlorite analyses.

Figure 6.3 Log fO_2 - pH diagram calculated for 300°C, $a_{K^+} = 0.1$, and $\Sigma S = 10^{-2.5} M$. Mole% FeS in sphalerite is indicated, along with (1) a black line indicating the conditions of sphalerite deposition, and (2) a hatched region indicating the conditions of chlorite associated pyrite deposition.

Figure 6.4 Log fO_2 - temperature (°C) diagram calculated for $\Sigma S = 10^{-2.5} M$ and $pH = 4$.

Figure 6.4a Log fS_2 - fO_2 calculated for 300°C. Chlorite data are plotted for the range $300 \pm 10^\circ C$.




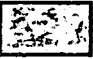

Figure 6.5 Log fO_2 - pH diagram calculated for 300°C, $a_{K^+} = 0.1$, $\Sigma S = 10^{-2.5} M$ with gold copper solubility contours. The shaded region represents the conditions of ore formation.

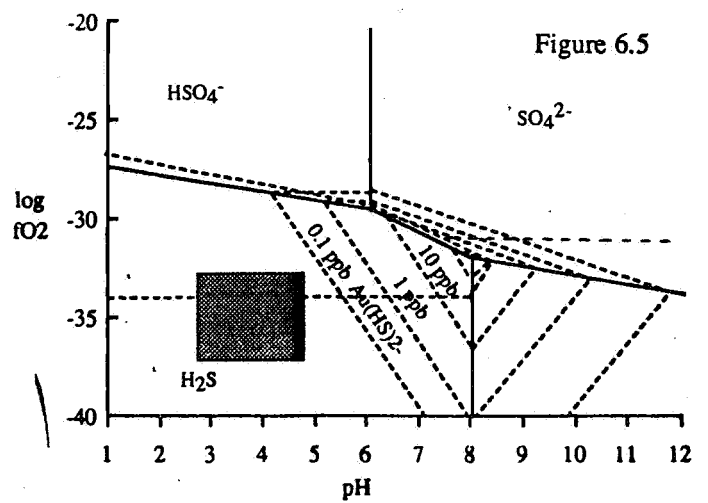
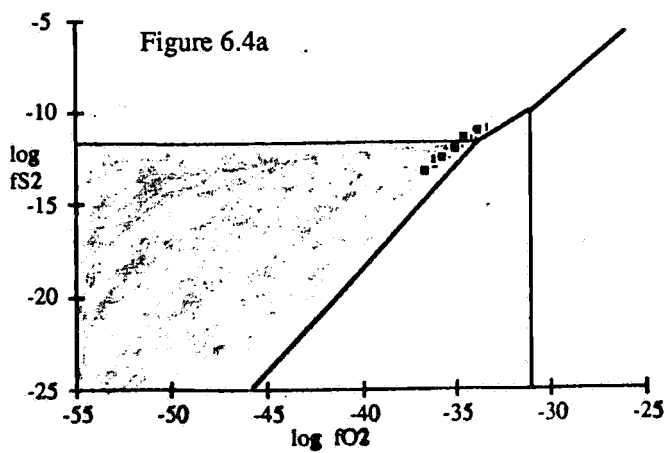
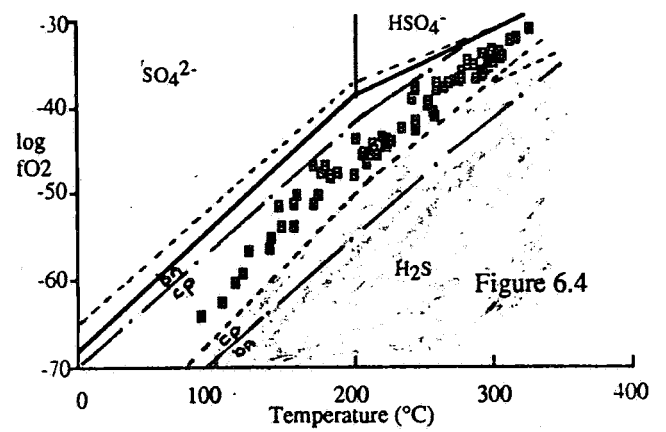
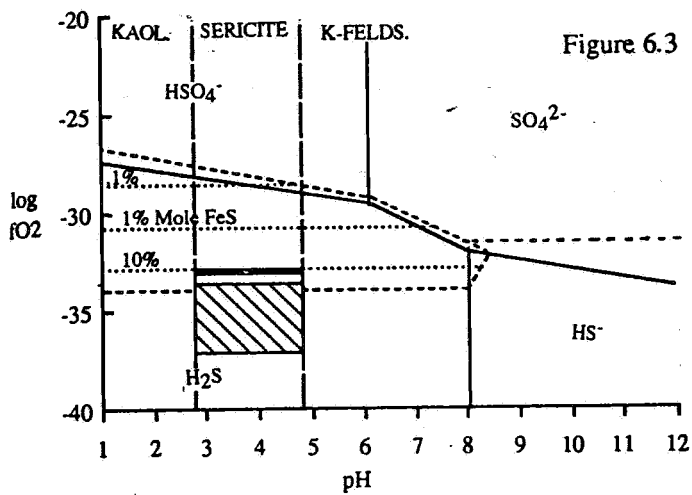
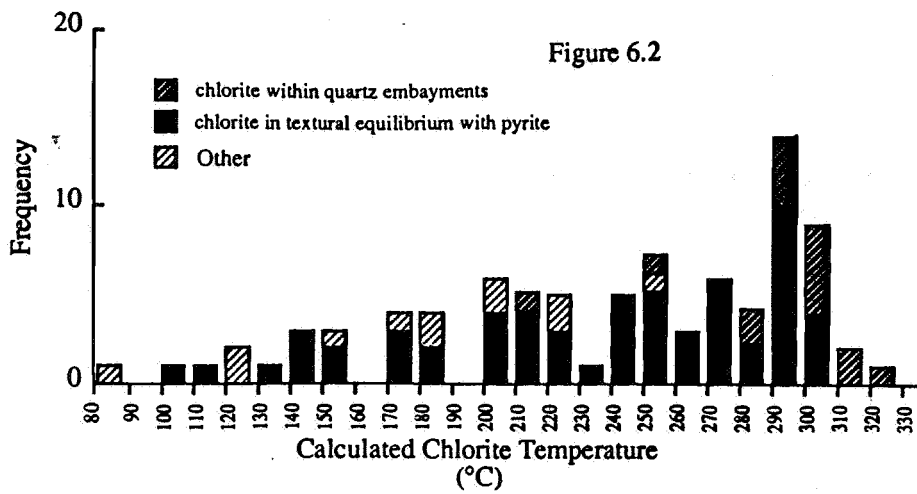
Boundaries

- Fe-S-O phases
- Sulphur species
- · — · — Chalcopyrite-bornite
- Kaolinite-sericite-K feldspar

Contours

- ppb Au(HS)₂ in solution
- mol% FeS in sphalerite

-  Magnetite field
-  Hematite field
-  Pyrite field
-  Pyrrhotite field
-  Chlorite data



7. GENETIC MODEL FOR MINERALISATION

Findings from the previous chapters will be used here to propose a feasible genetic model for the mineralisation seen within the Gibraltar I drill core.

7.1 Heat Source Driving the Hydrothermal System

It is likely that intrusive bodies associated with the Gawler Range Volcanics are present at depth. Such a body would have been a sufficient heat source to drive a convective hydrothermal system via heat conduction through the volcanic pile.

7.2 Fluid / Metal / Sulphur Source and Transport

Two possible metal and sulphur sources may be theorised, based on available sulphur isotope data:

(1) Leaching of metals from the volcanic pile

(2) Input of metals via devolatilisation from local intrusions

Neither can be distinguished as being a more favourable source, given that the sulphur isotopic signatures of both would be very similar.

Fluids, given the low proposed temperature range (200°-300°C), were most likely meteoric in nature, as distinct from higher temperature magmatic fluids. In this case, ground waters percolating vertically and laterally through the cooling volcanic pile would have had a convective hydrothermal system imposed upon them. Nevertheless, if any metal and / or sulphur input from a plutonic body is to be assumed, a corresponding fluid input is inevitable.

Characteristics of the fluid determined by measurement (fluid inclusion studies, sphalerite analyses and chlorite analyses), and by thermodynamic modelling are consistent with the low metal contents reported in assays of the mineralisation (Dubowski, 1992). As demonstrated in section 6.5, gold solubility in the fluid, for at least part of its history, would have been < 0.1 ppb. Copper solubility is low (≤ 0.1 ppm) at temperatures below 300°C (Crerar and Barnes, 1976), and the solubilities of lead and zinc are depressed in low salinity fluids.

Initial pyrite deposition (Stage 1) occurred at temperatures of the order of 300°C and a within a pH range of around 3 to 5. Homogenisation temperatures obtained from fluid inclusions in fluorite indicate hydrothermal fluids of lower temperatures were involved in its deposition. This stage also included minor sphalerite, galena, pyrrhotite and chalcopyrite. Based on the proposed paragenetic sequence, this indicates a decrease in temperature occurred towards the end of stage 1 mineralisation. It is likely that this decrease in temperature, coupled with an increase in pH, resulted in the later (Stage 2) mineralisation, which is interpreted to have been deposited at elevated pH, due to the presence of albite and calcite veins.

Deposition was most likely the result of mixing with less evolved groundwaters. Hayba et al. (1985) note two mechanisms of deposition; one of boiling, and one of fluid mixing. Devolatilisation due to boiling generates high acidity fluids which leach the surrounding host rocks, characteristically resulting in intense silicification at the depth at which boiling occurred. No horizon of such silicification is evident within the drill core, suggesting mixing to be the likely mechanism of precipitation of the sulphides.

7.3 Relation of the Gibraltar I Mineralisation to nearby Hydrothermally Mineralised Zones

Considering the proximity of all other hydrothermally altered / mineralised areas to the Gibraltar I drill site, it is quite probable that each was affected by the same mineralising event. Further, alteration in each area (ie. Zone 1 altered volcanics, the vent area and the quartz-sericite rock) is quite similar. The only exception is the quartz-hematite breccia and associated quartz veins; this breccia body displays a distinctly different mineral assemblage to that observed in the Gibraltar I drill core. Any explanation as to the source or nature of the fluids associated with this mineralisation is unwarranted from the information gathered in this study. However, it is probable that such mineralisation was fault controlled, based on the structural interpretation presented in Chapter 4.

8. CONCLUSIONS

(1) The Gibraltar I drill core intersected weak sulphide mineralisation consisting of pyrite, chalcopyrite, sphalerite, galena, pyrrhotite and marcasite, accompanied by sericite, quartz, chlorite, albite, calcite and fluorite. Two stages of mineralisation are evident (stage 1 and stage 2), with the first stage resulting in the majority of the sulphides.

(2) The mineralisation is hosted in rhyolitic members of the Middle Proterozoic Ealbara Rhyolite, a member of the Lower Gawler Range Volcanics. Tectonic implications of the geochemistry of these volcanics is consistent with the model of formation of the GRV; bimodal volcanism generated by basaltic underplating and associated dry partial melting of a sialic lower crust.

(3) All mineralisation in the area must have occurred prior to the intracontinental rifting and emplacement of the Gairdner Dyke Swarm (dated at 802 ± 35 and 867 ± 40 Ma (Zhao, 1992)).

(4) From the geochemical modelling performed (based on chlorite and sphalerite analyses, fluid inclusions and the observed mineral assemblages) stage 1 mineralisation appears to have occurred at 300°C within a pH range of 3 to 5, while stage 2 mineralisation occurring at higher pH and probably lower temperatures of around 200°C .

(4) The source of the ore sulphur is most likely felsic magmatic in origin, with two possible sources: the GRV volcanic pile and associated intrusions. The source of the metals is similar, but the fluid source was probably dominantly meteoric.

(5) Hydrothermal alteration and mineralisation proximal to the Gibraltar I drill site, aside from the quartz-hematite breccia, are probably related to the same hydrothermal event. The quartz-hematite breccia, due to its distinctively unique mineral assemblage, is most likely the result of separate hydrothermal activity.

ACKNOWLEDGEMENTS

Firstly, I wish to thank Dr Ross Both for supervising this project; his advice and guidance throughout the year was invaluable to say the least. Thanks are also extended to Dr John Foden, who also provided many helpful suggestions and comments.

I am indebted to the South Australian Department of Mines and Energy for their logistical assistance. Special thanks are extended to Ted Dubowski, Warwick Newton and Ric Horn, who helped organise the project; gourmet chefs Steve Ewen and Mark Flintoft for their extensive assistance during fieldwork; Peter Crittenden for technical assistance; Jo Janz for helping with geochemical assaying by Amdel; and Sue Daly for her inestimable comments and aid with regard to the regional geology and provision of geochemical data.

I would like to thank the staff of the Geology Department for the technical support received, in particular Wayne Mussared for polished thin sections and fluid inclusion work, Geoff Trevelyan for thin sections, Huw Rosser for assistance with microanalysis, Dr Keith Turnbull for guidance in sulphur isotope analyses, John Stanley and Phil McDuie for geochemical analyses, and Rick Barrett for photographic work.

Almost finally, I would like to thank the honours students that put up with me this year, and for the help and support they provided. In this regard I would particularly like to thank Andrea Smith and Scott Mildren, the igneous crew (Brian Cock, Graeme McDonald and Pete Smith) and the geophysics crew (Paul Basford, Alex Bontenakel and Angus McCoy).

Finally, I wish to express gratitude to my parents for all they have done for me throughout my University life; without them, I could not have achieved what I have.

REFERENCES

- Barker, D.S., 1983, *Igneous Rocks.*, Prentice Hall., p. 417.
- Blissett, A.H., 1975, Rock units in the Gawler Range Volcanics, South Australia., Q. Geol. Notes, Geol. Surv. S. Aust., No. 55, pp. 2-14.
- Collins, W.J., Beams, S.D., White, A.J.R. and Chappell, B.W., 1982, Nature and origin of A-type granites with particular reference to south eastern Australia., *Contrib. Mineral. Petrol.*, vol. 80, pp. 189-200.
- Cooper J.A., Mortimer, G.E., Rosier, C.M. and Uppill, R.K., 1985, Gawler Range magmatism - further isotopic age data., *Aust. J. Earth Sci.*, vol. 32, pp. 115-123.
- Crerar, D.A., and Barnes, H.L., 1976, Ore solution chemistry V. Solubilities of chalcopyrite and chalcocite assemblages in hydrothermal solution at 200°C to 300°C. *Econ. Geol.*, vol. 71, pp. 772-794.
- Daly, S.J., 1985, Tarcoola map sheet, Geological Atlas of South Australia, 1:250000 map series., Geol. Surv. S. Aust., Adelaide.
- Daly, S.J., 1986, The stratigraphy of the Tarcoola 1:250000 map sheet area., Rept. Bk. No. 81/5, Geol. Surv. S. Aust., Adelaide.
- Daly, S.J., Horn, C.M. and Fradd, W.P., 1990, Tarcoola gold field, In : *Geology of the Mineral Deposits of Australia and Papua New Guinea* (Ed. F.E. Hughes), pp. 1099-1053. (The Aust. Inst. Min. Metall., Melbourne).
- Dubowski, E.A., 1992, Image processing over the north west Gawler Craton., Rept. bk. 92/16, S. Aust. Dept. Mines and Energy, Adelaide.
- El Bouseily, A.M. and El. Sökkary, A.A., 1975, The relation between Rb, Ba, and Sr in granitic rocks., *Chem. Geol.*, vol. 16, pp. 207-219.
- Fanning, C.M., Flint, R.B., Parker, A.J., Ludwig, K.R. and Blissett, A.H., 1988, Refined Proterozoic evolution of the Gawler Craton, South Australia through U-Pb zircon geochronology., *Precamb. Res.*, vol. 40/41, pp. 363-386.
- Flint, R.B., (compiler), Chapter 5, In : Parker, A.J., Flint, R.B., Daly, S.J. and Preiss, W., "The Geology of South Australia", Bulletin 54, Geol. Surv. S. Aust., Adelaide. (in press).
- Giles, C.W., 1980, A study of Precambrian felsic volcanism in southern Australia. Ph.D. Thesis, University of Adelaide, 220 p.
- Giles, C.W., 1988, Petrogenesis of the Proterozoic Gawler Range Volcanics, South Australia., *Precamb. Res.*, vol. 40/41, pp. 407-427.
- Henley, R.W., 1984, Hydrolysis reactions in hydrothermal fluids, In : Henley, R.W., Truesdell, A.H. and Barton P.B. (eds), *Fluid-Mineral Equilibria in Hydrothermal Systems*, Society of Economic Geologists. *Rev. Econ. Geol.*, vol. 2.
- Huston, D.L. and Large R.R., 1989, A chemical model for the concentration of gold in volcanogenic massive sulphide deposits. *Ore Geol. Rev.*, vol. 4, pp. 171-200.

- Ishihara, S., 1981, The granitoid series and mineralisation. *Econ. Geol.* 75th Ann. Vol., pp. 458-484.
- Jagodzinski, E.A., 1985, The geology of the Gawler Range Volcanics in the Toondulya Bluff Area, and U-Pb dating of the Yardea dacite at Lake Acraman. Hons. Thesis, University of Adelaide, 86p.
- Ohmoto, H. and Rye, R.O., 1979, Stable isotopes in high temperature geological processes., *Min. Soc. Am., Rev. Min.*, vol. 16, pp. 491-560.
- Pearce, J.A., Harris, N.B. and Tindle, A.G., 1984, Trace element discrimination diagrams for the interpretation of granitic rocks. *J. Petrol.*, vol. 25, Part 4, pp. 956-983.
- Purvis, A.C., 1991, Mineralogy report no. 5985. In : Dubowski, E.A., 1992, Image processing over the north west Gawler Craton., Rept. bk. 92/16, S. Aust. Dept. Mines and Energy, Adelaide.
- Robertson, B.D., 1989, The geology, petrology and geochemistry of the volcanics in the Kokatha region, Gawler Ranges, South Australia. Hons. Thesis, University of Adelaide, 77p.
- Shepherd, T.J., Rankin, A.H. and Alderton, D.H.M., 1985, A practical guide to fluid inclusion studies. Blackie and Son, 239p.
- Streickeisen, A.L., 1975, To each plutonic rock its proper name., *Earth Sci. Rev.*, vol. 12, pp. 1-33.
- Streickeisen, A.L. and Le Maitre, R.W., 1979, A chemical approximation to the modal QAPF classification of igneous rocks. *Neues Jahr. Min. Abhand.*, vol. 136, pp. 169-206.
- Sun, S. and Mc Donough, W.F., 1989. Chemical and isotopic systematics of oceanic basalts : implications for mantle compositions and processes. *Magmatism in the ocean basins*, *Geol. Soc. Spec. Pub. No. 42*, pp. 313-345.
- Walshe, J. L., 1986. A six-component solid solution model and conditions of chlorite formation in hydrothermal systems. *Econ. Geol.*, vol. 81, pp. 681-703.
- Webb, A.W., Thomson, B.P., Blissett, A.H., Daly, S.J., Flint, R.B. and Parker, A.J., 1986, Geochronology of the Gawler Range Craton South Australia. *Aust. J. Earth Sci.*, vol. 33, pp. 119-143.
- Whalen, J.B., Currie, K.L. and Chappell, B.W., 1987, A-type granites : geochemical characteristics, discrimination and petrogenesis., *Contrib. Mineral. Petrol.*, vol. 95, pp. 407-419.
- Winchester, J.A. and Floyd, P.A., 1977, Geochemical discrimination of different magma series and their differentiation products using immobile elements., *Chem. Geol.*, vol. 20, pp. 325-343.

TN MN

5 1/2° approx.

Qp

GIBRALTAR 1 DDH

Qp

Qp

Qp

Qp

Qp

Qp

Qp

Qp

Qp

Qp

Qp

Qp

Qp

GEOLOGICAL REFERENCE

- Pleistocene**
- Qp Red-brown, clay-rich quartz sand partly indurated by iron oxide and calcrete
- Proterozoic (Ealbara Rhyolite)**
- rd Rhyolite dyke
 - bg Black glassy rhyolite
 - rl Rhyolite lava
 - bf Brown flow banded ash flow tuff
 - sw Strongly welded rhyolitic ash flow tuff
 - pw Porphyritic welded rhyolitic ash flow tuff

- ALTERED VOLCANICS**
- a1 Altered Volcanics - Zone 1
 - a2 Altered Volcanics - Zone 2
 - aV Altered Volcanics - Vent Area / Volcanic breccia
 - qs Quartz sericite rock
 - Qz Quartz - Hematite Breccia
 - BQV Barren quartz vein
 - cm Chloritic Microbreccia
 - Boxworks
 - Joint Zone

Legend

- Fence
- Vehicle track
- Creeks and drainage
- Outcrop boundary
- Alteration boundary
- Joint, vertical
- Joint set, conjugate (Dominant set = longest line)
- Flow banding



**GIBRALTAR 1 DRILL SITE
OUTCROP GEOLOGY**

TN
MN
5 1/2° approx.

GEOLOGICAL REFERENCE

FRESH VOLCANICS

Proterozoic (Ealbara Rhyolite)

- rd Rhyolite dyke
- bg Black glassy rhyolite
- rl Rhyolite lava
- bf Brown flow banded ash flow tuff
- sw Strongly welded rhyolitic ash flow tuff
- pw Porphyritic welded rhyolitic ash flow tuff

ALTERED VOLCANICS

- a1 Altered Volcanics - Zone 1
- a2 Altered Volcanics - Zone 2
- aV Altered Volcanics - "Vent Area"/ Volcanic breccia
- qs Quartz sericite rock
- Quartz - Hematite Breccia Observed / Interpreted
- Barren quartz vein
- cm Chloritic Microbreccia
- Boxworks
- Joint Zone

Legend

- Fence
- Vehicle track
- Creeks and drainage
- Outcrop boundary
- Proposed geological boundary
- Alteration boundary
- Joint, vertical
- Joint set, conjugate (Dominant set = longest line)
- Flow banding



**GIBRALTAR 1 DRILL SITE
INTERPRETIVE GEOLOGY**



APPENDIX 1

SELECTED THIN SECTION DESCRIPTIONS

Unaltered Volcanics

Sample: A972-28M

Unit: Porphyritic welded tuff

Hand Specimen Description

A dark brown, slightly altered porphyritic rhyolite. Quartz phenocrysts (to 2 mm) are less abundant than pink feldspars (to 3 mm). Frequently, feldspars are altered to white clay. Rare intense yellow sericite spots are noted.

Thin Section Description

The groundmass is a cryptocrystalline mass of alkali feldspar and quartz. Occasional devitrified glass shards are distinguishable. Discontinuous banding is noted, commonly contorted around the abundant phenocrysts.

Subhedral and angular resorbed phenocrysts of quartz are evident, the latter more abundant than the former. Orthoclase phenocrysts (up to 2.5 mm) with simple twinning are observed, also commonly with a micropertthitic to perthitic texture. Both phenocryst populations demonstrate in situ fracturing.

Feldspars are sericitised to varying degrees, and commonly hematized.

Plagioclase feldspars, rarely up to 1 mm, are sericitised, but appear to be less affected by hematization than the alkali feldspars.

Rare muscovite and leucoxene pseudomorphs of biotite (and possibly augite) are apparent.

Occasional lithic fragments are distinguishable, characterised by a sericitised intergrowth of quartz and alkali feldspar. Some fragments possess phenocryst of quartz, alkali feldspar and plagioclase are evident, the alkali feldspar notably hematized.

Rare, disseminated opaques (occasionally up to 0.5 mm) are present.

Phenocrysts

Quartz:	15 - 20%
Orthoclase:	20%
Plagioclase:	5%

Altered Biotite:	<1%
Lithic Fragments:	5%
Opagues:	<1%
Groundmass:	50-55%

Conclusion: A welded, porphyritic, crystal lithic rhyolitic tuff.

Sample: A972-121M

Unit: porphyritic welded tuff

Hand Specimen Description

A dark brown / black, alkali feldspar > quartz phyric rhyolite. Small white feldspars are also visible, with red lithic fragments also present. The volcanic appears relatively unaltered.

Thin Section Description

The groundmass in this rock is a cryptocrystalline mass of alkali feldspar and quartz. Quartz shards and feldspar microlites are pervasive throughout, and demonstrate preferential orientations parallel to layering observed in the groundmass. Such layering appears to be compactive in origin, due to local convolutions around phenocrysts.

Quartz phenocrysts (up to 2.5 mm) display both embayed subhedral and fragmental habits, with the smaller fragments in alignment with layering.

Orthoclase phenocrysts (up to 2 mm) are also represented by euhedral and fragmental morphologies. Commonly these demonstrate a distinct perthitic texture, occasionally to a mesoperthitic extent. Sericitisation is common in these crystals, generally concentrated in the cores.

Smaller (rarely up to 1.5 mm) subhedral plagioclase feldspars also demonstrate sericitisation, although to a lesser extent than the orthoclase.

Lithic fragments commonly consist of fine-grained intergrowths of quartz and (commonly sericitised) alkali feldspar. These fragments occasionally demonstrate alignment to the layering

plane. A number of these fragments appear lensoidal in shape, and possess abundant spherulites. These bodies may in fact be devitrified collapsed pumice fragments.

Muscovite pseudomorphs of biotite (rarely up to 1.5 mm long) are commonly present, occasionally associated with leucoxene.

Hematisation is manifest in both feldspar types, with greatest intensity evident in those feldspars without discernable sericitisation.

Phenocrysts

Quartz:	15%
Orthoclase:	15%
Plagioclase:	3-5%
Altered Biotite:	1%
Lithic / Pumice Fragments:	20%
Opagues:	<1%
Groundmass:	45%

Conclusion: a (pumaceous ?) crystal lithic rhyolitic tuff.

SAMPLE: A972-20M

Unit: porphyritic welded tuff.

Hand Specimen Description

A feldspar > quartz phyric rhyolite. The groundmass is green-brown, with red weathered feldspars (up to 2 mm) > quartz. A relatively linear quartz vein ~ 2 mm wide cuts through the sample.

Thin Section Description

The groundmass consists of cryptocrystalline intergrowths of quartz and sericitised feldspars. Trachytic quartz shards and sericitised feldspars are pervasive throughout.

Quartz phenocrysts occur both as embayed subhedral and fragmental crystals, the latter in greater abundance.

Alkali feldspars (up to 2 mm) are albitised, hematized and sericitised. Note that two suites of alteration are observed in these crystals:

(1) complete sericitisation (with minor hematization)

(2) albitisation with varying degrees of hematization, as a function of distance from the above mentioned quartz vein.

Plagioclase feldspars could not be recognised: any fine parallel twinning is obliterated, even in areas of minimal sericitisation. Rare muscovite pseudomorphs of biotite are evident.

Altered lithic / collapsed pumice fragments may be observed. the "more lithic" (in appearance" fragments occasionally contain altered feldspars up to 1 mm, and quartz crystals up to 1.5 mm. This alteration is homogeneous with that observed in the host rock.

The quartz vein possesses a sharply defined margin, and contains quartz crystals up to 1.5 mm. Colloform goethite associated with chalcedonic quartz may be identified at two locations within the vein. Aligned streaks of goethite possibly pseudomorph hematite; these are also local to the chalcedonic quartz. Later, thinner (0.1 mm) very fine grained quartz veins appear to have reintruded along the edges and within this vein.

Feldspars adjacent and proximal to the vein appear heavily hematized.

Phenocrysts

Quartz:	10-15%
Feldspars:	15%
Altered biotite:	<1%
Lithic / Pumice Fragments:	10-15%
Opaques:	<1%
Groundmass:	55-60%

Conclusion: A pumaceous crystal lithic rhyolitic tuff

Sample: A972-C122

Unit: Strongly welded tuff

Hand Specimen Description

Mottled orange-red / dark brown alkali feldspar = quartz phyric flow layered rhyolite.

Thin Section Description

The groundmass includes intimately associated cryptocrystalline quartz, alkali feldspar and hematite. Microcrystalline quartz bands are abundant delineating compactional layering and commonly drape around the phenocrysts present.

Quartz phenocrysts (up to 1.5 mm) display varying degrees of alignment to the layers, the degree of concordance increasing with decreasing phenocryst size. The crystals are only mildly embayed, in comparison to that observed within the porphyritic welded tuffs.

The feldspar population is comprised of alkali feldspars, (up to 1 mm) which have been moderately hematized. Sericitisation is rare, and confined to patches throughout the slide. As with the quartz, the smaller feldspars exhibit alignment to the layering.

Phenocrysts

Quartz:	10%
Alkali Feldspar:	10%
Groundmass:	80%

Conclusion: Crystal rhyolitic tuff, displaying a greater intensity of welding than the porphyritic tuff investigated previously.

Sample: A972-C48a

Unit: Brown flow banded rhy.

Hand Specimen Description

Flow layered / banded alkali feldspar > quartz phyric rhyolite. The matrix is a dark red-brown colour, with thin (~0.2 mm to 0.8 mm) brick red bands evident.

Thin Section Description

The groundmass consists of granular cryptocrystalline quartz and alkali feldspar, which display clear devitrification textures. Two types of layers are evident; one is comprised of spherulitically and axiolitically devitrified quartz and feldspar; the other of granular quartz and feldspar. The latter possesses a higher hematite content, making these layers appear dark red in hand specimen.

The phenocryst population consists of embayed quartz (up to 2 mm), with chloritised and sericitised feldspars.

Orthoclase commonly displays perthitic textures, commonly occurring as coarse (up to 0.1 mm) albite corridors within the host crystal. Chloritisation is common within the orthoclase, commonly being associated with sericitisation.

Plagioclase appears only to have suffered light sericitisation and hematisation, although this may be a biased interpretation as multiple twinning is difficult to recognise in even mildly altered crystals.

Rare clusters of rutile (to 0.3 mm) commonly associated with zircons (to 0.2 mm) are identified within the groundmass.

Fine disseminated pyrite to 0.1 mm is noted associated with sericite patches, and rarely in quartz phenocrysts.

Phenocrysts

Quartz:	5-10%
Plagioclase:	5%
Orthoclase:	15%

Zircon, rutile:	<1%
Groundmass:	75-80%

Conclusion: A flow banded rhyolitic tuff

Sample: A972-C23b

Unit: Brown flow banded rhy.

Hand Specimen Description

A dark red, flow banded alkali feldspar > quartz phyric rhyolite, with specks of green-white clay alteration.

Thin Section Description

The groundmass consists of intergrown cryptocrystalline quartz and alkali feldspar, and demonstrates flow banding via concordant anastomosing microcrystalline quartz layers 0.1 mm wide, and thicker (up to 3 mm) microcrystalline quartz and sericite bands, congruent with the above layers.

Quartz phenocrysts (up to 2 mm) occur both as embayed subhedral crystals and as fragments (up to 1 mm). Orthoclase crystals display relatively heavy hematization and coarse albitization, along with mild sericite and clay alteration.

Plagioclase crystals, rarely up to 2 mm wide, display coarse antiperthitic textures, along with speckle-like sericitization.

Phenocrysts

Quartz:	5-10%
Alkali Feldspar:	5-10%
Plagioclase:	1-3%
Groundmass:	80-85%

Conclusion: Quartz-alkali feldspar phyric tuff.

Sample: A972-S178

Unit: Rhyolite lava

Hand Specimen Description

A flow - banded, red / dark purple green clay altered volcanic. Small boxworks (up to 1 mm) are pervasive throughout the sample.

Thin Section Description

The groundmass has distinct flow banding, the bands alternating between cryptocrystalline quartz and sericite (generally 2 mm thick) interlayered with finely divided hematite rich, sericitised and axiolitically devitrified layers approximately 0.2 to 0.3 mm wide.

Subhedral quartz phenocrysts and fragments up to 1 mm wide are common, with embayments relatively rare in comparison to those slides examined previously. Feldspar crystals (up to 2 mm), have been heavily hematized and silicified. Most phenocrysts display parallel alignment to the flow bands.

Amygdales are common throughout the slide, playing host to quartz and sericite. Chalcedonic quartz, earthy hematite and possibly barite are also noted, although only in trace quantities.

Clay - chalcedonic quartz - limonite pseudomorphs of pyrite are disseminated throughout the rock, showing a preference for the finely divided hematite sericite flow layers.

Phenocrysts

Quartz :	10%
Alkali Feldspar:	5%
Groundmass:	80-85%
Amygdales:	1-3%

Disseminated Pyrite Pseudomorphs:

1%

Conclusion: A quartz-sericite altered rhyolitic lava.

Altered Volcanics

Sample: A972-96M

Zone: Vent Area, Halo 1

Hand Specimen Description

An altered, green - grey volcanic, with 2 mm quartz phenocrysts, and white feldspars up to 3 mm long.

Thin Section Description

The groundmass comprises intergrowths of cryptocrystalline quartz and feldspar, with abundant randomly orientated quartz and alkali feldspar shards and microlites. No layering is apparent.

Pseudomorphs of orthoclase are noted, with either very fine grained clay / quartz-sericite alteration, or sericitisation with goethite after pyrite. Perthitic textures are common within these crystals.

Occasional small (0.5 mm) crystals of both relatively fresh, and sericitised plagioclase are evidenced.

Quartz exists as embayed subhedral phenocrysts up to (2 mm diam.), as well as fragments. Rarely, some embayments play host to 50 µm wide euhedral pyrite grains.

Disseminated goethite pseudomorphs of pyrite are located throughout the groundmass, but are most commonly associated with the sericite pseudomorphs mentioned above.

Rare apatite fragments are noted, showing no sign of alteration.

Lithic fragments of microcrystalline (0.1 to 0.2 mm) intergrowths of quartz and altered feldspar occasionally possess similar minerals as phenocrysts. The intergrowths commonly display a granophyric habit, the quartz showing a spectacular branching morphology.

Phenocrysts

Quartz:	10-15%
Feldspar Pseudomorphs:	15%
Plagioclase:	1-3%
Lithic Fragments:	10%
Goethite:	1%
Groundmass:	60-65%

Conclusion: A quartz - sericite altered, crystal lithic rhyolitic tuff

Sample: A972-75M

Zone: Vent Area, Halo 1

Hand Specimen Description

Pink / grey mottled groundmass, altered rhyolite, with quartz phenocrysts, red and white feldspars. Most feldspars have been hematized or kaolinized.

Thin Section Description

The groundmass is comprised of cryptocrystalline intergrowths of quartz, sericite after alkali feldspar, and kaolinite. Layering is convoluted and discontinuous, and distinguished by the preferential sericitisation and kaolinisation of different groundmass layers, and commonly enveloping phenocrysts.

Quartz phenocrysts (up to 3 mm diameter) display both embayed subhedral and fragmental habits. Embayment is relatively intense in this slide. Some crystals display in situ fracturing.

Sericite / kaolinite / quartz pseudomorphs of feldspars (up to 2 mm diam.) with occasional hematization are evident. In the less altered alkali feldspars, albitisation is commonly recognisable.

Lithic fragments (up to 1 cm diam.) are characterised by microcrystalline quartz and sericite intergrowths, along with occasional quartz phenocrysts and sericite pseudomorphs of feldspars.

Occasional muscovite pseudomorphs of (presumably) actinolite after pyroxene, and muscovite pseudomorphs of biotite are noted.

Rare, thin quartz veinlets (0.1 up to 0.2 mm) crosscut sericitised feldspars.

Phenocrysts

Quartz:	10-15%
Sericite P'morphing feldspars:	15%
Altered biotite, pyroxene:	<1%
Lithic Fragments:	10%
Groundmass:	60%

Conclusion: Quartz - sericite - kaolinite altered welded crystal lithic tuff

Sample: A972-86MA

Zone: Vent Area, Halo 2

Hand Specimen Description

This rock is an obviously altered, quartz - alkali feldspar phyric rhyolite. The alteration is indicated by the sample's fawn - olive green mottled groundmass.

Thin Section Description

The matrix consists of cryptocrystalline sericite altered banded masses of (presumably) alkali feldspar and quartz. Numerous quartzitic shards and sericitised feldspar microlites are aligned with this banding.

Embayed subhedral quartz phenocrysts up to 2 mm are common, along, with smaller quartz fragments. The phenocrysts are rarely fractured.

The feldspars have been obliterated by a fine grained aggregate of sericite kaolinite and hematite, although relict shapes are still recognizable. Original phenocryst dimensions are estimated to be up

to 3 mm diameter, the majority being ~ 1 mm in size. Rare euhedral apatite grains up to 1 mm size can be found.

Lithic fragments are evident, up to 1.5 mm across, although most are ~2 mm average. These fragments are characterised by microcrystalline intergrowths of quartz and (originally) feldspars, and have undergone a similar alteration to the host rock.

Rare muscovite and leucoxene pseudomorphs of biotite are apparent.

Phenocrysts

Quartz:	15%
Feldspars:	15%
Altered biotite:	<1%
Lithic Fragments:	20%
Groundmass:	50 - 55%

Conclusion: a quartz - sericite altered lithic rhyolitic tuff

Sample: A972-ST7

Zone: Vent Area, Halo 2

Hand Specimen Description

A light green, white feldspar > quartz phyric rhyolite. The quartz phenocrysts appear angular. A 2 cm diameter, quartz + sericite altered lithic fragment is present.

Thin Section Description

The groundmass consists of cryptocrystalline quartz, feldspar and sericite, with an obvious flow / compaction layering. This layering warps around all phenocrysts and lithic fragments present, and controls the preferential alignment of quartz and feldspar microlites.

Quartz phenocrysts (up to 3 mm) are present both as embayed subhedral and fragmental bodies, the latter also aligned to the compactional fabric.

Alkali feldspars (up to 2 mm) are also subhedral and fragmental, and have been coarsely albitised. Sericitisation is the predominant alteration species within these crystals, along with minor hematisation and kaolinisation.

Plagioclase feldspars (where recognisable) are up to 1 mm in diameter.

Occasional lithic fragments can be distinguished, and consist of fine-grained intergrowths of (now altered) feldspar and quartz. As with A972-121M, lensoidal, commonly spherulitic bodies can also be found, again possibly indicating the presence of collapsed pumice fragments.

A 1.5 cm lithic fragment is present, displaying easily identifiable banding. This banding is characterised by alternating, 0.1 up to 1 mm wide quartz and earthy clay - like layers. It is probable that the altered layers originally possessed a feldspar component, thus leading to their preferential alteration. (Microprobe analysis reveals a fine grained aggregate of quartz, sericite and kaolinite.) The fragment is possibly a lava.

Phenocrysts

Quartz:	15%
Feldspars:	15%
Lithic / Pumice Fragments:	25%
Opagues:	<1%
Groundmass:	45%

Conclusion: Altered pumaceous crystal lithic rhyolitic tuff

Sample: A972-5M

Zone: Vent Area, Halo 2

Hand Specimen Description

An alkali feldspar > quartz phyric rhyolite. The groundmass of this specimen is brown, with red feldspar phenocrysts (up to 2 mm) > quartz (up to 2 mm). Red / brown lithic fragments are observable.

Thin Section Description

The groundmass of this specimen is typical of the other, less altered specimens of this area described previously. It consists of cryptocrystalline quartz and alkali feldspar, with trachytic quartz and alkali feldspar microlites outlining a layering. This layering is less evident in this sample than other samples examined.

Quartz phenocrysts (rarely up to 2 mm) display both embayed subhedral, and fragmental habits, the latter in greater abundance. Embayment is relatively intense.

Orthoclase (rarely up to 2 mm) displays both euhedral, subhedral and fragmental habits, and is also commonly microlitic. Albitisation in most of these crystals are noted, along with hematization and sericitization.

Plagioclase feldspars (commonly up to 1.5 mm) display similar modes of occurrence and alteration to the orthoclase crystals. Rare fragmental apatite (up to 1.5 mm lengths) is present, minimally altered.

Lithic fragments up to 1cm across are distinguishable. These possess quartz and alkali feldspar phenocrysts up to 2 mm diameters, and on average are larger than their host rock equivalents. Further, alteration is more intense in these fragments, with rare sericite tending to muscovite.

Disseminated goethite pseudomorphing pyrite crystals (up to 0.3 mm across) are evidenced. Where sericite coarsens to muscovite in one lithic fragment, goethite is intergrown with the muscovite flakes.

Phenocrysts

Quartz:	10-15%
Orthoclase:	15%
Plagioclase:	2-5%
Opagues:	<1%
Groundmass:	60-65%
Altered Biotite:	<1%

Lithic Fragments: 10%
Groundmass: 60-65%

Conclusion: Altered (predom. sericitic) crystal lithic rhyolitic tuff.

Sample: A972-85M

Zone: Vent Area, Halo 2

Hand Specimen Description

An intensely altered, white quartz phyric rhyolite. The white groundmass colour is undoubtedly the result of alteration, probably silicification and kaolinisation. Occasional rounded quartz phenocrysts (up to 2 mm diameter) can be found. Erratic limonite stringers are apparent.

Thin Section Description

The groundmass consists of cryptocrystalline quartz and sericite, the latter presumably after alkali feldspar. Occasional quartz sericitised feldspar microlites are visible. No apparent preferred orientation may be observed.

Quartz phenocrysts are predominantly rounded subhedral, and commonly display microfractures. Very fine grained pyrite crystals are located within quartz crystal embayments.

There are no feldspars visible; all have been sericitised. The intensity of sericitisation may be gauged by the common coarsening of the sericite to muscovite. Within these pseudomorphs, goethite flakes (and limonite stringers) are intergrown within the muscovite.

Goethite disseminations and veinlets pseudomorphing pyrite are abundant, the veinlets showing no preferred orientations.

Phenocrysts

Quartz: 10%
Sericite P'morphing F'spar: 10-15%

FeO Phases: 1-3%
Groundmass: 75%

Conclusion: A quartz-sericite altered rhyolite tuff.

Sample: A972-86M

Zone: Vent Area, Halo 3

Hand Specimen Description

Silicified / kaolinised ? volcanic. Only rounded quartz phenocrysts remain, and red iron oxide stringers are pervasive through the sample. Fine boxworks (just visible) are disseminated through the sample.

Thin Section Description

The groundmass is a banded, cryptocrystalline to microcrystalline intergrowth of quartz and sericite. Quartz is distinctly more abundant than sericite.

Quartz phenocrysts (rarely up to 2 mm) display both embayed subhedral and fragmental habits. Embayments are more abundant in this slide compared with previous slides. This, coupled with the elevated quartz abundance in the groundmass suggests silicification of this rock has occurred.

Cryptocrystalline quartz masses pseudomorphing feldspars (up to 2 mm long) indicate silicification to be the dominant mode of alteration here.

Numerous limonite stringers associated with vein goethite pseudomorphing pyrite are present throughout the specimen. These vary between ~ 0.1 and 0.4 mm thickness. The majority of these appear to be subperpendicular to the flow banding, the remainder being parallel to it. Disseminated colloform goethite (up to 0.02 mm), pseudomorphing pyrite is also pervasive throughout the sample.

Occasionally, quartz veinlets (up to 0.2 mm) are observed crosscutting the flow banding at ~ 45°. These appear to predate the pyrite (now goethite) veining episodes.

Phenocrysts

Quartz:	10%
Feldspar Pseudomorphs:	10%
FeO Phases:	10%
Groundmass:	70%

Conclusion: Intensely silicified rhyolitic tuff

Sample: A972-31M

Zone: Vent Area, Volcanic Breccia

Hand Specimen Description

Brecciated, silicified rock. Clasts (up to 2 cm) are subangular to subrounded, grey and contain quartz phenocrysts up to 2 mm. Iron hydroxide coated, white clay filled fractures separate the clasts.

Thin Section Description

The clasts in this sample are primarily defined by the presence of porous iron hydroxide filled fractures. Further, the clasts possess weak banding, which is truncated at the clast edges, thus aiding in their identification.

Clast mineralogy is characterised by angular and embayed subhedral quartz and obliterated feldspars in a layered / banded altered groundmass. The feldspars are now pseudomorphed by a fine - grained aggregate of quartz, sericite and kaolinite, and a similar alteration suite is noted within the groundmass.

Interstitial to the clasts, angular quartz fragments (up to 1 mm), altered rock fragments (up to 2 mm) and disseminated goethite crystals after pyrite (up to 0.2 mm) are noted within an altered matrix. Rare 0.1 mm wide pyrite euhedra are distinguished within this area.

Goethite veinlets after pyrite are commonly observed within the iron hydroxide stained fractures surrounding the clasts, as well as rare stringers passing erratically through the areas interstitial to the clasts.

Rare disseminated goethite (again after pyrite) is occasionally located within sericite pseudomorphs of feldspars.

Clast components		Interstices	
Quartz:	5-10%	Quartz Fragments:	10%
Feldspar Pseudomorphs:	10-15%	Feldspar Pseudomorphs:	10%
Goethite:	<1%	Pyrite:	<1%
Pyrite:	<1%	Groundmass:	80%
Groundmass:	75-80%		

Conclusion: A quartz - sericite - kaolinite altered rhyolitic breccia.

Sample: A972-S174

Zone: Zone 1 Altered Volcanics

Hand Specimen Description

Intensely silicified, pink/white fragment rich rock, demonstrating a weak layering.

Thin Section Description

This sample possesses intensely silicified fragments and groundmass. The groundmass consists cryptocrystalline to microcrystalline quartz and sericite, with a minor clay component. Finely divided hematite is pervasive throughout.

Three fragment populations exist. Population 1 displays complete silicification and minor sericite-clay alteration, with relict flow banding easily visible under normal light due to the variation in hematite content. These fragments are generally angular, and range in size from <1 mm to 5 mm. Population 2 consists of more heavily hematized, subangular lithic fragments with little silicification noted. These demonstrate spectacular spherulitic devitrification textures, and also possess quartz

and alkali feldspar phenocrysts (up to 0.7 mm). These fragments are relatively rare. Population 3 is comprised of variably angular alkali feldspar, plagioclase and quartz phenocrysts between 0.3 mm and 0.8 mm in size. Feldspars display light to moderate hematisation, and are occasionally completely replaced by sericite; alkali feldspars are commonly albitised.

Rare disseminated colloform goethite pseudomorphs of pyrite crystals are evident, rarely up to 0.1 mm.

Fragments

Population 1:		30%
Population 2:		1%
Population 3:	-Quartz:	5%
	-Alkali Feldspar:	5%
	-Plagioclase:	1-2%
Goethite pseudomorphs of pyrite:		<1%

Conclusion: A quartz-sericite-clay altered rhyolitic agglomerate.

Sample: A972-C134

Zone: Quartz-Hematite Breccia

Hand Specimen Description

A quartz vein brecciated, quartz > feldspar rhyolite porphyry. two sets of veins are apparent. One set consists of two perpendicular vein sets of hematite bearing quartz, the other set is characterised by a veins orientated at 45° to the earlier vein sets, apparently barren.

Thin Section Description

The rock brecciated in this sample is flow layered, as indicated by aligned quartz and hematite bands amongst a homogeneous cryptocrystalline quartz / sericite / hematite groundmass.

Subhedral quartz crystals and fragments (up to 2 mm) display appreciable embayment, occasionally along quartz crystal growth lines; rare in situ fracturing is noted.

Feldspar phenocrysts (up to 2 mm) distal from the quartz veins are mildly hematized and sericitized, making identification of plagioclase difficult. Those feldspars proximal to the quartz veins are almost completely obliterated by sericitization, the sericite commonly coarsening to muscovite. Sericitization is also intense along rare bands of spherulitic devitrification.

The quartz veins, as mentioned above, may be divided into two sets. Set 1 consists of 2 orthogonal subsets of quartz veins, hosting an abundance of thin blades of specular hematite. Rare areas of colloform goethite surrounding chalcedonic quartz are also present, along with minor sericite. Set 2, veins although not well represented in the thin section, are characterised by greater thickness and 45° orientation to Set 1 veins. This set appears to crosscut Set 1 veins, and contains substantially less hematite.

Brecciated Rock		Set 1 Vein Mineralogy	
Quartz Phenocrysts:	10%	Microcrystalline Quartz:	80-85%
Feldspar " " :	10-15%	Chalcedonic Quartz:	1%
Groundmass:	75-80%	Specular Hematite:	10-20%
		Goethite:	<1%
		Sericite:	1-5%

Conclusion: A quartz-hematite breccia.

Sample: A972-C141

Zone: Chloritic Microbreccia

Hand Specimen Description

An alkali feldspar > quartz phytic volcanic. The groundmass appears dark green, commonly infilling fractures within the relatively large (up to 2 cm) red alkali feldspar phenocrysts.

Thin Section Description

Thin section examination immediately reveals the brecciated nature of this sample. Large alkali feldspar and quartz phenocrysts up to 1cm in length display in situ fragmentation and

microbrecciation, with chlorite and clay filling the interstices. Alkali feldspar phenocrysts (orthoclase) commonly display a distinct perthitic texture (albitic), while both alkali and plagioclase feldspars demonstrate cross-hatched clay alteration.

The brecciated matrix of this sample consists of unsorted angular to subrounded quartz and feldspar fragments amongst microcrystalline to cryptocrystalline chlorite and clay.

Fractures (rarely 0.2 mm wide) display both an abundance of microcrystalline chlorite and goethite. No textural clues are available to suggest as to whether the goethite has replaced any iron phase.

Phenocrysts

Quartz:	25-30%
Alkali feldspar:	20%
Plagioclase:	5%
Breccia Matrix:	45-50%
Goethite:	<1%

Conclusion: A chloritic microbreccia.

Sample: A972-C143

Zone: Chloritic microbreccia

Hand Specimen Description

Pink / Brown, altered quartz = alkali feldspar phyric rhyolite. Phenocrysts display abundant microfractures.

Thin Section Description

This sample bears a strong resemblance to the chloritic microbreccia, in regard to both the fragmental fabric and the phenocryst population. However, hydrothermal biotite, rather than chlorite, resides in the interstices of the phenocryst / groundmass fragments. Spherulitic

devitrification textures are common, along with plagioclase phenocrysts. Partially filled vesicles are also present, exhibiting an abundance of biotite and limonite.

Phenocrysts

Quartz:	15-20%
Alkali Feldspar:	15%
Plagioclase:	10%
Microcrystalline Fragments:	30%
Hydrothermal Biotite:	25%
Limonite:	<1%
Vesicle:	1%

Conclusion: A biotitic microbreccia

Sample: A972-S10

Zone: Zone 2 Altered Volcanics

Hand Specimen Description

An altered, fragment rich volcanic. Clasts are sericitised/chloritised, with a fine grained red groundmass.

Thin Section Description

This rock is heavily altered; relict spherulitic devitrification textures are almost all that remain of the original volcanic features. The groundmass, which comprises 90% of this lithology, consists of very fine grained quartz with disseminated clays. Rare feldspars demonstrate hematisation and sericitisation, and are occasionally crosscut by quartz veins.

Clasts, completely altered to clays, display angular morphologies and infrequently possess feldspar phenocrysts.

Boxworks of limonite pseudomorphing euhedral pyrite crystals (rarely up to 0.5 mm) are either associated with quartz veins, or are disseminated throughout the groundmass.

Feldspar Phenocrysts:	<5%
Groundmass	
Quartz:	50%
Clays:	30%
Quartz Veins:	<5%
Limonite:	<1%
Clasts:	10%

Conclusion: A quartz-clay altered volcanic agglomerate.

Sample: A972-S92

Zone: Zone 2 Altered Volcanics

Hand Specimen Description

A brick red, heavily altered volcanic. Fine stringers of quartz are pervasive throughout the rock, along with patches of green clay alteration.

Thin Section Description

Immediately evident in this slide is the abundance of finely divided hematite within the groundmass (giving the rock its red colour) and the abundance of thin (0.5 mm to 1.5 mm wide), erratic quartz veinlets. Other components of the groundmass probably include quartz and sericite, with most feldspar obliterated during alteration.

Phenocrysts of any type are rare in this rock; no quartz crystals are distinguished (although some may be obscured by the quartz veinlets) and feldspar phenocrysts (hematised and up to 1 mm) are infrequent. The green clay patches mentioned in the hand specimen description are identified as sericitised alkali feldspars, also notably hematised and silicified.

Feldspar Phenocrysts:	1-3%
Sericitised Feldspars:	1-3%

Groundmass: 70%
Quartz Veinlets: 25%

Conclusion: A quartz-sericite altered volcanic, probably originally rhyolitic.

Drill Core Mineralisation

Sample: A972-GI104.1

Location: Gib. I drill core, 104.1m

Hand Specimen Description

A red-brown, quartz > feldspar phyrlic rhyolite. A pyrite-bearing sericite vein cuts through the sample, parallel to the banding. Abundant disseminated pyrite is noted in the proximity of the veins.

Thin Section Description

The groundmass in this sample consists of cryptocrystalline quartz and feldspar, possibly with minor sericite. Weak compactional layering is indicated by thin bands of microcrystalline quartz, commonly contorted around phenocrysts.

Quartz phenocrysts occur both as mildly embayed, fractured subhedral crystals and as fragments up to 1 mm wide. Alkali feldspar phenocrysts are more abundant than quartz phenocrysts, displaying minor hematization and sericitization.

A zone of sericitic microbrecciation cuts through the sample, playing host to subhedral aggregates of pyrite which themselves exhibit a microbrecciated morphology. Inclusions of sphalerite, galena, chalcopyrite and pyrrhotite, are noted, up to a maximum of 0.05 mm in size.

Euhedral pyrite (up to 1 mm) is pervasive throughout the sample, rarely associated with local aggregates of rutile and zircon (up to 0.04 mm).

Phenocrysts

Quartz:	1-3%
Alkali Feldspar:	5-10%
Groundmass:	75-80%

Sericite:	5%
Pyrite:	5%
Chalco., Sphal., Pyrrh., Gal.,	<1%
Rutile-Zircon Aggregates:	<1%

Conclusion: A mildly altered rhyolitic crystal tuff, containing minor sulphide minerals.

Sample: A972-GI107.7

Location: Gib. I drill core, 107.7 m

Hand Specimen Description

A light brown, slightly silicified, quartz > feldspar phyric rhyolite, containing disseminated and vein hosted pyrite. Veins appear to consist of quartz and sericite / clay.

Thin Section Description

The groundmass in this volcanic is a silicified mass of quartz and sericite, with abundant quartz rich bands presumably defining relict compaction layering.

Large embayed subhedral quartz phenocrysts (up to 4 mm) display in situ fragmentation, smaller quartz fragments demonstrating preferential alignment to the layer fabric. Feldspar phenocrysts (up to 1 mm) are variably hematized and sericitized, rarely displaying chloritization. No plagioclase is discerned, possibly due to this alteration.

Patches of leucoxene (up to 0.5 mm) are spotted throughout the section, frequently associated with zircons.

Disseminated euhedral pyrite (up to 1 mm) is abundant, commonly observed within feldspar phenocrysts.

Minor amounts of brecciated and euhedral pyrite, rarely 0.5 mm wide, reside within quartz and sericite veins. These veins crosscut each other, and are pervasive throughout the section, exhibiting widths of up to 0.5 mm.

Phenocrysts	
Quartz:	5-10%
Feldspar:	3-5%
Groundmass:	80-85%
Quartz-sericite veinlets:	3-5%
Disseminated pyrite:	3-5%
Vein Pyrite:	<1%
Leucoxene and zircon:	<1%

Conclusion: A silicified, pyrite bearing rhyolite.

APPENDIX 2

WHOLE ROCK ANALYSES

MAJOR AND TRACE ELEMENT GEOCHEMISTRY

A. Personally Prepared Samples (Table A2.1, 2.2)

SAMPLE PREPARATION AND ANALYSIS

1. Samples were broken down using a geopick to remove weathered surfaces, and to reduce their size for jaw crushing (5-8 cm diameter).
2. Reduced samples were then crushed to sub-centimetre size via a Sturtevant jaw crusher.
3. Crushed samples were powdered using a Siebtechnik tungsten carbide mill.
4. For trace element analysis, 5g of this powder was combined with a binder solution and compressed into a pellet ready for X-ray spectrometry.
5. For major element analysis, 3-4g of powder was ignited overnight at 960° C and loss on ignition recorded. 1g of this ignited powder was then mixed evenly with 4g of flux, finally being fused together into a glass disc for X-ray spectrometry.
6. Trace and major element concentrations were investigated using a Phillips PW1480 X-ray spectrometer.

(i) Trace elements analysed include Ba, Ce, Cr, Cu, Ga, La, Nb, Nd, Ni, Pb, Rb, Sc, Sr, Th, U, V, Y, Zr.

(ii) Major elements analysed include Al₂O₃, CaO, FeO, K₂O, MgO, MnO, Na₂O, P₂O₅, SiO₂, TiO₂, SO₃.

Results are presented in table A overleaf. Note that "*" implies data from SADME (Dubowski, 1992).

B. Analyses provided by SADME (Table A2.3)

Analyses of these rock samples were conducted at Amdel.

A number of geochemical analyses were provided by SADME before and during the course of this study. These results are presented in table B.

Table A2.1 - Fresh Outcrop Volcanics

Sample No.:	972-GC1	972-GC3	972-GC5	972-GC6	972-GC11	972-GC27	972-GC38	972-GC42
Location or Unit	Porph. Weld. Tuff	Porph. Weld. Tuff	Porph. Weld. Tuff	Porph. Weld. Tuff	Porph. Welded Tuff	Porph. Weld. Tuff	porph. weld. tuff	Brown F.B. Rhyolite
Maj. El (%)								
SiO ₂	76.5	75.77	75.47	76.61	75.94	76.53	76.22	77.97
Al ₂ O ₃	12.93	12.81	13	13.06	12.97	13.16	12.82	11.57
Fe ₂ O ₃ T	1.11	1.06	0.94	0.65	0.96	0.6	0.95	1.01
MnO	0.03	0.02	0.02	0.02	0.03	0.02	0.05	0.02
MgO	0.21	0.22	0.2	0.21	0.19	0.14	0.21	0.14
CaO	0.23	0.27	0.18	0.32	0.33	0.26	0.44	0.09
Na ₂ O	2.74	2.71	2.24	2.49	3.19	2.66	3.07	1.49
K ₂ O	5.33	5.35	5.58	5.15	5.06	5.51	5.27	6.73
TiO ₂	0.15	0.14	0.15	0.15	0.15	0.16	0.15	0.13
P ₂ O ₅	0.02	0.02	0.02	0.02	0.02	0.01	0.02	0.02
SO ₃	0	0	0	0.01	0	0	0	0
LOI	0.69	0.67	0.83	0.95	0.69	0.8	0.57	0.61
Total	99.94	99.04	98.63	99.64	99.53	99.86	99.76	99.78
Tr. El (ppm)								
Ga	15.7	17	18.4	16.7	No Data	16.8	16.7	17.4
Cu	3	1	0	2	No Data	2	3	8
Zn	25	30	19	28	No Data	12	28	24
Ni	0	5	0	0	No Data	0	0	0
Ba	295	323	382	864	No Data	384	255	783
Sc	1.3	1.6	1.3	2.4	No Data	2.5	1.6	0.9
Cr	24	44	22	23	No Data	25	25	23
V	5.1	3.7	7	7.1	No Data	6.9	6.3	6.1
Co	72.3	64.7	51.5	78.9	No Data	68.5	80.2	65.9
Ce	106	104	119	92	No Data	99	99	125
Nd	39	35	40	31	No Data	34	33	53
La	67	61	69	51	No Data	51	59	67
Y	21.1	24	23.2	21.9	No Data	22.1	23.7	29.1
Sr	64.3	77.7	61.3	104.4	No Data	93.6	66.8	79.5
Rb	180	181.6	209	171.7	No Data	186.2	180.1	268.5
Nb	14.1	15.7	15.4	14.3	No Data	15.1	14.9	13.7
Zr	129	125.9	133.9	126.8	No Data	134.9	127.5	120.3
Th	24.5	25.3	28.3	24.4	No Data	25.6	24.7	22.1
Pb	61.3	37.4	36.7	39	No Data	29.6	27.2	44.9
U	4.4	4.3	5	4	No Data	4.1	4.1	3.5
Mo	0.5	0.4	0.9	0.6	No Data	3.3	1	1.3
CIPW Norm								
qtz	39.04	38.36	40.17	41.34	36.79	39.11		42.88
ort	31.45	31.56	32.96	30.4	29.89	32.51		39.75
ab	23.18	22.92	18.93	21.03	26.96	22.5		12.59
an	1.05	1.24	0.8	1.49	1.52	1.28		0.35
ne	0.52	0	0	0	0	0		0
hy-en	0.83	0.54	0.49	0.52	0.47	0.34		0.34
hy-fs	0	0.77	0.65	0.37	0.69	0.3		0.74
mt	0.46	0.44	0.39	0.28	0.42	0.25		0.42
hm	0	0	0	0	0	0		0
il	0.27	0.26	0.27	0.27	0.27	0.3		0.24
ru	0	0	0	0	0	0		0
cor	2.28	2.11	2.99	2.84	1.7	2.36		1.71
ap	0.03	0.03	0.03	0.03	0.033	0		0.03

Table A2.1 - Fresh Outcrop Volcanics

Sample No.:	972-GC43	972-GC45	972-GC48	972-GC50	972-GC51	RS 1089*
Location or Unit	Porph. Weld. Tuff	Brown F.B. Rhyolite	Rhyolite Lava	Stongly Weld. Tuff	Strongly Weld. Tuff	Black Glassy Rhy.
Maj. El (%)						
SiO ₂	76.54	70.22	81.77	77.6	77.82	76.5
Al ₂ O ₃	12.58	14.03	9.25	12.13	12.15	12
Fe ₂ O ₃ T	0.92	3.56	1.37	0.79	1.14	2.62
MnO	0.02	0.07	0.07	0.01	0.01	0.02
MgO	0.14	0.37	0.22	0.12	0.11	0.15
CaO	0.2	0.33	0.05	0.1	0.09	0.12
Na ₂ O	2.53	3.18	0.13	3.28	3.26	4.1
K ₂ O	5.83	6.4	5.25	4.59	4.82	3.89
TiO ₂	0.14	0.45	0.15	0.08	0.08	0.07
P ₂ O ₅	0.02	0.11	0.03	0.01	0.01	0.01
SO ₃	0	0	0.02	0	0	no Data
LOI	0.59	0.92	1.05	0.66	0.53	0.5
Total	99.52	99.63	99.37	99.37	100.01	99.98
Tr. El (ppm)						
Ga	15.9	20.3	16.2	20.6	23.5	
Cu	2	2	41	4	4	10
Zn	26	51	146	21	26	20
Ni	1	2	0	0	0	<5
Ba	460	916	1760	250	221	89
Sc	2.1	8.8	4.5	1.6	2.1	2
Cr	24	23	20	29	29	20
V	6	6.2	12.3	4.5	3.6	2
Co	50.2	58	68.1	89.6	76.3	<5
Ce	103	143	178	17	21	49
Nd	37	63	52	7	7	20
La	61	75	63	6	7	26
Y	26	52.4	132.8	41.3	52.8	54
Sr	56.8	69	43.4	35.9	33.6	48
Rb	225.9	206.1	275.3	234.9	260.9	No Data
Nb	16.1	17.7	19.2	27.9	28	22
Zr	120.3	587.7	265.3	224.9	226.1	263
Th	27.3	19.3	29.9	25.6	25.4	33
Pb	31.6	23.6	362.7	17.5	21.8	<5
U	4.6	4.6	6.2	2.6	4.5	2
Mo	0.2	1.3	5.1	1.4	0.8	No Data
CIPW Norm						
qtz	38.67	25.08		40.31	39.7	36.1
ort	34.4	37.8		27.11	28.45	22.94
ab	21.39	26.91		27.74	27.54	34.67
an	0.88	0.96		0.47	0.45	0.58
ne	0	0		0	0	0
hy-en	0.34	0.91		0.29	0.27	0.37
hy-fs	0.63	2.63		0.61	0.91	2.7
mt	0.39	1.53		0.32	0.49	1.09
hm	0	0		0	0	0
il	0.26	0.85		0.15	0.15	0.12
ru	0	0		0	0	0
cor	1.79	1.52		1.59	1.42	0.84
ap	0.03	0.24		0	0	0

Table A2.2 - Altered Volcanics

Sample No:	972-GC2	972-GC4	972-GC7	972-GC9	972-GC10	972-GC12	972-GC15	972-GC16
Location or zone	Vent Area	Vent Area	Vent Area	Vent Area	Vent Area	Vent Area	Vent Area	Vent Area
Maj. El (%)								
SiO ₂	82.85	77.88	76.63	79.13	79.51	76.35	77.39	78.67
Al ₂ O ₃	10.57	12.03	12.66	12.2	12.85	12.76	13.11	12.96
Fe ₂ O ₃ T	1.44	0.3	0.92	0.25	0.87	0.87	0.6	2.08
MnO	0.04	0.03	0.01	0.02	0.03	0.04	0.03	0.02
MgO	0.12	0.16	0.2	0.09	0.11	0.19	0.18	0.16
CaO	0.03	0.28	0.04	0.12	0.03	0.08	0.04	0.04
Na ₂ O	0.05	0.24	0.31	0.18	0.1	1.24	0.43	0.08
K ₂ O	3.18	6.19	6.02	5.87	3.88	5.44	5.66	3.67
TiO ₂	0.12	0.16	0.16	0.16	0.15	0.16	0.15	0.16
P ₂ O ₅	0.01	0.01	0.02	0.01	0.01	0.02	0.01	0.02
SO ₃	0	0.03	0.03	0.02	0	0.01	0.04	0
LOI	1.62	1.79	1.45	1.37	1.78	1.37	1.58	1.86
Total	100.03	99.11	98.45	99.43	99.33	98.52	99.24	99.73
Tr. El (ppm)								
Ga	17.5	16.8	17.7	17.3	16.7	No Data	16.6	16.6
Cu	18	2	1	2	0	No Data	1	5
Zn	15	12	15	10	13	No Data	13	9
Ni	1	2	2	0	2	No Data	3	0
Ba	65	1294	1568	1060	230	No Data	1588	82
Sc	3.5	2.2	1.5	1.9	2.3	No Data	1.8	2.8
Cr	29	30	29	25	28	No Data	30	23
V	6.9	9.2	7.8	9	7.4	No Data	6.1	8.6
Co	37.6	62.9	52.7	60.9	50.7	No Data	40.7	51.2
Ce	53	74	81	81	47	No Data	80	55
Nd	21	27	26	27	16	No Data	26	19
La	25	43	43	45	25	No Data	50	29
Y	40.3	19.8	20.6	18	19.2	No Data	20.8	18.3
Sr	5	141.6	60	64.8	13.7	No Data	48.9	6
Rb	136.5	214.2	217.8	188.1	164.4	No Data	224.1	145.9
Nb	16.3	15.4	15.4	14.9	14.1	No Data	16.3	15.2
Zr	180.8	144.3	139.5	134.7	133.5	No Data	133.2	137.2
Th	21.5	25.6	28.8	24.2	24.6	No Data	26.1	23.5
Pb	10.8	27.2	26.8	23.6	16.9	No Data	88.6	12.3
U	5.7	2	2.1	3.9	3.8	No Data	3.7	3.6
Mo	1.1	1.3	1	2.3	0.5	No Data	1.1	4.1

Table A2.2 - Altered Volcanics

Sample No:	972-GC17	972-GC18	972-GC19	972-GC21	972-GC23	972-GC26	972-GC31	972-GC32
Location or zone	Vent Area	Vent Area	Vent Area	Vent Area	Vent Area	Vent Area	Alt. Volcs. Zone 2	Alt. Volcs. Zone 2
Maj. El (%)								
SiO ₂	79.3	78.5	82.48	76.63	79.35	82.71	76.69	77.34
Al ₂ O ₃	12.74	13.55	12.43	11.94	12.19	10.64	12.06	12.61
Fe ₂ O ₃ T	1.08	0.9	0.56	0.39	1.88	1.19	1.17	1.07
MnO	0.02	0.03	0	0.1	0.02	0.01	0.02	0.03
MgO	0.15	0.13	0.07	0.59	0.23	0.11	0.15	0.26
CaO	0.04	0.03	0.02	0.41	0.05	0.03	0.18	0.07
Na ₂ O	0.07	0.1	0.07	0.12	0.09	0.1	2.08	1.45
K ₂ O	3.64	4.02	1.45	5.85	3.5	2.91	5.62	5.45
TiO ₂	0.15	0.16	0.15	0.16	0.26	0.13	0.18	0.18
P ₂ O ₅	0.02	0.01	0.02	0.02	0.02	0.05	0.03	0.01
SO ₃	0.01	0	0	0.01	0	0	0	0.01
LOI	1.82	1.85	2.12	2.47	1.9	1.61	1.1	1.38
Total	99.04	99.29	99.37	98.7	99.51	99.48	99.29	99.86
Tr. El (ppm)								
Ga	16.8	17.1	15.4	17.2	19.8	18.5	20.3	17.2
Cu	2	2	5	2	5	4	1	1
Zn	7	10	6	19	11	7	80	31
Ni	-1	0	-2	3	3	1	-3	0
Ba	146	137	251	689	211	151	887	560
Sc	2.6	2.7	1.2	1.9	5	3.1	6.1	2.5
Cr	25	27	23	27	33	25	18	27
V	7.2	8.6	7.1	9.8	9.2	4.5	6	5.1
Co	75	60.3	74.8	71.6	29.3	50.3	81	55.2
Ce	61	24	74	50	45	31	146	50
Nd	18	9	23	14	18	11	59	17
La	39	13	43	35	19	17	73	27
Y	18.7	16.6	16.2	16.2	51	39.7	57.1	24.2
Sr	10.2	7.6	11.9	75.2	10.4	11.7	63	56.8
Rb	140.6	172.7	67.8	198.1	188.2	153.1	245.7	267.5
Nb	15	15.5	14.8	15.8	26.3	24.7	22	18
Zr	134.1	137.2	133.9	142	290.7	220.1	321.7	175.2
Th	24.6	25.9	25.2	25.2	28.3	28	30.1	29
Pb	44.6	9.7	11.2	44.9	11	26.6	50.6	107
U	2.4	3.7	3.4	2.7	5.1	4.7	6.5	4.8
Mo	1.1	1.2	0.5	1.8	4.1	2.9	8.6	2.2

Table A2.2 - Altered Volcanics

Sample No:	972-GC33	972-GC34	972-GC36	972-GC44	972-GC46	972-GC53
Location or zone	Alt. Volcs. Zone 2	Alt. Volcs. Zone 2	Alt. Volcs. Zone 2	Quartz Breccia	Qtz-Ser Rock	Chl. M'breccia
Maj. El (%)						
SiO ₂	77.3	74.91	75.45	79.35	75.03	73.68
Al ₂ O ₃	12.52	13.92	13.26	10.3	13.81	12.99
Fe ₂ O ₃ T	1.08	0.93	1.15	3.03	1.25	2.74
MnO	0.03	0.02	0.04	0.14	0.05	0.11
MgO	0.14	0.16	0.23	0.27	0.24	0.62
CaO	0.06	0.08	0.05	0.04	0.09	0.34
Na ₂ O	1.45	1.59	0.13	0.1	1.64	3.04
K ₂ O	5.63	6.69	7.06	3.66	5.99	5.17
TiO ₂	0.18	0.19	0.3	0.18	0.21	0.28
P ₂ O ₅	0.01	0.01	0.02	0.03	0.02	0.07
SO ₃	0	0	0.01	0.01	0.01	0
LOI	1.19	1.36	1.48	1.78	1.33	0.91
Total	99.59	99.86	99.17	98.89	99.67	99.94
Tr. El (ppm)						
Ga	18.7	18.1	18.4	19.8	19.9	15.7
Cu	3	3	5	52	3	24
Zn	36	22	35	234	29	105
Ni	-1	0	1	1	4	13
Ba	338	440	2111	1178	1178	732
Sc	2	3.2	5.5	3.4	2.7	4.8
Cr	23	25	24	16	25	22
V	5.3	6.3	14.9	14.7	10.1	17.5
Co	69.7	57.3	50.1	40.6	31.6	47.2
Ce	60	54	101	131	124	102
Nd	22	19	36	58	45	40
La	28	25	43	71	71	61
Y	28	28	35.2	44.3	32.8	28.3
Sr	48.7	46.9	52.7	25.4	74.4	84.5
Rb	289.4	283.3	345.6	316.9	310	179.1
Nb	20.1	19.8	14	19.8	19	13.6
Zr	181.3	181	297.9	324	193.6	166.7
Th	28.5	31.9	16.9	52.6	31.5	23.3
Pb	41.9	28.9	81.8	622.4	37.3	47.6
U	5.1	4.6	4	13.8	5.1	5.9
Mo	3.5	1.1	48.3	44.5	0.4	1.1

Table A2.3: Amdel Geochemical Analyses

Sample No.:	75MGC13	32MGC14	31MGC20	82MGC24	83MGC25
Location or Unit	Vent Halo 2	Vent Halo 2	Vent Halo 3	Vent Halo 3	Vent Halo 2
Major Element (%)					
SiO ₂	80.2	78.7	83.6	83.1	81.8
TiO ₂	0.15	0.14	0.14	0.18	0.12
Al ₂ O ₃	12.3	12.9	11.8	10.5	10.8
Fe ₂ O ₃	1.27	1.29	0.71	0.68	1.85
MnO	0.02	0.05	<0.01	<0.01	<0.01
MgO	0.05	0.03	<0.01	0.05	0.02
CaO	0.07	0.13	<0.01	0.01	0.01
Na ₂ O	0.25	0.09	0.07	0.11	0.09
K ₂ O	3.58	3.9	0.98	2.98	3.08
P ₂ O ₅	<0.01	0.02	<0.01	<0.01	0.04
LOI	1.85	2.26	2.54	1.64	1.74
Total	99.74	99.49	99.84	99.25	99.55
Trace Element (ppm)					
Ag	<1	<1	<1	<1	<1
As	30	8	6	10	58
Au	<0.02	<0.02	<0.02	<0.02	<0.02
Ba	100	65	65	450	150
Bi	0.5	1	<0.05	<0.05	2
Co	<2	<2	<2	<2	<2
Cr	<2	2	<2	2	<2
Cu	7	7	8	5	5
Hg	<0.05	<0.05	<0.05	<0.05	<0.05
Mn	155	380	45	70	70
Mo	<0.05	7	<0.05	<0.05	<3
Ni	<2	<2	<2	<2	<2
Pb	5	25	10	10	10
Rb	165	180	48	155	165
Sb	<4	<4	10	4	<4
Se	<0.5	<0.5	<0.5	<0.5	1
Sr	12	9	10	24	14
Te	0.5	1	<0.5	<0.5	1.5
Ti	970	960	850	970	770
Tl	<10	<10	<10	10	10
U	<4	4	5	<4	<4
V	6	8	4	4	2
W	<10	<10	<10	<10	<10
Zn	7	18	7	5	4

APPENDIX 3

CIPW NORMALISATION PROGRAM

A program has been constructed in BASIC to calculate CIPW normative mineralogies for silica oversaturated igneous rocks, based on major element abundances. The program structure is based on calculative methodology from Barker (1983). Note that the program was developed for use with both silica oversaturated and undersaturated rocks, however results obtained for the undersaturated rocks are suspect. A listing of the program is presented overleaf.


```

10 REM CIPW NORM PROGRAM
20 INPUT "SiO2%", SI
25 SI=SI/60.09: X=SI: GOSUB 3000: SI=X
30 INPUT "TiO2%", TI
35 TI=TI/79.9: X=TI: GOSUB 3000: TI=X
40 INPUT "Al2O3%", AL
45 AL=AL/101.96: X=AL: GOSUB 3000: AL=X
50 INPUT "Fe2O3", FE
55 FE=FE/159.69: X=FE: GOSUB 3000: FE=X
60 INPUT "FeO", FO
65 FO=FO/71.85: X=FO: GOSUB 3000: FO=X
70 INPUT "MnO", MN
75 MN=MN/70.94: X=MN: GOSUB 3000: MN=X
80 INPUT "MgO"; MG
85 MG=MG/40.3: X=MG: GOSUB 3000: MG=X
90 INPUT "CaO"; CA
95 CA=CA/56.08: X=CA: GOSUB 3000: CA=X
100 INPUT "Na2O"; NA
105 NA=NA/61.98: X=NA: GOSUB 3000: NA=X
110 INPUT "K2O", K
115 K=K/94.2: X=K: GOSUB 3000: K=X
120 INPUT "P2O5"; P
125 P=P/141.95: X=P: GOSUB 3000: P=X
130 INPUT "Cr2O3"; CR
135 CR=CR/151.99: X=CR: GOSUB 3000: CR=X
136 INPUT "CO2"; CO
137 CO=CO/44.01: X=CO: GOSUB 3000: CO=X
140 LET FO=FO+MN
190 LET AP=P: LET CA=CA-(3.333*P)
195 LET CC=CO: CO=0
197 LET CA=CA-CC
200 LET CM=CR: LET CR=0: REM STEP 11
210 LET FO=FO-CM: REM STEP 11
220 REM STEP 12
230 IF FO>TI, THEN GOSUB 1200 ELSE GOSUB 1250
240 REM STEP 13
250 IF AL>K, THEN GOSUB 1300 ELSE GOSUB 1350
300 REM STEP 14
310 IF AL>NA THEN GOSUB 1400 ELSE GOSUB 1450
330 LET Y=Y+(6*AB): PRINT "14:", Y
340 REM STEP 15
350 IF NA>FE THEN GOSUB 1500 ELSE GOSUB 1550
370 REM STEP 16
380 IF AL>CA THEN GOSUB 1600 ELSE GOSUB 1650
390 Y=Y+(2*AN): PRINT "16:", Y
400 REM STEP 17
410 IF CA>TI THEN GOSUB 1700 ELSE GOSUB 1750
420 Y=Y+TN: PRINT "17:", Y
430 REM STEP 18
440 IF FE>FO THEN GOSUB 1800 ELSE GOSUB 1850
450 REM STEP 19
460 M=MG/(MG+FO)
465 REM STEP 20
470 IF CA>(MG+FO) THEN GOSUB 2000 ELSE GOSUB 2050
489 PRINT "20:", Y
490 IF SI>Y THEN QZ=SI-Y ELSE GOSUB 600
500 GOTO 1000
600 D=Y-SI
605 REM STEP 22
610 IF D < .5*(HYEN+HYFS) THEN GOTO 2200
620 IF D > .5*(HYEN+HYFS) THEN GOSUB 2250
630 LET D1=D-.5*(HYEN+HYFS)
640 REM STEP 23
650 IF TN=0 THEN D2=D1: GOTO 690
660 IF D1<TN THEN GOTO 2300
670 IF D1>TN THEN GOSUB 2350
680 LET D2=D1-TN
690 REM STEP 24

```

```

700 IF D2<(A+BS) THEN GOTO 2400 ELSE GOSUB 2450
710 D3=D2-(4*AB)
715 REM STEP 25
720 IF D3<2*ORT THEN GOTO 2500 ELSE GOSUB 2550
730 D4=D3-2*ORT
740 REM STEP 26
750 IF D4<.5*WO THEN GOTO 2600 ELSE GOSUB 2650
760 D5=D4-.5*WO
770 REM STEP 27
780 IF D5<(DIDI+DIHD) THEN GOTO 2700 ELSE GOSUB 2750
790 D6=D5-(DIDI+DIHD)
800 REM STEP 28
810 LET KPP=D6/2 AND LCP=LC-D6/2
1000 REM Conversion of mineral proportions to weight percentages
1100 REM Output of mineral weight %'s are as follows:
1105 PRINT "Mineral weight %'s are as follows:"
1110 PRINT "qz",QZ*60.09;PRINT "ort",ORT*556.7;"ortp",ORTP*556.7; PRINT "ab",AB*
524.48;"apb",APB
1120 PRINT "an",AN*278.22;"ne",NE*284.12; PRINT "hyen",HYEN*100.39;"hyfs",HYFS*1
31.94
1125 FOR Z = 1 TO 30000:NEXT Z
1130 PRINT "didi",DIDI*216.56;"didip",DIDIP*216.56; PRINT "dihd",DIHD*248.11;"di
hdp",DIHDP*248.11
1140 PRINT "olfo",OLFO;"olfa",OLFA; PRINT "lc",LC;"lcp",LCP
1150 PRINT "ks",KS;"kpp",KPP; PRINT "pf",PF;"csp",CSP
1155 PRINT "wo",WO*116.17;"wop",WOP*116.17; PRINT "cm",CM*223.84;"ac",AC*462.03
1160 PRINT "pf",PF;"csp",CSP; PRINT "mt",MT*231.54;"hm",HM*159.69
1162 PRINT "il",IL*151.75;"ru",RU*79.9;PRINT "tn",TN*196.07;"tnp",TNP*196.07
1165 PRINT "cc",CC;"corundum",C*101.96;"APATITE",AP*336.22
1170 PRINT "finished"
1180 END
1200 LET IL=TI: FO=FO-II
1210 TI=0
1240 RETURN
1250 LET IL=FO: TI=TI-FO
1260 FO=0
1290 RETURN
1300 LET ORT = K: AL=AL-K
1305 LET K=0
1320 LET Y=6*ORT: PRINT "13:",Y
1340 RETURN
1350 LET ORT=AL: K=K-AL
1360 LET AL=0
1370 LET KS = K: K=0
1380 LET Y=(6*ORT)+KS: PRINT "13:",Y
1390 RETURN
1400 LET AB=NA: AL=AL-NA
1410 LET NA=0
1440 RETURN
1450 LET AB=AL: NA=NA-AL
1460 LET AL=0
1490 RETURN
1500 LET AC=FE: NA=NA-FE
1502 LET FE=0
1505 LET NS=NA: NA=0
1510 Y=Y+(4*AC)+NS: PRINT "15:",Y
1540 RETURN
1550 LET AC=NA: FE=FE-NA
1555 LET NA=0
1560 Y=Y+(4*AC): PRINT "15:",Y
1590 RETURN
1600 LET AN=CA: AL=AL-CA
1605 LET CA=0
1610 LET C=AL: AL=0
1640 RETURN
1650 LET AN=AL: CA=CA-AL
1660 LET AL=0
1690 RETURN
1700 LET TN=TI: CA=CA-TI
1710 LET TI=0

```

```

1700 RETURN
1750 LET TN=CA: T1=TI-CA
1755 LET CA=0
1760 LET RU=TI: TI=0
1790 RETURN
1800 LET MT=FO: FE=FE-FO
1805 LET FO=0
1810 LET HM=FE: FE=0
1840 RETURN
1850 LET MT=FE: FO=FO-MT
1860 LET FE=0
1890 RETURN
2000 DIDI=M*(MG+FO): DIHD=(1-M)*(MG+FO)
2010 CA=CA-(DIDI+DIHD)
2030 LET WO=CA: CA=0
2035 Y=Y+2*(DIDI+DIHD)+WO
2040 RETURN
2050 DIDI=M*CA: DIHD=(1-M)*CA
2060 HYEN=MG: HYFS=FO: MG=0: FO=0
2070 Y=Y+2*(DIDI+DIHD)+(HYEN+HYFS)
2090 RETURN
2200 OLFO=M*D: OLFA=(1-M)*D
2210 HYEN=M*D: HYFS=(1-M)*D: REM ERROR IS HERE
2240 GOTO 1000
2250 OLFO=M*.5*(HYEN+HYFS)
2260 OLFA=(1-M)*.5*(HYEN+HYFS)
2270 RETURN
2300 TNF=TN-D1
2310 FF=D1
2340 GOTO 1000
2350 PF=TN
2360 TNF=0
2390 RETURN
2400 LET NE=(D2/4)
2410 LET ABP=AB-(D2/4)
2440 GOTO 1000
2450 NE=AB
2460 APB=0
2490 RETURN
2500 LET LC=D3/2
2510 ORTP=ORT-D3/2
2540 GOTO 1000
2550 LC=ORT
2560 ORTP=0
2590 RETURN
2600 CSP=D4
2610 WOP=WO-2*D4
2640 GOTO 1000
2650 CSP=.5*WO
2660 WO=0
2690 RETURN
2700 CSP=CSP+D5/2
2710 OLFO=OLFO+M*(D5/2)
2720 OLFA=OLFA+(1-M)*(D5/2)
2730 DIDIP=DIDI-M*D5
2735 DIHDP=DIHD-(1-M)*(D5/2)
2740 GOTO 1000
2750 CSP=CSP+2*(DIDI+DIHD)/2
2760 OLFO=OLFO+M*(DIDI+DIHD)/2
2770 OLFA=OLFA+(1-M)*((DIDI+DIHD))/2
2780 DIDIP=0: DIHDP=0
2790 RETURN
3000 X=(INT(X*10000)/10000)
3010 RETURN

```

APPENDIX 4

GIBRALTAR I DRILL CORE LOG

Logging of the drill core was performed by E. Dubowski during drilling of the Gibraltar I drill hole. A copy of the log is provided here, after Dubowski (1992).

Depth (m)	Sample Interval	Sample RS Nos.	DESCRIPTION
0			0-1.0m : Open hole : rotary bit (NB-Sample RS Numbers are prefixed by 5737)
1			1.0-2.18m : RHYOLITE, finely laminated, slightly porphyritic; laminations < 0.5mm thick, phenocrysts of qtz (1mm) and pinkish red feldspar (< 0.5mm); feldspars altered to lg pale yellowish ?sericite; fine discontinuous fractures perpendicular to lamination
2			2.18-4.08m : RHYOLITE, vfg. massive relatively structureless, pale reddish brown with disseminated vfg sericite flecks; cobs of 5mm large green ?sericite/koolinite; rare angular fragments
3			
4	4.18 4.47	786	4.08-4.18m : RHYOLITE, porphyritic with minor laminated zone; altered green feldspars to 5mm
5	S		4.18-7.90 : ?RHYOLITE, fg, silicified, colour mottled brown-red, purplish red, light brown, with disseminated yellow sericite, and thin green ?sericite/koolinite veins/cobs; fracture surfaces coated with yellowish FeOx.
6	S		
7	S		6.8m : brecciated appearance
8			7.90-9.53m: RHYOLITE, vfg brownish purplish red with trace disseminated pale yellowish sericite; orange FeOx and pale green clay deposited on fracture surfaces; colour of unit changes to light - pale brown adjacent to fractures.
9			
10	9.95 10.05	787	9.53-9.85m: RHYOLITE, finely laminated, porphyritic, dark brownish red, subhedral qtz phenocrysts - 2-5%; fine fracture stockwork and FeOx and yellow sericite on surface.
11	S		9.85-22.3m: RHYOLITE, massive, fg, silicified, mottled colour, brown red-brown, orange brown, brownish purplish red; coarse fracture stockwork developed; thin, <0.5mm, dark grey qtz veins visible throughout unit.
12	S		10.65-10.70m: green ?koolinitised/sericitised fragments
13	S		
14	S		
15	S		14.61-15.43m: colour mottles becoming pale greenish brown and darker purplish red; occasional small fine dark fractures sub perpendicular to CA.
16	S	15.26 16.15	788 15.7-16.57m: intense fracturing with possible associated host rock alteration - more pale colouring; possibly minor brecciation.
17	S	16.9 17.06	789 16.57m : fracture infilled with pale yellowish clay below a fragmental zone. 16.95m : rhyolite, 40cm thick, finely laminated, dark reddish, highly contorted; weakly porphyritic
18	S	18.38 18.43	790
19	S		19.35m : breccia, 6cm thick zone, pale yellow to yellow orange FeOx qtz matrix.
20	S		
21	S		20.7-22.3m: purplish red, highly fractured, showing host rock altm along margins of fractures.
22	S		
23			22.5-22.5m: RHYOLITE, poorly layered, fractured with traces of yellowish sericite on fracture surfaces. 22.5-23.25m: RHYOLITE, brown weakly porphyritic grading to porphyritic by 23.25m; phenocrysts of 3mm grey anhedral-subhedral qtz and sericitised feldspars; silicification adjacent to fractures.
24			23.25-85.46m: RHYOLITE, porphyritic, brownish red; phenocrysts comprise grey subhedral qtz to 4mm and pink subhedral to euhedral feldspar to 3mm (rare to 5mm); well developed fracture stockwork showing altm of host and FeOx on surfaces; developing to porphyritic, layered rhyolite
25			24.1-25.8 : Rhyolite shows well developed layering
26			

Depth (m)	Sample Interval	Sample RS Nos.	DESCRIPTION
26			
27	27.21	791	
28	28.08		28.1-33.32: extensively fractured and altered; feldspars altered to yellowish green; pale green sericite/clay on fracture surfaces; ?silicification of host rock adjacent to fractures; possibly trace chlorite on fracture surfaces.
29			
30			
31	31.40	792	
32	31.98 32.05	793	
33	32.50 32.79 32.84	794 795	32.54m : Rhyolite, 30cm thick, red, matrix with green feldspars; fine fracture stockwork with qtz and chlorite on surface; disseminated lg aggregates of sulphide to 2-3mm 33.17-35.64m: laminated on fine and broad scale; some thin qtz veins. x-cutting layering; disseminated sulphides as fine aggregates to 2mm.
34			
35			Slightly ?amethystine thin qtz and chlorite veins @: 34.54m 35.33m - trace sulphides 36.75m - trace sulphides
36			35.85m : more massive, redder coloured rhyolite, lacking laminations; disseminated sulphide aggregates.
37	36.75	796	
38	37.75		
39			
40	40.60	797	39.8-40.3m: fracture zone, margin altered to vlg red colour; disseminated sulphide aggregates and crystals to 1mm associated with chlorite cils and along fine fractures
41	41.51		40.9m : 10mm clt of ?amethystine qtz and chlorite with small fragments of host rock; minor orange FeOx staining
42			41.5-43.3m: Rhyolite, slightly lighter colour, porphyritic, layering less conspicuous; anhedral-euhedral pale pink feldspar phenocrysts to 4mm and anhedral-subhedral grey qtz phenocrysts to 2-3mm; traces of disseminated sulphide.
43			
44	44.64	798	43.9m : thin 2mm white qtz vein perpendicular to layering.
45	44.77	799	44.76m : 12cm zone red, orange red fracture zone with disseminated sulphide 44.97 : sulphide and chlorite at intersection of fractures
46			45.0-46.5m: well developed fracture stockwork with trace chlorite
47			
48			
49	49.43 49.56	800	48.3m : dark green chlorite and pale green ?sericite/clay on fracture surface.
50	50.10		49.18-51.4m disrupted and brecciated - producing slightly vuggy core
51	51.28	801	
52			51.7-52.2m: Rhyolite red, massive, with contorted fine layering

Depth (m)	Sample Interval	Sample RS Nos.	DESCRIPTION
52			
53			52.5 : 2 cm thick breccia zone.
54			
55	55.25 55.40	802 803	
56			
57			56.86m : fracture along which is developed dark green clay and pale green chlorite.
58	57.84 57.98	804	
59			58.54-60.4m: green feldspar zone; fine fracture stockwork; rhyolite more reddish, lacks layering.
60	59.80 60.47	805	59.8-60.8m: disseminated fg aggregates of sulphides.
61			
62			61.5m : 5mm thick green clay/chlorite - ?shear zone
63			62.5-62.9m: disrupted/brecciated rhyolite pervaded by chlorite and pale green clay along fractures. 62.9-68.2m: rhyolite lacks definite layering, appears to be disrupted; green feldspars present, veins of chlorite and pale green ?clay/sericite.
64	63.75 63.90	806	63.84m : ?quartzitic fragment mantled by ?chlorite.
65	64.80 65.80	807	
66			65.44m : thin very pale creamish green vein (?sericitic) showing minor brecciation
67			66-67.9m : core lost out of barrel and tube - recovered most)
68			
69			69.2-69.9m: green feldspar zone
70	69.73 69.90	808	69.6m : breccia associated with pale green to green ?clay/sericite alteration.
71			
72			71.8-74.25m: fracture stockwork pale greenish ?clay/sericite on fracture surfaces; minor green feldspars.
73			
74	74.23		
75	75.30	809	
76			75.9-76.1m: minor fracture stockwork with pale green altered feldspars; trace fg disseminated sulphides.
77			
78			

Depth (m)	Sample Interval	Sample RS Nos.	DESCRIPTION
78			
79	79.40 79.46	810	79.5m : 1 cm breccia fragment
80			
81			80.9-81.3m: vf white ?carbonate veins (<0.5mm thick)
82	81.53 82.53	811	
83			
84			
85			
86	85.68 85.83 85.90	812 813	85.46-103m: RHYOLITE, layered, porphyritic with zones of disruption, brecciation and fracture stockwork unit carries sulphides along fracture system, which intensely alters host rock; also cross-cut by thin carbonate, chlorite and qtz veins.
87	86.63 86.95	814	
88			
89	88.90	815	88.5m : TROPARI Measurement - 67° to 297° M.
90	89.60 89.69 89.75	816	
91	90.61 90.75	817	
92			
93	93.42 93.50	818	
94	94.32	819	
95			
96			
97	96.52 97.10 97.25	820 821	
98			
99	99.28 99.50	822 823	
100			
101			
102	101.6 102.0	824	
103			103.0-107.1m: RHYOLITE, massive red, increased content of sulphides (approximately 1%) disseminated and aggregate in matrix and with qtz and chl and CO ₂ in veins
104			

Depth (m)	Sample Interval	Sample RS Nos.	DESCRIPTION
104	104.04 104.35 104.26	825 826	
105	104.98 105.26 105.54	827 828	104.96 : layered red rhyolite - layering highlighted by qtz and sulphide; pronounced brittle fracturing to 107.1m
106	106.37 106.55	829	
107	107.11 107.18 107.48 107.64	830 831	107.1-111m: AGGLOMERATE, massive with fragments to 60cm; minor chlorite and ?CO ₂ with traces of sulphide on fracture surfaces.
108	Ag 108.46 108.59	832	108.3m : TROPARI Measurement - 675° to 300° M
109	Ag		
110	Ag 109.60 110.53	833	
111			EOH : 111 metres

APPENDIX 5

FLUID INCLUSION MICROTHERMOMETRY

Sample No.	Mineral	Inclusion Type	Phases	% Vapour	Inclusion Area	Te	Tm	NaCl%	TCO2 Vap	Th av.
A972-C23	quartz	2°	L + V	30%	18 x 7.5 µm	-35.4	-0.5	0.5	n/a	148.6
A972-DDH	fluorite	1°	L + V	10%	24 x 13 µm	-53.2	-1.0	1.0	n/a	168.4
A972-DDH	fluorite	1°	L + V	5%	16 x 9.5 µm	-59.0	-0.5	0.5	n/a	200.2
A972-S184	quartz	1°	L + V	5%	13.5 x 7.5 µm	-27.8	-1.2	1.5	n/a	211.2
A972-S184	quartz	2°	L + V	10%	6 x 5 µm	?	?		n/a	172.0
A972-S184	quartz	1°	L + V	15%	6 x 12 µm	-28.0	-0.8	1.0	n/a	198.5
A972-S184	quartz	2°	L + V	50%	6 x 3 µm	?	?		n/a	173.0
A972-S184	quartz	2°	L + V	10%	9 x 7.5 µm	-26.0	-1.5	2.0	n/a	195.2
A972-S184	quartz	1°	L + V	30%	10.5 x 5 µm	-39.4	-1.7	2.5	n/a	231.8
A972-S184	quartz	1°	L + V	20%	4.5 x 5 µm	-39.5	-1.8	2.8	n/a	260.7
A972-S184	quartz	1°	L + V	20%	4.5 x 3.5 µm	?	?		n/a	231.7
A972-S184	quartz	1°	L + V	10%	7 x 4.5 µm	?	-1.0	1.0	n/a	256.6
A972-C134	quartz	1°	L + V	10%	6 X 4.5 µm	?	?		n/a	271.9
A972-C134	quartz	1°	L + V	25%	4.5 x 3 µm	-41.3	-1.3	2.0	n/a	296.5
A972-C134	quartz	2°	L + V	50%	3.75 x 9 µm	?	-1.3	2.0	n/a	130.0

Hand specimens considered suitable for fluid inclusion work were thin sectioned to approximately 0.03 mm thickness. Fluid inclusions were then identified using optical microscopy. Once located, the rock slide was removed from its glass mount using an acetone bath to dissolve the backing glue. Areas of a slide considered to have fluid inclusions suitable for analyses were then broken off, to give pieces ready for use.

A Reynolds heating and freezing stage was used for the microthermometry. fluid inclusions were located using 40x magnification on the transmitted light microscope. First melt and final melt temperatures were obtained by freezing the sample with a jet of liquid nitrogen gas, and then reheating the inclusion to observe any phase changes. Homogenisation temperatures were determined by heating the sample using a copper coil conduction filament, capable of temperatures of 500°C. On the disappearance of bubbles within the observed inclusion, homogenisation temperature had been reached.

Results are presented in the following table.

APPENDIX 6

CHLORITE ELECTRON MICROPROBE ANALYSES

Thin sections made from both outcrop and drill core samples were investigated for chlorites evidently in equilibrium with sulfide and other alteration mineralogies. Selected sections were carbon - coated and analysed in a Jeol 733 Superprobe model electron microscope, using rhodonite as a standard for calibration. Electron beam potential was set at 15kV running a 3nA current. Analyses were recorded using an ACER 386 computer employing the "DD SOILS" EDS package.

From the wt % oxide values temperature, $\log fO_2$ and $\log fS_2$ were calculated on computer by Dr J Walshe of the Australian National University, using a six component solid solution model (Walshe, 1986). These results are presented the table following, associated with their corresponding microprobe analysis.

Wt (%) Oxide	808-01A	808-01B	808-01C	808-01D	808-01E	808-01F	808-07B	808-07C	808-08B	808-08D	808-08E	808-08F
SiO2	23.92	22.55	22.47	22.57	23.80	23.33	22.83	22.78	28.39	28.47	22.66	24.66
Al2O3	21.84	20.20	19.86	19.25	19.41	19.41	20.51	20.62	22.03	22.02	20.62	20.39
Fe2O3	0.00	0.00	0.00	0.00	0.00	0.00	0.00	0.00	0.00	0.00	0.00	0.00
FeO	35.08	34.78	36.38	34.36	35.16	33.41	32.59	32.55	26.17	27.39	34.03	31.83
MnO	2.02	2.79	1.99	2.71	2.30	3.07	3.05	3.24	3.04	2.83	2.35	2.45
MgO	6.30	5.20	4.97	5.23	6.23	6.05	7.11	6.99	5.02	5.50	5.23	5.72
Na2O	0.01	0.59	0.00	0.01	0.34	0.16	0.24	0.00	0.41	0.27	0.00	0.00
K2O	0.00	0.00	0.02	0.00	0.04	0.06	0.00	0.02	1.82	1.59	0.16	0.42
TiO2	0.16	0.15	0.08	0.00	0.07	0.00	0.00	0.01	0.00	0.18	0.05	0.08
CaO	0.08	0.15	0.13	0.03	0.09	0.06	0.11	0.01	0.27	0.11	0.16	0.13
Mg No.	27.45	25.80	23.01	25.99	27.64	29.37	32.59	32.59	31.48	31.62	25.58	28.48
Temp (°C)	299	303	306	298	293	292	300	299	141	148	300	234
log fO2	-34.8	-34.4	-34.3	-35.4	-36.1	-36.0	-33.5	-33.5	-54.9	-53.8	-35.0	-42.3
log fS2	-11.7	-11.5	-11.6	-12.4	-12.9	-12.7	-11.0	-11.0	-22.2	-21.7	-12.0	-16.0
Wt (%) Oxide	808-10A	808-02C	808-02D	808-02E	808-02F	808-02G	808-05A	808-05B	808-05C	808-05D	808-03A	808-03B
SiO2	26.56	23.87	22.91	23.89	26.36	24.68	21.59	21.24	21.29	21.84	22.47	23.28
Al2O3	22.17	20.98	21.18	20.65	20.92	20.38	20.89	20.81	19.34	21.55	19.98	20.13
Fe2O3	0.00	0.00	0.00	0.00	0.00	0.00	0.00	0.00	0.00	0.00	0.00	0.00
FeO	29.84	33.62	34.96	33.78	32.24	32.08	36.52	37.74	34.50	35.11	33.30	33.85
MnO	2.69	3.47	2.77	2.62	2.52	4.03	2.12	2.84	2.64	2.61	2.44	2.35
MgO	6.29	5.71	5.59	5.84	6.58	6.32	4.61	3.55	4.08	4.66	6.24	6.66
Na2O	0.04	0.20	0.22	0.22	0.01	0.00	0.00	0.00	0.11	0.08	0.00	0.15
K2O	1.18	0.12	0.00	0.21	0.20	0.08	0.00	0.00	0.03	0.03	0.00	0.00
TiO2	0.08	0.10	0.08	0.00	0.18	0.08	0.22	0.15	0.04	0.05	0.12	0.11
CaO	0.03	0.07	0.14	0.12	0.18	0.18	0.07	0.02	0.16	0.40	0.07	0.06
Mg No.	31.83	28.94	26.75	27.88	30.69	32.35	22.10	19.60	22.37	23.77	28.98	29.62
Temp (°C)	206	292	305	282	215	259	317	327	307	313	300	297
log fO2	-45.6	-33.8	-33.7	-35.1	-44.9	-38.0	-32.0	-31.1	-34.1	-32.2	-34.3	-34.9
log fS2	-17.7	-11.0	-11.1	-11.7	-17.5	-13.2	-10.2	-9.8	-11.4	-10.3	-11.4	-11.8
Wt (%) Oxide	808-03C	808-04B	808-04F	808-04G	808-04J	808-09B	808-09C	080-09D	808-11A	806T-02A	806T-02B	806B-08A
SiO2	24.39	23.81	22.85	25.85	25.47	25.71	28.78	22.87	23.52	27.99	28.01	25.32
Al2O3	21.54	19.21	18.24	20.07	18.58	18.62	17.81	17.65	20.74	19.78	20.02	17.84
Fe2O3	0.00	0.00	0.00	0.00	0.00	0.00	0.00	0.00	0.00	0.00	0.00	0.00
FeO	33.22	34.59	33.51	31.53	28.58	29.48	17.96	32.82	33.86	28.00	29.95	28.40
MnO	2.42	9.08	9.56	8.13	7.08	7.26	3.70	9.15	2.55	4.48	3.90	4.39
MgO	6.59	1.85	1.34	4.30	6.72	6.84	15.47	2.59	5.71	9.73	9.18	8.34
Na2O	0.04	0.15	0.31	0.40	0.37	0.21	0.09	0.59	0.29	0.00	0.19	0.00
K2O	0.39	0.00	0.03	0.35	0.10	0.00	0.05	0.00	0.12	0.04	0.04	0.18
TiO2	0.03	0.21	0.00	0.00	0.25	0.00	0.11	0.12	0.09	0.21	0.15	0.13
CaO	0.05	0.19	0.08	0.20	0.17	0.14	0.24	0.17	0.09	0.20	0.24	0.22
Mg No.	29.94	26.53	26.48	33.52	40.12	39.86	63.55	29.73	27.37	43.86	40.41	40.47
Temp (°C)	282	273	278	223	214	221	146	288	293	183	189	207
log fO2	-34.8	-36.8	-36.3	-43.6	-44.2	-43.3	-51.5	-36.7	-33.9	-48.0	-47.5	-45.1
log fS2	-11.5	-12.7	-12.4	-16.6	-16.7	-16.2	-19.9	-13.3	-11.1	-18.4	-18.4	-17.2

Wt (%) Oxide	808-01A	808-01B	808-01C	808-01D	808-01E	808-01F	808-07B	808-07C	808-08B	808-08D	808-08E	808-08F
SiO2	23.92	22.55	22.47	22.57	23.80	23.33	22.83	22.78	28.39	28.47	22.66	24.66
Al2O3	21.84	20.20	19.86	19.25	19.41	19.41	20.51	20.62	22.03	22.02	20.62	20.39
Fe2O3	0.00	0.00	0.00	0.00	0.00	0.00	0.00	0.00	0.00	0.00	0.00	0.00
FeO	35.08	34.78	36.38	34.36	35.16	33.41	32.59	32.55	26.17	27.39	34.03	31.83
MnO	2.02	2.79	1.99	2.71	2.30	3.07	3.05	3.24	3.04	2.83	2.35	2.45
MgO	6.30	5.20	4.97	5.23	6.23	6.05	7.11	6.99	5.02	5.50	5.23	5.72
Na2O	0.01	0.59	0.00	0.01	0.34	0.16	0.24	0.00	0.41	0.27	0.00	0.00
K2O	0.00	0.00	0.02	0.00	0.04	0.06	0.00	0.02	1.82	1.59	0.16	0.42
TiO2	0.16	0.15	0.08	0.00	0.07	0.00	0.00	0.01	0.00	0.18	0.05	0.08
CaO	0.08	0.15	0.13	0.03	0.09	0.06	0.11	0.01	0.27	0.11	0.16	0.13
Mg No.	27.45	25.80	23.01	25.99	27.64	29.37	32.59	32.59	31.48	31.62	25.58	28.48
Temp (°C)	299	303	306	298	293	292	300	299	141	148	300	234
log fO2	-34.8	-34.4	-34.3	-35.4	-36.1	-36.0	-33.5	-33.5	-54.9	-53.8	-35.0	-42.3
log fS2	-11.7	-11.5	-11.6	-12.4	-12.9	-12.7	-11.0	-11.0	-22.2	-21.7	-12.0	-16.0
Wt (%) Oxide	808-10A	808-02C	808-02D	808-02E	808-02F	808-02G	808-05A	808-05B	808-05C	808-05D	808-03A	808-03B
SiO2	26.56	23.87	22.91	23.89	26.36	24.68	21.59	21.24	21.29	21.84	22.47	23.28
Al2O3	22.17	20.98	21.18	20.65	20.92	20.38	20.89	20.81	19.34	21.55	19.98	20.13
Fe2O3	0.00	0.00	0.00	0.00	0.00	0.00	0.00	0.00	0.00	0.00	0.00	0.00
FeO	29.84	33.62	34.96	33.78	32.24	32.08	36.52	37.74	34.50	35.11	33.30	33.85
MnO	2.69	3.47	2.77	2.62	2.52	4.03	2.12	2.84	2.64	2.61	2.44	2.35
MgO	6.29	5.71	5.59	5.84	6.58	6.32	4.61	3.55	4.08	4.66	6.24	6.66
Na2O	0.04	0.20	0.22	0.22	0.01	0.00	0.00	0.00	0.11	0.08	0.00	0.15
K2O	1.18	0.12	0.00	0.21	0.20	0.08	0.00	0.00	0.03	0.03	0.00	0.00
TiO2	0.08	0.10	0.08	0.00	0.18	0.08	0.22	0.15	0.04	0.05	0.12	0.11
CaO	0.03	0.07	0.14	0.12	0.18	0.18	0.07	0.02	0.16	0.40	0.07	0.06
Mg No.	31.83	28.94	26.75	27.88	30.69	32.35	22.10	19.60	22.37	23.77	28.98	29.62
Temp (°C)	206	292	305	282	215	259	317	327	307	313	300	297
log fO2	-45.6	-33.8	-33.7	-35.1	-44.9	-38.0	-32.0	-31.1	-34.1	-32.2	-34.3	-34.9
log fS2	-17.7	-11.0	-11.1	-11.7	-17.5	-13.2	-10.2	-9.8	-11.4	-10.3	-11.4	-11.8
Wt (%) Oxide	808-03C	808-04B	808-04F	808-04G	808-04J	808-09B	808-09C	808-09D	808-11A	806T-02A	806T-02B	806B-08A
SiO2	24.39	23.81	22.85	25.85	25.47	25.71	28.78	22.87	23.52	27.99	28.01	25.32
Al2O3	21.54	19.21	18.24	20.07	18.58	18.62	17.81	17.65	20.74	19.78	20.02	17.84
Fe2O3	0.00	0.00	0.00	0.00	0.00	0.00	0.00	0.00	0.00	0.00	0.00	0.00
FeO	33.22	34.59	33.51	31.53	28.58	29.48	17.96	32.82	33.86	28.00	29.95	28.40
MnO	2.42	9.08	9.56	8.13	7.08	7.26	3.70	9.15	2.55	4.48	3.90	4.39
MgO	6.59	1.85	1.34	4.30	6.72	6.84	15.47	2.59	5.71	9.73	9.18	8.34
Na2O	0.04	0.15	0.31	0.40	0.37	0.21	0.09	0.59	0.29	0.00	0.19	0.00
K2O	0.39	0.00	0.03	0.35	0.10	0.00	0.05	0.00	0.12	0.04	0.04	0.18
TiO2	0.03	0.21	0.00	0.00	0.25	0.00	0.11	0.12	0.09	0.21	0.15	0.13
CaO	0.05	0.19	0.08	0.20	0.17	0.14	0.24	0.17	0.09	0.20	0.24	0.22
Mg No.	29.94	26.53	26.48	33.52	40.12	39.86	63.55	29.73	27.37	43.86	40.41	40.47
Temp (°C)	282	273	278	223	214	221	146	288	293	183	189	207
log fO2	-34.8	-36.8	-36.3	-43.6	-44.2	-43.3	-51.5	-36.7	-33.9	-48.0	-47.5	-45.1
log fS2	-11.5	-12.7	-12.4	-16.6	-16.7	-16.2	-19.9	-13.3	-11.1	-18.4	-18.4	-17.2

Wt (%) Oxide	806B-08C	806B-08D	806B-08E	806B-08F	806B-08G	806B-04A	806B-04B	806B-05B	806B-07A	806B-07C	806B-07D
SiO2	33.03	26.94	26.73	23.91	27.38	25.53	24.42	29.55	24.47	24.46	25.33
Al2O3	19.69	17.05	18.56	18.02	19.23	18.59	18.31	18.53	18.59	18.48	18.36
Fe2O3	0.00	0.00	0.00	0.00	0.00	0.00	0.00	0.00	0.00	0.00	0.00
FeO	19.89	26.98	30.39	36.95	34.67	31.51	33.55	21.29	34.39	32.66	34.84
MnO	3.10	3.50	4.15	5.06	5.10	4.73	4.44	3.17	4.95	5.09	4.18
MgO	11.91	6.48	7.02	2.14	2.95	6.14	4.14	12.16	3.44	4.25	3.74
Na2O	0.00	0.21	0.15	0.06	0.53	0.00	0.14	0.21	0.32	0.16	0.53
K2O	0.54	1.00	0.36	0.01	0.17	0.02	0.02	0.13	0.00	0.14	0.06
TiO2	0.00	0.09	0.25	0.00	0.05	0.14	0.09	0.04	0.00	0.03	0.00
CaO	0.28	0.20	0.19	0.13	0.19	0.22	0.07	0.21	0.47	0.23	0.15
Mg No.	55.05	35.87	35.48	19.48	23.11	33.30	26.14	53.89	24.47	28.04	23.83
Temp (°C)	89	120	174	258	157	210	223	124	227	224	201
log fO2	-64.0	-59.3	-50.1	-41.1	-53.8	-45.5	-44.4	-56.6	-44.0	-44.2	-47.7
log fS2	-26.3	-24.8	-20.1	-16.3	-22.6	-17.8	-17.6	-22.6	-17.4	-17.4	-19.6
Wt (%) Oxide	810-06C	810-07A	810-07B	810-04B	810-04C	810-03A	810-03B	810-03C	810-02A	810-02B	02a
SiO2	25.82	27.46	29.64	27.86	28.01	27.18	25.41	24.50	28.54	27.89	23.26
Al2O3	20.83	20.57	20.74	19.89	19.94	18.72	19.76	18.74	18.64	18.98	20.14
Fe2O3	0.00	0.00	0.00	0.00	0.00	0.00	0.00	0.00	0.00	0.00	0.00
FeO	25.23	21.95	17.90	23.23	22.22	20.92	29.17	29.59	21.45	27.84	33.89
MnO	2.28	2.97	1.24	4.37	3.39	3.41	2.25	1.53	3.23	1.98	3.36
MgO	12.09	13.71	17.61	9.63	12.88	13.69	11.27	10.61	14.02	11.94	5.65
Na2O	0.00	0.12	0.00	0.00	0.01	0.13	0.24	0.00	0.58	0.10	0.28
K2O	0.17	0.33	0.68	0.72	0.53	0.37	0.09	0.05	0.30	0.24	0.07
TiO2	0.03	0.00	0.08	0.06	0.06	0.07	0.11	0.23	0.00	0.02	0.00
CaO	0.14	0.03	0.00	0.14	0.21	0.05	0.09	0.12	0.16	0.04	0.19
Mg No.	48.60	55.56	64.58	48.17	54.29	57.10	43.39	40.88	56.85	45.54	28.44
Temp (°C)	242	201	171	157	177	180	259	276	159	184	296
log fO2	-39.2	-43.7	-46.8	-51.2	-47.4	-46.7	-37.3	-36.6	-50.2	-47.8	-35.3
log fS2	-13.8	-16.0	-17.5	-19.9	-17.9	-17.5	-12.8	-12.6	-19.3	-18.2	-12.2
Wt (%) Oxide	02b	02e	02f	03b	03d	03e	03h	04a	04b	04c	04e
SiO2	23.06	24.08	22.68	22.96	23.99	23.31	22.50	24.19	22.91	24.80	29.37
Al2O3	20.47	19.94	19.21	20.00	18.16	19.81	20.11	19.69	19.07	19.95	20.11
Fe2O3	0.00	0.00	0.00	0.00	0.00	0.00	0.00	0.00	0.00	0.00	0.00
FeO	35.86	34.70	35.58	35.81	36.97	34.93	35.89	35.66	36.44	35.67	28.00
MnO	4.60	3.58	5.47	5.51	3.53	4.81	4.72	3.99	3.79	3.74	3.74
MgO	3.82	4.62	3.91	3.51	2.75	3.62	3.61	3.63	3.53	4.56	3.70
Na2O	0.06	0.33	0.33	0.01	0.13	0.20	0.01	0.28	0.00	0.05	0.21
K2O	0.03	0.05	0.00	0.02	0.94	0.13	0.08	0.18	0.07	0.05	1.43
TiO2	0.00	0.13	0.00	0.05	0.00	0.00	0.00	0.11	0.08	0.02	0.00
CaO	0.11	0.55	0.02	0.01	0.16	0.00	0.09	0.29	0.02	0.08	0.19
Mg No.	24.23	25.47	26.01	24.84	18.65	24.48	23.81	22.76	21.75	25.04	27.05
Temp (°C)	301	264	301	301	244	287	305	253	296	253	105
log fO2	-35.0	-37.9	-34.7	-34.9	-42.6	-35.1	-34.3	-39.7	-34.5	-39.6	-62.6
log fS2	-12.1	-13.2	-11.8	-12.1	-17.0	-11.7	-11.5	-14.4	-11.5	-14.3	-26.7

Wt (%) Oxide	04h	0x1	0x2	0x3	0x4	0x7	0x9	05e	05g	05h	05i
SiO2	23.43	23.44	24.20	24.60	25.39	27.78	25.60	25.20	27.31	24.15	24.64
Al2O3	18.79	19.01	19.66	18.91	19.26	19.83	20.13	19.75	21.05	20.45	20.21
Fe2O3	0.00	0.00	0.00	0.00	0.00	0.00	0.00	0.00	0.00	0.00	0.00
FeO	36.52	36.16	34.98	34.29	35.01	31.86	35.23	34.63	32.56	35.67	35.23
MnO	4.10	3.76	3.85	3.79	3.82	3.56	4.18	4.50	4.28	5.00	5.07
MgO	3.34	3.62	3.60	3.56	3.64	3.67	3.81	3.32	3.38	4.10	4.35
Na2O	0.01	0.33	0.10	0.38	0.33	0.00	0.47	0.21	0.22	0.08	0.00
K2O	0.04	0.18	0.23	0.37	0.60	0.49	0.69	0.56	0.78	0.00	0.10
TiO2	0.11	0.38	0.00	0.00	0.00	0.14	0.03	0.09	0.14	0.00	0.23
CaO	0.18	0.10	0.24	0.13	0.07	0.08	0.16	0.04	0.15	0.06	0.09
Mg No.	21.67	22.10	22.77	22.90	22.83	24.15	23.83	23.22	24.13	25.75	26.78
Temp (°C)	278	276	257	217	209	140	223	213	172	292	268
log fO2	-36.8	-36.9	-40.6	-45.4	-46.5	-56.2	-44.5	-45.4	-51.2	-36.6	-37.3
log fS2	-12.7	-12.7	-15.6	-18.3	-18.9	-23.6	-17.7	-18.0	-21.0	-13.3	-12.9
Wt (%) Oxide	05k	05m	05n	05o	05j						
SiO2	24.90	23.50	25.90	24.38	24.61						
Al2O3	20.54	20.15	21.43	21.19	20.47						
Fe2O3	0.00	0.00	0.00	0.00	0.00						
FeO	36.21	34.57	35.64	35.91	35.95						
MnO	4.42	3.12	4.00	4.61	4.94						
MgO	3.75	5.56	4.31	3.80	3.73						
Na2O	0.00	0.00	0.00	0.08	0.31						
K2O	0.13	0.07	0.08	0.00	0.18						
TiO2	0.05	0.12	0.08	0.21	0.06						
CaO	0.03	0.14	0.05	0.14	0.08						
Mg No.	23.56	27.43	24.77	24.16	24.48						
Temp (°C)	254	295	244	278	265						
log fO2	-39.4	-35.7	-41.6	-36.0	-37.8						
log fS2	-14.1	-12.5	-15.9	-12.2	-13.1						

APPENDIX 7

SPHALERITE ELECTRON MICROPROBE ANALYSES

Sphalerite crystals were recognised within pyrite in polished thin sections cut from the Gibraltar I drill core. The thin sections were coated with carbon, in preparation for electron microanalysis.

The sphalerites were analysed using a Jeol 733 superprobe electron microprobe; all analyses were performed applying the WDS system. The incident beam operated under a potential difference of 20 KeV, with a current of 3nA. The resulting analyses are presented in the following table.

Mole % FeS (see chapter 6) was calculated via the equation:

$$\text{mole \% FeS} = \frac{\text{atomic \% Fe}}{\text{atomic \% S}} \times 100$$

Sphalerite Microprobe Analyses

Sample No.	104.1-01a	104.1-01AA	104.1-01AB	104.1-01AC	104.1-01AD
S	33.80	33.34	33.03	32.61	33.45
Mn	No Data	0.31	0.30	0.33	0.33
Fe	6.64	6.95	6.97	7.12	6.96
Ni	No Data	0.00	0.03	0.00	0.02
Cu	0.00	0.00	0.00	0.00	0.00
Zn	59.16	60.20	59.93	59.67	59.63
As	0.00	0.06	0.08	0.01	0.09
Total	99.60	100.85	100.35	99.73	100.48
Mole% FeS	19.66	20.83	21.11	21.82	20.80

Sample No.	104.1-01AE	104.1-01BA	104.1-01BB	104.1-01BC	104.1-01BD	104.1-01BE
S	33.75	32.16	32.44	32.22	32.65	32.32
Mn	0.32	0.29	0.33	0.35	0.36	0.35
Fe	7.32	7.34	7.51	7.33	7.55	7.43
Ni	0.03	0.04	0.03	0.01	0.02	0.02
Cu	0.00	0.01	0.00	0.00	0.00	0.02
Zn	59.78	59.99	58.98	59.05	59.89	59.59
As	0.03	0.00	0.05	0.06	0.00	0.00
Total	101.22	99.82	99.33	99.02	100.47	99.72
Mole% FeS	21.68	22.83	23.15	22.76	23.11	22.97

APPENDIX 8

SULPHUR ISOTOPE ANALYSES

METHOD OF PREPARATION

The sulphide used in this analysis was pyrite. Other species present (chalcopyrite and sphalerite) lacked sufficient quantity for any analysis to be performed. All pyrite was extracted from the Gibraltar I drill core, due to the absence of sulphide in outcrop samples.

Sample material was extracted from the core using a dental drill, equipped with a 1mm diamond coated bit. This method ensured identification of the sample with regard to its location, crystallinity, etc.

The sample was then weighed, finely ground (mortar and pestle) and mixed with 200 mg of Cu₂O flux in preparation for SO₂ gas production.

GENERATION OF SO₂ GAS

The method described by Robinson and Kusakabe (1975) was employed as a means of SO₂ gas production. The sample and flux were placed in a ceramic boat and heated at 1060° C for 12-15 minutes under vacuum. The evolved gas was then separated into condensables and non-condensables via freezing with liquid nitrogen, to tap off the non-condensable fraction. Water vapour was then removed using a cold ethanol bath, the remainder being collected again with liquid nitrogen. SO₂ and CO₂ were then separated using an n-pentane bath, where the condensed CO₂ was tapped off after entrapment of SO₂ with the liquid nitrogen. The SO₂, now pure, was trapped and sealed in a glass tube, in readiness for mass spectrographic analysis.

ISOTOPIC ANALYSIS OF SULPHUR

All sulphur isotope ratios were measured using a Micromass VG 602E stable isotope mass spectrometer. The ³⁴S/³²S ratios were compared with the Canon Diablo troilite international standard, and are expressed in per mil (‰).

$$\delta^{34}\text{S} (\text{‰}) = \frac{^{34}\text{S}/^{32}\text{S} \text{ sample} - ^{34}\text{S}/^{32}\text{S} \text{ standard}}{^{34}\text{S}/^{32}\text{S} \text{ standard}} \times 1000$$

APPENDIX 9

THERMODYNAMIC EQUATIONS

EQUATION

LOG K (300 °C)

(1) $\text{KAl}_2(\text{AlSi}_3\text{O}_8)(\text{OH})_2 + 6\text{SiO}_2 + 3\text{Na}^+ = 3\text{NaAlSi}_3\text{O}_8 + \text{K}^+ + 2\text{H}^+$	-10.53
(2) $3\text{Al}_2\text{Si}_2\text{O}_5(\text{OH})_4 + 2\text{K}^+ = 2\text{KAl}_2(\text{AlSi}_3\text{O}_{10})(\text{OH})_2 + 2\text{H}^+$	-3.60
(3) $\text{HSO}_4^- = \text{H}^+ + \text{SO}_4^{2-}$	-6.08
(4) $\text{H}_2\text{S} = \text{HS}^- + \text{H}^+$	-8.06
(5) $\text{H}_2\text{S} + 2\text{O}_2 = \text{HSO}_4^- + \text{H}^+$	53.40
(6) $\text{H}_2\text{S} + 2\text{O}_2 = \text{SO}_4^{2-} + 2\text{H}^+$	47.32
(7) $\text{HS}^- + 2\text{O}_2 = \text{SO}_4^{2-} + \text{H}^+$	55.38
(8) $4\text{Fe}_3\text{O}_4 + \text{O}_2 = 6\text{Fe}_2\text{O}_3$	31.04
(9) $4\text{FeS}_2 + 8\text{H}_2\text{O} + 15\text{O}_2 = 2\text{Fe}_2\text{O}_3 + 8\text{HSO}_4^- + 8\text{H}^+$	372.21
(10) $4\text{FeS}_2 + 8\text{H}_2\text{O} + 15\text{O}_2 = 2\text{Fe}_2\text{O}_3 + 8\text{SO}_4^{2-} + 16\text{H}^+$	323.57
(11) $3\text{FeS}_2 + 6\text{H}_2\text{O} + 11\text{O}_2 = \text{Fe}_3\text{O}_4 + 6\text{SO}_4^{2-} + 12\text{H}^+$	234.92
(12) $3\text{FeS}_2 + 6\text{H}_2\text{O} = \text{Fe}_3\text{O}_4 + 6\text{H}_2\text{S} + \text{O}_2$	-49.00
(13) $2\text{FeS}_2 + 2\text{H}_2\text{O} = 2\text{FeS} + 2\text{H}_2\text{S} + \text{O}_2$	-39.13
(14) $6\text{FeS} + 6\text{H}_2\text{O} + \text{O}_2 = 2\text{Fe}_3\text{O}_4 + 6\text{H}_2\text{S}$	19.39
(15) $5\text{CuFeS}_2 + 2\text{H}_2\text{S} + \text{O}_2 = 2\text{H}_2\text{O} + \text{Cu}_5\text{FeS}_4 + 4\text{FeS}_2$	33.89
(16) $5\text{CuFeS}_2 + 2\text{H}_2\text{O} = \text{FeS} + \text{Cu}_5\text{FeS}_4 + 2\text{H}_2\text{S} + \text{O}_2$	-42.29
(17) $2\text{FeS}_2 = \text{S}_2 + 2\text{FeS}$	-11.92
(18) $4\text{FeS}_2 + 3\text{O}_2 = 2\text{Fe}_2\text{O}_3 + 4\text{S}_2$	53.85
(19) $6\text{FeS} + 4\text{O}_2 = 3\text{S}_2 + 2\text{Fe}_3\text{O}_4$	110.19
(20) $4\text{Fe}_3\text{O}_4 + \text{O}_2 = 6\text{Fe}_2\text{O}_3$	-31.04
(21) $3\text{FeS}_2 + 2\text{O}_2 = 3\text{S}_2 + \text{Fe}_3\text{O}_4$	32.52
(22) $\text{Au} + \text{H}_2\text{S} + \text{HS}^- = \text{Au}(\text{HS})_2^- + 1/2\text{H}_2$	-1.35

References for equations: (1) to (15) = Huston and Large (1989).
 (16) & (17) = Ohmoto et al. (1983).
 (23) = Shenberger and Barnes (1989).

Primary Industries SA

L00022379

